INVESTIGATING THE DYNAMICS AND BIOMECHANICS OF ACTIN STRESS FIBER REMODELING

by

Laura Marie Chapin

A dissertation submitted to the faculty of
The University of Utah
in partial fulfillment of the requirements for the degree of

Doctor of Philosophy

Department of Oncological Sciences

The University of Utah

May 2013

The University of Utah Graduate School

STATEMENT OF DISSERTATION APPROVAL

The dissertation of **Laura Marie Chapin**

has been approved by the following supervisory committee members:

Mary Beckerle	, Chair	**Dec 11, 2012** Date Approved
Vladimir Hlady	, Member	**Dec 11, 2012** Date Approved
Dean Li	, Member	**Dec 11, 2012** Date Approved
Yan-Ting Shiu	, Member	**Dec 11, 2012** Date Approved
Katharine Ullman	, Member	**Dec 11, 2012** Date Approved

and by **Brad Cairns**, Chair of the Department of **Oncological Sciences**

and by Donna M. White, Interim Dean of The Graduate School.

ABSTRACT

Cells encounter mechanical cues from the environment to which they sense and respond. The actin cytoskeleton is the main network that can not only sense mechanical changes, but can also reorganize in response. Actin stress fibers are predominant in cultured fibroblast cells and are load-bearing structures of the cell. Here, in collaboration with others, I have investigated the mechanisms of stress fiber strain response and remodeling using fluorescently-labeled cytoskeletal proteins and live cell microscopy, traction force microscopy, and genetic manipulation to assess these mechanisms. High resolution image acquisition and analysis have provided novel insight into the mechanosensitivity of actin stress fibers. Specifically, the actin-associated protein zyxin has been implicated in an actin repair mechanism with mechanical consequences. We discovered a novel zyxin-mediated actin repair mechanism that restored structural and mechanical integrity to stress fibers following a hyperleongation event in a single stress fiber sarcomere. We also discovered that while these spontaneously occurring hyperelongation events impact single sarcomeres along a stress fiber, they coincide with compensatory shortening in the near-by regions of stress fiber sarcomeres, suggesting there is active remodeling that occurs in actin stress fibers in order to maintain the structure and mechanical homeostasis in live cells. Lastly, we designed a computational model to test whether actin and myosin-based mechanical changes drive some of these dynamic changes in stress fibers. We discovered that variable differences in actin stiffness and myosin contractility may be the main factors in spontaneous changes in

stress fiber sarcomere length. The findings presented in this dissertation have made exciting contributions to the field of actin cytoskeletal dynamics, and will provide groundwork to future studies dissecting the role of actin-associated proteins in structural and mechanical homeostasis in stress fibers.

CONTENTS

LIST OF TABLES

ACKNOWLEDGMENTS

I would like to thank Rocky and Barb Chapin, Eric Chapin and Ellie Lewis, Robert Luettjohann, and Linda Luettjohann for their support during grad school. My good friends at Huntsman Cancer Institute and the Center for Human Toxicology were invaluable to me during this process for keeping me motivated and focused on finishing.

Mary Beckerle, my adviser, was incredibly helpful and supportive while I've been in her lab. I enjoyed learning from her while writing manuscripts and gaining her perspective on my work during our lab meetings.

Yan-Ting Shiu, a committee member, became involved in my project a couple years into my program. She was extremely helpful in preparing manuscripts, and I learned a lot from her by reviewing her grant submissions and other manuscripts.

I would like to thank my committee for their help and advice over the last few years. Katharine Ullman, Dean Li, Vladimir Hlady, and Yan-Ting Shiu were all very helpful and supportive.

Everyone in the Beckerle lab was extremely helpful. I contributed to Mark Smith's project when I first joined the lab and I continued to work on certain aspects of that project on my own towards the end of my time in the Beckerle lab. He provided helpful feedback regarding experiments, microscopy, and image analysis. Elizabeth Blankman was immensely helpful technically as well as a great friend. Laura Hoffman provided positive feedback and support throughout my time in lab. Chris Jensen kept me laughing, and Julie Kadrmas, Steve Pronovost, Masaaki Yoshigi, and Kathleen Clark were all great to work with. The other grad students and undergrads in lab were also very fun to get to know during my time in the Beckerle lab.

CHAPTER 1

INTRODUCTION

1.1 Broad roles of the actin cytoskeleton

In order to maintain homeostasis, cells within tissues adapt to changing conditions via cell division, apoptosis, cell migration, and differentiation. There are three main types of cytoskeletal networks used for support and movement. Intermediate filaments are made up of single helices that contain vimentin, desmin or keratin. They contribute to overall cell elasticity and support and have been called a cell's "security belt" due to their absorption of large and fast deformations (1). Microtubules are another kind of cytoskeletal structure and they are made of protofilaments comprised of tubulin, which polymerize to form ordered hollow cables. They are well-known for their involvement in kinetochore separation during cell division and intracellular trafficking using molecular motors (2). The actin cytoskeleton is the cytoskeletal structure responsible for processes such as forming the contractile ring during cell division, and coordinating leading edge protrusion, and generating contractile forces during cell migration (3). Actin monomers, known as globular actin (G-actin), polymerize to form filamentous-actin (F-actin). Bundled strands of F-actin form stress fibers (SFs). Characterizing and understanding actin cytoskeleton dynamics in live cells became the main topic of my thesis.

Actin SFs form the central architecture of mouse embryonic fibroblasts. They can span across the width of a cell and terminate in clusters of proteins that make up the integrin based focal adhesion (FA) (Figure 1.1). Actin SFs have often been compared to striated muscle fibers (4), in that they too have a striated pattern of alternating myosin and actin-bundling proteins

which form sarcomeres (Figure 1.2). And like muscle fibers, SF sarcomeres have long been thought to be the contractile subunits of SFs (5, 6). SFs have been identified in vivo and are commonly found in cells that experience tension and contraction. For example, SFs were identified in migrating cells in wound beds (7, 8) and in the endothelium of the vasculature (9) and spleen (10). SFs found in cultured cells provide us with relatively easy access for studying cell mechanics and actin dynamics.

Proteins associated with actin SFs have roles in adhesion to the extracellular matrix (ECM), actin polymerization, and signal transduction (11, 12). FAs link SFs to the underlying ECM and it is here that mechanical cues are sent in and out of the cell; a process called mechanotransduction (13, 14). There have been many proteins implicated in both sensing and responding to mechanical stimuli, though the mechanisms by which mechanosensing and responding occurs are not well understood.

1.2 The actin cytoskeleton and mechanotransduction

Mechanotransduction is the transfer of mechanical stimuli from the extracellular matrix to the cell with subsequent conversion into chemical activity. In terms of responding to mechanical forces, all three cytoskeletal networks are sensitive to mechanical changes. Microtubule growth rate and persistence are linked to mechanosensing (15), and microtubules sense shape asymmetries during cytokinesis and remodel to restore symmetry (16). Intermediate filaments have been shown to reorganize and thicken upon exposure to shear stress (17-19), and the network also stiffens in response to external stress (20). The actin cytoskeleton also stiffens with increased substrate stiffness (21) in addition to realigning SFs in response to shear stress (18), and reinforcing SFs in response to substrate stretch (22). Cells use specific components of their cytoskeleton and attachment sites to process mechanical cues.

The main hub for mechanotransduction is thought to be integrin-rich FAs that connect the actin cytoskeleton to its extracellular matrix (13, 14). In addition to mechanosensing that occurs at FAs, the cytoskeleton itself is sensitive to mechanical change. Sawada and Sheetz prepared Triton-insoluble cytoskeletons and exposed them to stretch (23). Cytoskeletal strain was shown to lead to the recruitment of cytoskeletal proteins independent of ion channels which have traditionally been hypothesized to be involved in mechanosensing (23). It is possible the actin cytoskeleton reveals cryptic binding sites along its length upon stretch, similar to the ECM protein fibronectin (24). Several cytoskeletal proteins including p130Cas (25), talin (26), and spectrin, myosin IIA, and vimentin (27) have stretch-induced changes in conformation. The exact mechanism of cytoskeletal protein recruitment to stretched actin SFs has not been fully characterized.

Mechanotransduction also involves the generation of cell-driven contractile forces on the extracellular environment. Though microtubules have been shown to be involved in fibroblast-populated collagen-gel contraction (28), they contribute only 13% towards load-bearing functions (29). The actin cytoskeleton is hypothesized to be the main contributor to generating contractile forces. Intermediate filaments are less understood regarding their force generating ability. Unlike polymerization of microtubules and actin filaments, the assembly of intermediate filaments has not been shown to generate force for two main reasons: 1) Instead of monomer or dimer addition the ends of filaments, intermediate filaments add unit-length filaments to increase their width as well as their length (30) and therefore do not participate in filament polymerization to generate protrusive forces; and 2) Intermediate filaments are relatively soft compared to microtubules and actin filaments (1) and do not have the strength or rigidity to generate these forces. The actin cytoskeleton is the predominant network involved in generating forces via its myosin II contractile activity, yet the entire mechanism of traction force generation continues to be uncovered.

1.3 Discovery of zyxin and its role in mechanotransduction

1.3.1 Location, protein structure, and binding partners

Zyxin is a 564 amino acid protein that was first identified over 25 years ago (31). Zyxin was first observed to localize at the junction of actin SFs and FAs (Figure 1.3), and is therefore named after the Greek word *zeuxis* for "joining" (32). Zyxin associates with many actin-binding proteins with diverse roles in actin dynamics, though there is no evidence that zyxin directly binds actin (Figure 1.4).

Zyxin has three LIM domains; structures characterized by double zinc finger domains and are named after the Lin-11, Isl-1 and Mec-3 proteins in which they were first identified (33). Protein domain analysis revealed that the LIM domains of zyxin are involved in mechanically-induced FA and SF localization (34, 35). Once localized to FAs and SFs, zyxin is hypothesized to facilitate actin polymerization to presumably alleviate the increased tension, and does so via its interaction with Ena/VASP (36). Zyxin is necessary for the accumulation of Ena/VASP at FAs (37), where actin polymerization is known to occur (38-40).

In addition to binding proteins involved in actin polymerization, zyxin also binds α-actinin, an actin-bundling protein (41). Both zyxin and α-actinin colocalize at FAs and along SFs in a periodic distribution similar to that in muscle sarcomeres, and both zyxin and α-actinin can be used to identify the Z-disk proteins that define sarcomere borders in SF and muscle fiber sarcomeres. α-Actinin cross-links parallel and anti-parallel actin filaments in vitro (42, 43); a useful characteristic in a dynamic actin cytoskeleton. α-Actinin isoforms 1 and 4 are found at FAs and SFs in nonmuscle cells (44), and are both implicated in glioma cell mechanosensing, motility, and contractility (45). Elimination of zyxin's α-actinin binding domain led to insufficient rescue of SF thickening following stretch (35). The α-actinin-zyxin relationship became a topic of interest for this thesis and is included in Chapter 2 (46).

1.3.2 Actin reinforcement

Within the last 10 years the role of zyxin has been more fully characterized in vivo, which can be largely attributed to the creation of a zyxin -/- mouse (47). Although zyxin -/- mice have no obvious phenotype, zyxin -/- fibroblasts exhibit compromised actin reinforcement in stretched cells.

In an initial survey, fibroblasts were plated on the silicone membrane and exposed to uniaxial stretch. SFs in wild type cells became significantly thicker and appeared more robust upon stretch (22). In order to directly test zyxin's role in this mechanosensing behavior, zyxin -/- cells were also exposed to uniaxial stretch and displayed a reduced phalloidin-stained SF signal compared to zyxin -/- cells rescued with zyxin-GFP (22). These stretch experiments suggested zyxin was important in mechanically-stimulated actin SF reinforcement. Zyxin's role in actin SF repair is further investigated in Chapter 2 (46).

1.3.3 Zyxin: a strain sensor?

The exact mechanism and extent of zyxin's mechanosensitivity has yet to be fully characterized. Hirata et al. investigated the role zyxin plays in mechanosensing and actin polymerization at FAs (34). It was reported that zyxin accumulated at FAs under resting tension, but decreased during myosin II inhibition with blebbistatin (34), illustrating zyxin dissociates from SFs under decreased or no tension. Actin polymerization at FAs appeared most prevalent when zyxin was present (34), supporting the hypothesis zyxin gets recruited to sites of strain in an effort to mediate actin repair (22), thereby decreasing tension. Additionally, zyxin dense-bodies move from FAs onto the associated SF in a force-dependent manner (39). A more recent paper expanded on zyxin's mechanosensitivity and showed zyxin-GFP intensity was rapidly decreased following laser severing of actin SFs (48), suggesting zyxin's localization at FAs and along SFs is governed by tension. Further characterization of zyxin's mechanosensitivity and actin

reinforcement was the topic of investigation in the Smith et al. publication, included here as Chapter 2 (46).

1.4 Mechanics of the dynamic actin cytoskeleton

1.4.1 Generating contractile forces

The sarcomeric structure of actin SFs mimics that found in striated muscle fibers (4), and suggests sarcomeres found in cells are also contractile units as they are in muscle (5, 6). Plating chick embryonic fibroblasts on a silicone membrane and observing the deformation of the underlying substrate first suggested that cells in culture generate contractile forces (49). Since then more sophisticated techniques have been developed to quantify these cellular forces.

Multiple techniques of traction force microscopy (TFM) were first described in the 1990s and provided a means to quantify traction strain, stress, or force exerted by live cells. These techniques included plating cells on elastic nonwrinkling silicone substrates (50-52), UV-cured wrinkling elastomers (53), micromachined force transducing cantilevers (54), and polyacrylamide gels embedded with fluorescent beads (55, 56). The basis for most TFM methods is to measure feature displacement over time, and include known physical variables—such as substrate stiffness—to collect stress or force data. The use of TFM has led to significant findings about how cells interact with their environment. For example, the kinetics of actin retrograde flow at the leading edge has been linked to changes in traction stress (57). TFM has been instrumental in linking mechanical changes with molecular dynamics.

Cells must coordinate a number of complex processes in order to generate contractile forces to ultimately achieve cell movement. Nonmuscle myosin II is a molecular motor that generates force across the actin cytoskeleton (3). Changes in myosin activity can impact cell contractility, as well as the maintenance and formation of SFs (3). Protrusive forces at the cell's leading edge are created by actin polymerization and coordination of the formation and break-

down of FA contacts at the front and rear of the cell also result in net cell movement (58, 59). The overall strength of the actin cytoskeleton and its ability to quickly remodel has also been hypothesized to contribute to the generation of global cell contractility, though the mechanosensitive proteins that may be involved in this process are not known. The link between actin remodeling and the generation of contractile forces became a topic of investigation in Chapter 2 (46).

1.4.2 Mechanical properties of the actin cytoskeleton

Single actin filaments have been polymerized in vitro and have been used to answer questions regarding the actin cytoskeleton's physical properties (60, 61), though only more recently have intact SFs been successfully isolated and tested by quantifying tensile strength (62). One of the most successful attempts at characterizing the mechanical properties of whole SFs was published in 2006 (63). Here single SFs were isolated from cultured smooth muscle cells and tensile tests were carried out in vitro (63), which provided valuable information about whole SFs as opposed to single actin filaments, whose mechanics are indeed different (60, 61, 64). SFs are anchored to the underlying extracellular matrix via integrin-based FAs, and due to this anchorage are thought to generate isometric tension along their length (6, 62).

The physical properties of actin SFs have been elucidated in SF severing experiments. In these experiments a laser is used to sever a SF and the SF retraction through the cytoplasm is tracked by time-lapse microscopy (48, 65, 66). By tracking sarcomere proteins like zyxin, α-actinin or myosin II, these groups were able to deduce forces from the cytosol and mechanical properties of the SFs. For example, Kumar et al. showed cut, retracting SFs experience viscous drag forces from the cytosplasm, and also exhibit viscoelastic properties (65). Physical properties of actin SFs have become valuable tools for studying the mechanics of single SFs.

1.4.3 Nonhomogeneous stress fiber sarcomere contraction

Although a long-held assumption has been that there is homogeneous contraction and shortening of SF sarcomeric units due to the presumed identical physical properties of sarcomeres in series (4-6), which was observed in isolated cardiac cells (67, 68), this has not been experimentally demonstrated in SFs in either stimulated or unstimulated conditions. For example, treatment with the serine/threonine phosphatase inhibitor Calyculin A to induce constitutively active myosin, causes sarcomeres nearest to the FA to shorten, while sarcomeres in the central portion of the same fiber lengthened (69). This is an example of regional compensatory changes in sarcomere lengths along the SF, but it is not known whether these changes in sarcomere lengths have a more localized level of compensation. Understanding the level of compensation could reveal details of actin remodeling and SF mechanics. Studying a highly localized mechanism of strain compensation during dynamic actin remodeling became the topic of investigation in the Chapin et al. 2012 publication, which is included here as Chapter 3 (70).

Nonhomogeneous simultaneous shortening and lengthening of sarcomeres was more recently reported in unstimulated live cells, as well as in SFs experiencing localized pulling force (71, 72). These random episodes of negative and positive strain in sarcomere length had no obvious links to changes in force, and this relationship is further described in the Appendix.

1.4.4 Using mathematical models to predict actin stress fiber dynamics

Due to challenges in imaging resolution, computational modeling has been used to study many variables in SF dynamics such as actin polymerization, physical properties, and myosin II activity. Along with the creation of these models have come certain conflicting assumptions about the properties of SFs, summarized in Table 1.1. For example, a long held assumption is that SFs have homogeneous density (73), while more recently there has been data to suggest actin density

and elasticity vary along the length of SFs (74, 75). The field has yet to come to a consensus on a core list of assumptions regarding the biological state of actin SF mechanics.

An additional problem in modeling actin SFs is relying too heavily on models of striated muscle fiber mechanics. Although actin SFs have been compared to the highly organized structure of striated muscle fiber, our own results challenge the assumption that their biophysical properties are shared. Specifically, actin SFs are far more dynamic than muscle fibers and are capable of sarcomere addition and deletion (our observations, (72)). A key contributor to the highly dynamic nature of the actin cytoskeleton is actin polymerization and depolymerization (76), which can occur at focal adhesions and along the lengths of SFs (77). We used our mathematical model to study whether SF sarcomere length fluctuations were due to elastic properties of the SF and myosin contractility, and whether actin polymerization kinetics may be involved. This project is described here in Chapter 4.

1.5 Summary

Although the actin SF has been described in the literature for over 25 years, there is still much to be investigated regarding SF structural and mechanical dynamics in living cells. In the following chapters I investigate the mechanisms of actin reinforcement and repair, including the role of zyxin as a mechanosensing protein in a dynamic actin cytoskeleton. I also focus on spontaneously severing SFs in live cells to deduce molecular mechanisms present in the cytoskeleton. Lastly, the structure of the SF sarcomere is studied in the context of extremely dynamic localized strain events, as well as its ability for trans-sarcomeric lateral communication of strain across multiple sarcomeres in series. The answers to these questions will provide a more accurate picture of the kinds of forces actin SFs can experience in a live cell, and what proteins are involved in cytoskeleton maintenance and repair.

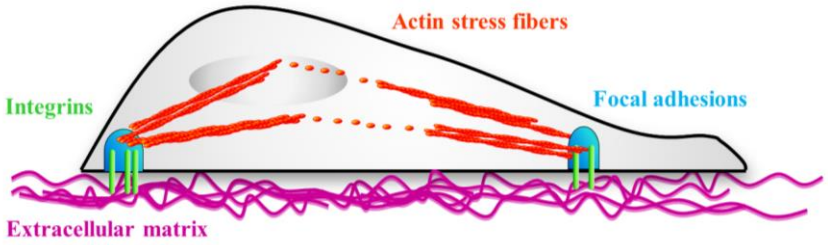

Figure 1.1: Actin stress fibers connect to focal adhesions. Actin stress fibers span across the cell and terminate at integrin-based focal adhesions. The cytoskeleton can sense and respond to the extracellular matrix through its transmembrane integrin proteins.

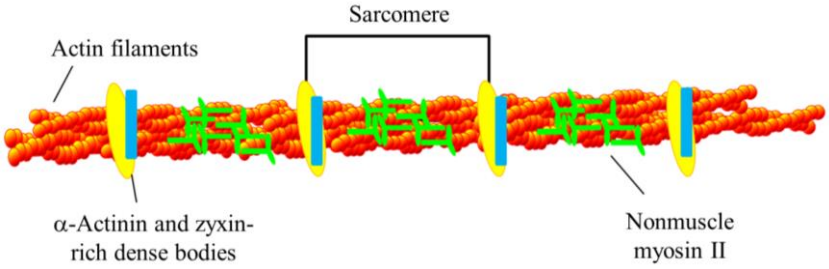

Figure 1.2: Stress fiber sarcomere. α-Actinin (yellow oval) and zyxin (blue line) are often used to identify the edges of individual stress fiber sarcomeres, while nonmuscle myosin II (green) is distributed along the actin within the unit and provides contractility.

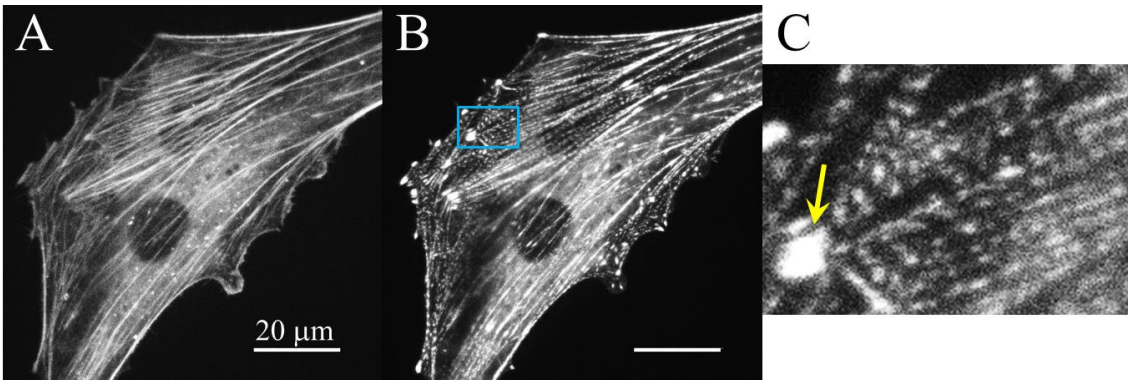

Figure 1.3: Zyxin localizes at focal adhesions and along actin stress fibers. Mouse embryonic fibroblast expressing actin-mCherry (A), and zyxin-GFP (B). Blue box indicates enlarged area shown in (C). Yellow arrow identifies a focal adhesion.

Figure 1.4: Zyxin protein and binding domains. Zyxin binds α-actinin and Mena/VASP, and contains two nuclear export sequences and three LIM domains at its C-terminus.

Table 1.1: Common assumptions made about actin stress fiber properties.

Assumption	**References**
Homogeneous actin density along their length	(48, 73, 78)
SF sarcomeres contract uniformly	(67, 68)
Local differences in actin density and elasticity	(74, 75)
Contract nonhomogeneously	(69, 71, 72, 79)
Anchored to integrin-based FAs	(80)
Anchored to substrate via FA attachments along their lengths	(48)
Tension is constant along the length of a SF	(80)

1.6 References

1. Ackbarow T, Sen D, Thaulow C, & Buehler MJ (2009) Alpha-helical protein networks are self-protective and flaw-tolerant. *PloS one* 4(6):e6015.

2. de Forges H, Bouissou A, & Perez F (2012) Interplay between microtubule dynamics and intracellular organization. *The international journal of biochemistry & cell biology* 44(2):266-274.

3. Lecuit T, Lenne PF, & Munro E (2011) Force generation, transmission, and integration during cell and tissue morphogenesis. *Annual review of cell and developmental biology* 27:157-184.

4. Weber K & Groeschel-Stewart U (1974) Antibody to myosin: the specific visualization of myosin-containing filaments in nonmuscle cells. *Proceedings of the National Academy of Sciences of the United States of America* 71(11):4561-4564.

5. Isenberg G, Rathke PC, Hulsmann N, Franke WW, & Wohlfarth-Bottermann KE (1976) Cytoplasmic actomyosin fibrils in tissue culture cells: direct proof of contractility by visualization of ATP-induced contraction in fibrils isolated by laser micro-beam dissection. *Cell and tissue research* 166(4):427-443.

6. Katoh K, Kano Y, Masuda M, Onishi H, & Fujiwara K (1998) Isolation and contraction of the stress fiber. *Molecular biology of the cell* 9(7):1919-1938.

7. Gabbiani G, Ryan GB, & Majne G (1971) Presence of modified fibroblasts in granulation tissue and their possible role in wound contraction. *Experientia* 27(5):549-550.

8. Hergott GJ, Sandig M, & Kalnins VI (1989) Cytoskeletal organization of migrating retinal pigment epithelial cells during wound healing in organ culture. *Cell motility and the cytoskeleton* 13(2):83-93.

9. Wong AJ, Pollard TD, & Herman IM (1983) Actin filament stress fibers in vascular endothelial cells in vivo. *Science* 219(4586):867-869.

10. Drenckhahn D & Wagner J (1986) Stress fibers in the splenic sinus endothelium in situ: molecular structure, relationship to the extracellular matrix, and contractility. *The Journal of cell biology* 102(5):1738-1747.

11. Dominguez R (2010) Structural insights into de novo actin polymerization. *Current opinion in structural biology* 20(2):217-225.

12. DeMali KA, Wennerberg K, & Burridge K (2003) Integrin signaling to the actin cytoskeleton. *Current opinion in cell biology* 15(5):572-582.

13. Geiger B, Spatz JP, & Bershadsky AD (2009) Environmental sensing through focal adhesions. *Nature reviews. Molecular cell biology* 10(1):21-33.

14. Geiger B & Bershadsky A (2001) Assembly and mechanosensory function of focal contacts. *Current opinion in cell biology* 13(5):584-592.

15. Myers KA, Applegate KT, Danuser G, Fischer RS, & Waterman CM (2011) Distinct ECM mechanosensing pathways regulate microtubule dynamics to control endothelial cell branching morphogenesis. *The Journal of cell biology* 192(2):321-334.

16. Effler JC, *et al.* (2006) Mitosis-specific mechanosensing and contractile-protein redistribution control cell shape. *Current biology : CB* 16(19):1962-1967.

17. Flitney EW, Kuczmarski ER, Adam SA, & Goldman RD (2009) Insights into the mechanical properties of epithelial cells: the effects of shear stress on the assembly and remodeling of keratin intermediate filaments. *FASEB journal : official publication of the Federation of American Societies for Experimental Biology* 23(7):2110-2119.

18. Helmke BP (2005) Molecular control of cytoskeletal mechanics by hemodynamic forces. *Physiology (Bethesda)* 20:43-53.

19. Helmke BP, Goldman RD, & Davies PF (2000) Rapid displacement of vimentin intermediate filaments in living endothelial cells exposed to flow. *Circulation research* 86(7):745-752.

20. Sivaramakrishnan S, DeGiulio JV, Lorand L, Goldman RD, & Ridge KM (2008) Micromechanical properties of keratin intermediate filament networks. *Proceedings of the National Academy of Sciences of the United States of America* 105(3):889-894.

21. Solon J, Levental I, Sengupta K, Georges PC, & Janmey PA (2007) Fibroblast adaptation and stiffness matching to soft elastic substrates. *Biophysical journal* 93(12):4453-4461.

22. Yoshigi M, Hoffman LM, Jensen CC, Yost HJ, & Beckerle MC (2005) Mechanical force mobilizes zyxin from focal adhesions to actin filaments and regulates cytoskeletal reinforcement. *The Journal of cell biology* 171(2):209-215.

23. Sawada Y & Sheetz MP (2002) Force transduction by Triton cytoskeletons. *The Journal of cell biology* 156(4):609-615.

24. Baneyx G, Baugh L, & Vogel V (2002) Fibronectin extension and unfolding within cell matrix fibrils controlled by cytoskeletal tension. *Proceedings of the National Academy of Sciences of the United States of America* 99(8):5139-5143.

25. Sawada Y, *et al.* (2006) Force sensing by mechanical extension of the Src family kinase substrate p130Cas. *Cell* 127(5):1015-1026.

26. del Rio A, *et al.* (2009) Stretching single talin rod molecules activates vinculin binding. *Science* 323(5914):638-641.

27. Johnson CP, Tang HY, Carag C, Speicher DW, & Discher DE (2007) Forced unfolding of proteins within cells. *Science* 317(5838):663-666.

28. Redden RA & Doolin EJ (2006) Complementary roles of microtubules and microfilaments in the lung fibroblast-mediated contraction of collagen gels: Dynamics and the influence of cell density. *In vitro cellular & developmental biology. Animal* 42(3-4):70-74.

29. Stamenovic D, Mijailovich SM, Tolic-Norrelykke IM, Chen J, & Wang N (2002) Cell prestress. II. Contribution of microtubules. *American journal of physiology. Cell physiology* 282(3):C617-624.

30. Sokolova AV, *et al.* (2006) Monitoring intermediate filament assembly by small-angle x-ray scattering reveals the molecular architecture of assembly intermediates. *Proceedings of the National Academy of Sciences of the United States of America* 103(44):16206-16211.

31. Beckerle MC (1986) Identification of a new protein localized at sites of cell-substrate adhesion. *The Journal of cell biology* 103(5):1679-1687.

32. Beckerle MC (1997) Zyxin: zinc fingers at sites of cell adhesion. *BioEssays : news and reviews in molecular, cellular and developmental biology* 19(11):949-957.

33. Kadrmas JL & Beckerle MC (2004) The LIM domain: from the cytoskeleton to the nucleus. *Nature reviews. Molecular cell biology* 5(11):920-931.

34. Hirata H, Tatsumi H, & Sokabe M (2008) Mechanical forces facilitate actin polymerization at focal adhesions in a zyxin-dependent manner. *Journal of cell science* 121(Pt 17):2795-2804.

35. Hoffman LM, Jensen CC, Chaturvedi A, Yoshigi M, & Beckerle MC (2012) Stretch-induced actin remodeling requires targeting of zyxin to stress fibers and recruitment of actin regulators. *Molecular biology of the cell*.

36. Bear JE & Gertler FB (2009) Ena/VASP: towards resolving a pointed controversy at the barbed end. *Journal of cell science* 122(Pt 12):1947-1953.

37. Drees B, *et al.* (2000) Characterization of the interaction between zyxin and members of the Ena/vasodilator-stimulated phosphoprotein family of proteins. *The Journal of biological chemistry* 275(29):22503-22511.

38. Endlich N, Otey CA, Kriz W, & Endlich K (2007) Movement of stress fibers away from focal adhesions identifies focal adhesions as sites of stress fiber assembly in stationary cells. *Cell motility and the cytoskeleton* 64(12):966-976.

39. Guo WH & Wang YL (2007) Retrograde fluxes of focal adhesion proteins in response to cell migration and mechanical signals. *Molecular biology of the cell* 18(11):4519-4527.

40. Hotulainen P & Lappalainen P (2006) Stress fibers are generated by two distinct actin assembly mechanisms in motile cells. *The Journal of cell biology* 173(3):383-394.

41. Crawford AW, Michelsen JW, & Beckerle MC (1992) An interaction between zyxin and alpha-actinin. *The Journal of cell biology* 116(6):1381-1393.

42. Liu J, Taylor DW, & Taylor KA (2004) A 3-D reconstruction of smooth muscle alpha-actinin by CryoEm reveals two different conformations at the actin-binding region. *Journal of molecular biology* 338(1):115-125.

43. Taylor KA, Taylor DW, & Schachat F (2000) Isoforms of alpha-actinin from cardiac, smooth, and skeletal muscle form polar arrays of actin filaments. *The Journal of cell biology* 149(3):635-646.

44. Vallenius T, Luukko K, & Makela TP (2000) CLP-36 PDZ-LIM protein associates with nonmuscle alpha-actinin-1 and alpha-actinin-4. *The Journal of biological chemistry* 275(15):11100-11105.

45. Sen S, Dong M, & Kumar S (2009) Isoform-specific contributions of alpha-actinin to glioma cell mechanobiology. *PloS one* 4(12):e8427.

46. Smith MA, *et al.* (2010) A zyxin-mediated mechanism for actin stress fiber maintenance and repair. *Developmental cell* 19(3):365-376.

47. Hoffman LM, *et al.* (2003) Targeted disruption of the murine zyxin gene. *Molecular and cellular biology* 23(1):70-79.

48. Colombelli J, *et al.* (2009) Mechanosensing in actin stress fibers revealed by a close correlation between force and protein localization. *Journal of cell science* 122(Pt 10):1665-1679.

49. Harris AK, Wild P, & Stopak D (1980) Silicone rubber substrata: a new wrinkle in the study of cell locomotion. *Science* 208(4440):177-179.

50. Dembo M, Oliver T, Ishihara A, & Jacobson K (1996) Imaging the traction stresses exerted by locomoting cells with the elastic substratum method. *Biophysical journal* 70(4):2008-2022.

51. Lee J, Leonard M, Oliver T, Ishihara A, & Jacobson K (1994) Traction forces generated by locomoting keratocytes. *The Journal of cell biology* 127(6 Pt 2):1957-1964.

52. Oliver T, Jacobson K, & Dembo M (1998) Design and use of substrata to measure traction forces exerted by cultured cells. *Methods in enzymology* 298:497-521.

53. Burton K, Park JH, & Taylor DL (1999) Keratocytes generate traction forces in two phases. *Molecular biology of the cell* 10(11):3745-3769.

54. Galbraith CG & Sheetz MP (1997) A micromachined device provides a new bend on fibroblast traction forces. *Proceedings of the National Academy of Sciences of the United States of America* 94(17):9114-9118.

55. Wang N, Ostuni E, Whitesides GM, & Ingber DE (2002) Micropatterning tractional forces in living cells. *Cell motility and the cytoskeleton* 52(2):97-106.

56. Wang YL & Pelham RJ, Jr. (1998) Preparation of a flexible, porous polyacrylamide substrate for mechanical studies of cultured cells. *Methods in enzymology* 298:489-496.

57. Gardel ML, *et al.* (2008) Traction stress in focal adhesions correlates biphasically with actin retrograde flow speed. *The Journal of cell biology* 183(6):999-1005.

58. Maheshwari G & Lauffenburger DA (1998) Deconstructing (and reconstructing) cell migration. *Microscopy research and technique* 43(5):358-368.

59. Pellegrin S & Mellor H (2007) Actin stress fibres. *Journal of cell science* 120(Pt 20):3491-3499.

60. Liu X & Pollack GH (2002) Mechanics of F-actin characterized with microfabricated cantilevers. *Biophysical journal* 83(5):2705-2715.

61. Tsuda Y, Yasutake H, Ishijima A, & Yanagida T (1996) Torsional rigidity of single actin filaments and actin-actin bond breaking force under torsion measured directly by in vitro micromanipulation. *Proceedings of the National Academy of Sciences of the United States of America* 93(23):12937-12942.

62. Stricker J, Falzone T, & Gardel ML (2010) Mechanics of the F-actin cytoskeleton. *Journal of biomechanics* 43(1):9-14.

63. Deguchi S, Ohashi T, & Sato M (2006) Tensile properties of single stress fibers isolated from cultured vascular smooth muscle cells. *Journal of biomechanics* 39(14):2603-2610.

64. Ingber DE (1997) Tensegrity: the architectural basis of cellular mechanotransduction. *Annual review of physiology* 59:575-599.

65. Kumar S, *et al.* (2006) Viscoelastic retraction of single living stress fibers and its impact on cell shape, cytoskeletal organization, and extracellular matrix mechanics. *Biophysical journal* 90(10):3762-3773.

66. Russell RJ, Xia SL, Dickinson RB, & Lele TP (2009) Sarcomere mechanics in capillary endothelial cells. *Biophysical journal* 97(6):1578-1585.

67. Iribe G, Helmes M, & Kohl P (2007) Force-length relations in isolated intact cardiomyocytes subjected to dynamic changes in mechanical load. *American journal of physiology. Heart and circulatory physiology* 292(3):H1487-1497.

68. Tarr M, Trank JW, & Goertz KK (1983) Effect of external force on relaxation kinetics in single frog atrial cardiac cells. *Circulation research* 52(2):161-169.

69. Peterson LJ, *et al.* (2004) Simultaneous stretching and contraction of stress fibers in vivo. *Molecular biology of the cell* 15(7):3497-3508.

70. Chapin LMB, E.; Smith, M.A.; Shiu Y.; Beckerle M.C. (2012) Lateral communication between stress fiber sarcomeres facilitates a local remodeling response. *Biophysical journal* 103(10).

71. Guolla L, Bertrand M, Haase K, & Pelling AE (2012) Force transduction and strain dynamics in actin stress fibres in response to nanonewton forces. *Journal of cell science* 125(Pt 3):603-613.

72. Russell B, Curtis MW, Koshman YE, & Samarel AM (2010) Mechanical stress-induced sarcomere assembly for cardiac muscle growth in length and width. *Journal of molecular and cellular cardiology* 48(5):817-823.

73. Satcher RL, Jr. & Dewey CF, Jr. (1996) Theoretical estimates of mechanical properties of the endothelial cell cytoskeleton. *Biophysical journal* 71(1):109-118.

74. Charras GT & Horton MA (2002) Determination of cellular strains by combined atomic force microscopy and finite element modeling. *Biophysical journal* 83(2):858-879.

75. Haga H, *et al.* (2000) Elasticity mapping of living fibroblasts by AFM and immunofluorescence observation of the cytoskeleton. *Ultramicroscopy* 82(1-4):253-258.

76. Pollard TD (1986) Rate constants for the reactions of ATP- and ADP-actin with the ends of actin filaments. *The Journal of cell biology* 103(6 Pt 2):2747-2754.

77. Turnacioglu KK, Sanger JW, & Sanger JM (1998) Sites of monomeric actin incorporation in living PtK2 and REF-52 cells. *Cell motility and the cytoskeleton* 40(1):59-70.

78. Cramer LP, Siebert M, & Mitchison TJ (1997) Identification of novel graded polarity actin filament bundles in locomoting heart fibroblasts: implications for the generation of motile force. *The Journal of cell biology* 136(6):1287-1305.

79. Besser AS, U. S. (2007) Coupling biochemistry and mechanics in cell adhesion: a model for inhomogeneous stress fiber contraction. *Journal of New Physics* 9.

80. Kirchenbuchler D, *et al.* (2010) Substrate, focal adhesions, and actin filaments: a mechanical unit with a weak spot for mechanosensitive proteins. *Journal of physics. Condensed matter : an Institute of Physics journal* 22(19):194109.

CHAPTER 2

A ZYXIN-MEDIATED MECHANISM FOR ACTIN STRESS FIBER MAINTENANCE AND REPAIR

My specific contributions to this manuscript included transfecting live cells with fluorescently-labeled proteins and live cell imaging. I developed a method of image analysis as a journal, a file of sequential image analysis commands, for MetaMorph, an image analysis program, which allowed us to measure intensity data in identical regions for two separate image stacks. This approach improved accuracy and efficiency of data collection. I also performed traction force microscopy to see whether zyxin -/- cells or zyxin -/- cells expressing zyxin-GFP were able to generate greater traction forces (Figure 3H and Supplemental Figure S2). This contribution included image acquisition, traction stress analysis, and data presentation. Lastly, I completed a second round of analysis of Margaret Gardel's traction force data to obtain traction strain data for the "Post SF strain event" in Figure 2H.

Reprinted with permission from *Developmental Cell* editor Daniel Wainstock.
Smith M. A., E. Blankman, M. L. Gardel, L. C. Luettjohann, C. M. Waterman, and M. C. Beckerle. 2010 A zyxin-mediated mechanism for actin stress fiber maintenance and repair. *Developmental Cell* 19:365-376.

A Zyxin-Mediated Mechanism for Actin Stress Fiber Maintenance and Repair

Mark A. Smith,[1] Elizabeth Blankman,[1] Margaret L. Gardel,[2] Laura Luettjohann,[1] Clare M. Waterman,[3,4,*] and Mary C. Beckerle[1,4,*]
[1]Departments of Biology and Oncological Sciences, Huntsman Cancer Institute, University of Utah, Salt Lake City, UT 84112, USA
[2]Department of Physics, University of Chicago, Chicago, IL 60637, USA
[3]Cell Biology and Physiology Center, National Heart, Lung and Blood Institute, National Institutes of Health, Bethesda, MD 30105, USA
[4]These authors contributed equally to this work
*Correspondence: watermancm@nhlbi.nih.gov (C.M.W.), mary.beckerle@hci.utah.edu (M.C.B.)
DOI 10.1016/j.devcel.2010.08.008

SUMMARY

To maintain mechanical homeostasis, cells must recognize and respond to changes in cytoskeletal integrity. By imaging live cells expressing fluorescently tagged cytoskeletal proteins, we observed that actin stress fibers undergo local, acute, force-induced elongation and thinning events that compromise their stress transmission function, followed by stress fiber repair that restores this capability. The LIM protein zyxin rapidly accumulates at sites of strain-induced stress fiber damage and is essential for stress fiber repair and generation of traction force. Zyxin promotes recruitment of the actin regulatory proteins α-actinin and VASP to compromised stress fiber zones. α-Actinin plays a critical role in restoration of actin integrity at sites of local stress fiber damage, whereas both α-actinin and VASP independently contribute to limiting stress fiber elongation at strain sites, thus promoting stabilization of the stress fiber. Our findings demonstrate a mechanism for rapid repair and maintenance of the structural integrity of the actin cytoskeleton.

INTRODUCTION

Organized tissues respond adaptively to mechanical changes in their environment. For example, muscle tissue undergoes a hypertrophic response to increased mechanical load, and an atrophic response to lack of load (Sadoshima and Izumo, 1997). Although much less well understood, nonmuscle cells are also acutely sensitive to mechanical changes in their surroundings. The ability to sense and respond to changes in mechanical input is essential for many developmental processes (Wozniak and Chen, 2009) including tissue morphogenesis (Hutson et al., 2003), proliferation (Iwamoto et al., 2000; Peyton et al., 2006) and differentiation (Farge, 2003). Experimental disruption of intracellular force generation impedes a range of functions, including directed migration (Lo et al., 2004), cell sorting in tissues (Krieg et al., 2008), and stem cell lineage commitment (McBeath et al., 2004). Moreover, misregulation of the ability to sense and respond to mechanical cues is involved in many disease processes including pathological cardiac hypertrophy (Heydemann and McNally, 2007; Palmer, 2005) and tumor metastasis (Clark et al., 2000; Paszek and Weaver, 2004). Consequently, understanding how cells sense mechanical cues within a physically diverse environment and respond by balancing forces and mechanical properties has emerged as a key to understanding how tissue homeostasis is maintained.

The actomyosin cytoskeleton is the major mediator of cellular mechanical properties. Actin filaments in nonmuscle cells form linear contractile bundles of filaments called stress fibers (SFs) that are induced to assemble by activation of Rho, which promotes myosin-dependent contractility (Chrzanowska-Wodnicka and Burridge, 1996). SFs are common in cells cultured in vitro and are also found in vivo where they are induced to assemble when cells are exposed to mechanical stress, as in the vasculature (Byers et al., 1984). SFs possess a periodic distribution of α-actinin and myosin II, reminiscent of, although less organized than, the sarcomeric banding pattern in muscle (Langanger et al., 1986; Lazarides and Burridge, 1975). SFs terminate at extracellular attachment sites, such as focal adhesions (FAs), where they are linked via a network of proteins to integrins, transmembrane receptors that bind extracellular matrix (ECM) (Burridge et al., 1988). This transmembrane linkage enables bidirectional communication of mechanical information for sensing, generating, and responding to physical cues. For example, actomyosin-dependent contractile forces generated by SFs are transmitted to the extracellular environment (Harris et al., 1980; Lauffenburger and Horwitz, 1996; Wang et al., 1993), a process critical for cell motility, extracellular matrix remodeling, and tissue morphogenesis. Reciprocally, externally applied strains and stresses promote SF thickening and reorientation (Iba and Sumpio, 1991; Yoshigi et al., 2005). Although it is well established that the actomyosin cytoskeleton is essential for physical cell behavior and mechanosensing, and responds dynamically to a variety of biochemical signals, little is known about the molecular mechanism by which SFs sense or respond to mechanical perturbations.

The LIM protein, zyxin, is responsive to mechanical cues. Zyxin localizes to SFs and is required for SF thickening in response to cyclic cell stretch (Yoshigi et al., 2005). The K_{off} of FA-localized zyxin is increased when the associated SF is severed by laser surgery (Lele et al., 2006). Retrograde fluxes

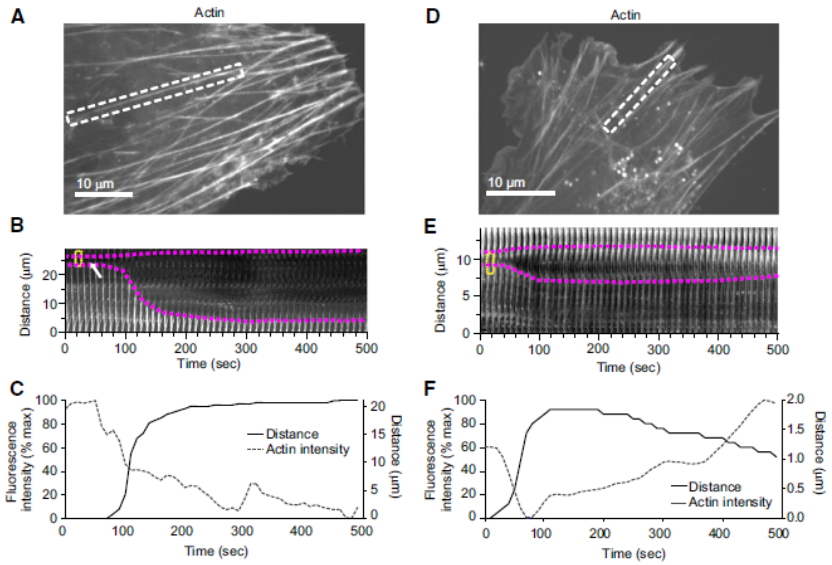

Figure 1. SFs Display the Capacity to Repair Local Damage

The micrographs and kymographs are of actin-mCherry in mouse fibroblasts. For this and subsequent figures, plots below kymographs show normalized average fluorescence intensity in the dotted yellow box over time and distance change between the fiducials highlighted with magenta dots (see Movie S1).

(A) Stress fiber in dashed white box undergoes catastrophic break.

(B) Kymograph showing SF highlighted in (A) that thins, breaks, and recoils. White arrow shows region of SF thinning prior to the break.

(C) Intensity and distance plot of (B) catastrophic SF break. Lack of rise in actin fluorescence intensity after ~100 s indicates a catastrophic break.

(D) Stress fiber in dashed white box undergoes strain followed by repair.

(E) Kymograph showing SF highlighted in (D) undergoes thinning, elongation, and then repair.

(F) Intensity and distance graph of SF thinning, elongation, and repair. Rise in actin fluorescence intensity after ~100 s indicates SF repair.

of zyxin at FAs are abated in response to decreased myosin contractility and increase in response to applied force (Guo and Wang, 2007). Finally, zyxin has been shown to be recruited to substrate anchor points on laser severed SFs (Colombelli et al., 2009), and to reversibly accumulate on SFs and FAs in response to mechanical perturbation (Colombelli et al., 2009). However, little is known about what role zyxin's mechanical responsiveness plays in cells in the absence of externally applied stress. Furthermore, the mechanism by which zyxin drives functional adaptation and remodeling of the actin cytoskeleton remains uncharacterized.

Here, we have dissected a molecular mechanism by which actin SFs in nonmuscle cells maintain their integrity in response to acute mechanical failure. We observed that SFs undergo local, acute, stress-induced elongation and thinning events. Some of these events are repaired, while others progress to catastrophic breaks. These strain events are triggered by stress increases in the SF and they compromise SF force transmission function. Zyxin and its partners accumulate at SF strain sites and facilitate their repair. In cells lacking zyxin the strain site repair capacity is compromised, and as a result of the diminished structural integrity of SFs, whole cell force transmission is attenuated. Our findings demonstrate a SF-resident system for rapid repair and maintenance of the actin cytoskeleton.

RESULTS

Actin Stress Fibers Exhibit Acute, Local Thinning and Elongation, Leading to Either Catastrophic Breakage or Repair

To understand how SFs in living cells maintain their physical integrity, we performed time-lapse imaging of mouse fibroblasts expressing actin-mCherry and looked for evidence of SF remodeling. This revealed spontaneous catastrophic breakage of SFs that occurred at a frequency of 0.03 ± 0.01 breaks/minute/cell (n = 83 cells, 1100 min of observation). Prior to a break, SFs displayed elongation and thinning within a localized region that subsequently became the breakage site. The elongation/thinning phase persisted for 10–60 s. Immediately following development of a distinct discontinuity, the flanking regions of the SF underwent rapid retraction, and we observed a persistent loss of actin fluorescence along the previous path of the SF indicating catastrophic breakage (Figures 1A–1C; Movie S1 available online), reminiscent of myosin II-dependent SF elastic recoil after laser severing (Kumar et al., 2006).

We also noted that for many sites of acute, local SF elongation and thinning, instead of progressing to a catastrophic break, the strain site exhibited spontaneous restoration of actin integrity (Figures 1D–1F; Movie S1) providing the first indication of a mechanism for SF repair. We refer to this actin remodeling as

SF repair, since, as is described below, when the remodeling machinery is compromised, the incidence of SF breaks increases. Local, acute SF thinning, elongation, and restoration events arose spontaneously at a rate of 0.18 ± 0.03 events/minute/cell (n = 83 cells, 1100 min of observation). Quantitative features of these events are summarized in Table S1. Following SF thinning, the mean recovery rate of actin fluorescence signal within the strain site was 1.20 ± 0.18 fluorescence intensity units/second (n = 10), resulting in recovery to 142.6% ± 12% (n = 11) of the original actin fluorescence signal during a 500 s analysis period. Kymograph analysis of fiducial marks flanking the strain site showed that the average maximum elongation distance was 2.5 ± 0.2 μm (n = 10), nearly twice the intersarcomeric SF banding distance which ranges from 0.4 to 1.75 μm (our observation; Peterson et al., 2004). Local SF elongation occurred at a rate of 4.0 ± 1.4 μm/min (n = 10). The half-time to cessation of elongation was 77 ± 6 s (n = 10). Actin fluorescence signal recovery typically occurred at a uniform rate across the strain site and was not accompanied by rejoining of the separated fiducial marks. This suggests that restoration occurred primarily by addition of new actin along the length of the residual thinned SF, as opposed to reversal of the elongation phase. Of SFs that experienced an acute, local elongation event, 82% recovered, while 18% progressed to a catastrophic break. These events are distinct from previously described internal SF elongations (Peterson et al., 2004), with 5- to 10-fold greater elongation length and >100-fold higher elongation velocities. Thus, our findings demonstrate that SFs undergo spontaneous, acute, local strain events that may or may not repair, providing evidence for a mechanism by which the majority of damaged SFs are repaired in situ.

Zyxin Is Recruited to Sites of Stress Fiber Strain

How are acute, local SF strain events detected, stabilized, and restored? Previous findings showing that the LIM protein zyxin responds to mechanical stress (Hoffman et al., 2006; Yoshigi et al., 2005) led us to consider a role for zyxin in repair of acute, local SF strain. Consistent with this hypothesis, in cells expressing zyxin-GFP and actin-mCherry, we observed that in addition to normal localization at FAs and periodic punctae along SFs, zyxin rapidly and robustly accumulated at sites of acute, local SF strain (Figures 2A–2C; Movies S2 and S3). Analysis of kymographs (Figure 2B) revealed that local SF strain immediately preceded zyxin accumulation, which in turn preceded restoration of actin at the strain site (Figure 2C). The average t1/2 for zyxin accumulation at SF strain sites was 28.6 ± 3.7 s (n = 24). From its maximum intensity, zyxin associated with the strain site displayed a half-life of 112 ± 12 s (n = 10), leaving the SF more slowly than it accumulated. The dissociation rate of zyxin from sites of acute SF damage is an order of magnitude slower than the dissociation rate of zyxin we measured by FRAP from stable SF regions (t1/2 = 13 ± 1.5 s [n = 61]) (Figures S1A–S1C). Thus, acute, local SF strain elicits rapid zyxin recruitment through a novel mode of zyxin/SF interaction.

Mechanical Stimulation Triggers Local Accumulation of Zyxin at Sites of Stress Fiber Strain

The accumulation of zyxin that we observed at sites of acute SF strain, coupled with the finding that zyxin exhibits force-sensitive binding to cellular structures (Lele et al., 2006; Yoshigi et al., 2005) led us to hypothesize that acute, local zyxin accumulation on a SF could be induced by physical perturbation. To test this, we grew zyxin-GFP-expressing cells on fibronectin-coupled elastic polyacrylamide substrates (Beningo et al., 2002) and then prodded the cell cortex with a polished micropipette (Figure 2D; Movie S4). At the site of cortical deformation, we observed SF deflection and concomitant rapid, local accumulation of zyxin-GFP on the SF. This finding supports the hypothesis that direct application of mechanical force is sufficient to initiate rapid zyxin accumulation to regions of local SF strain.

Stress Fiber Strain Events Do Not Generate New Focal Adhesions

It is possible that the rapid accumulation of zyxin to sites of acute SF strain could represent the formation of new FAs. Formation of a FA would be indicated by accumulation of the FA protein vinculin (Zamir and Geiger, 2001) and local induction of stress transmission to the substrate (Beningo et al., 2002; Gardel et al., 2008). Observation of cells coexpressing zyxin-GFP and vinculin-mCherry revealed lack of coordinate vinculin accumulation with zyxin at sites of SF strain (Figures 2E and 2F). To determine if local zyxin accumulation at SF strain sites was correlated with stress transmission to the substrate, we plated cells expressing zyxin-GFP on fiducial-embedded polyacrylamide substrates and performed high-resolution traction-force microscopy (Sabass et al., 2008). Although we detected extensive substrate strain at FAs, changes in traction force were not observed at zyxin-rich SF strain sites (Figure 2G; Movie S5). Many sites of rapid zyxin accumulation underwent lateral movement that was coordinated with movement of the SF, providing further evidence that these sites were not substrate bound. These data show that local, rapid zyxin accumulation at strain sites is not associated with formation of new FAs, but rather represents targeted accumulation of zyxin on a SF.

Stress Fiber Strain Events Are Preceded by Elevated Contractility and Reduce Traction Force

What induces SF strain events in steady state cells, and what is the mechanical output of these events? Since mechanical perturbation is sufficient to induce strain events, we wanted to test whether SFs exerted increased contractile force prior to the strain event. To test this, we used traction force microscopy to simultaneously measure local zyxin-GFP accumulation on a SF and relative substrate traction at the FA where the associated SF terminates (Figures 2G–2I; Movie S5). We compared local substrate traction forces at FAs during periods of quiescence and during acute, local SF elongation accompanied by rapid accumulation of zyxin. During quiescent periods, substrate traction force was relatively stable during a 30 s measurement interval (Figure 2H). In contrast, immediately prior to periods of rapid SF elongation and zyxin accumulation, substrate traction force at the site of associated FAs increased by an average of 15% (Figure 2H). This indicates that increasing SF contractility precedes the development of SF strain events.

We reasoned that acute, local SF strain may reduce the transmission of force through the cytoskeleton to the ECM. A zyxin-mediated repair process could restore this capacity. Immediately after periods of rapid SF elongation and zyxin

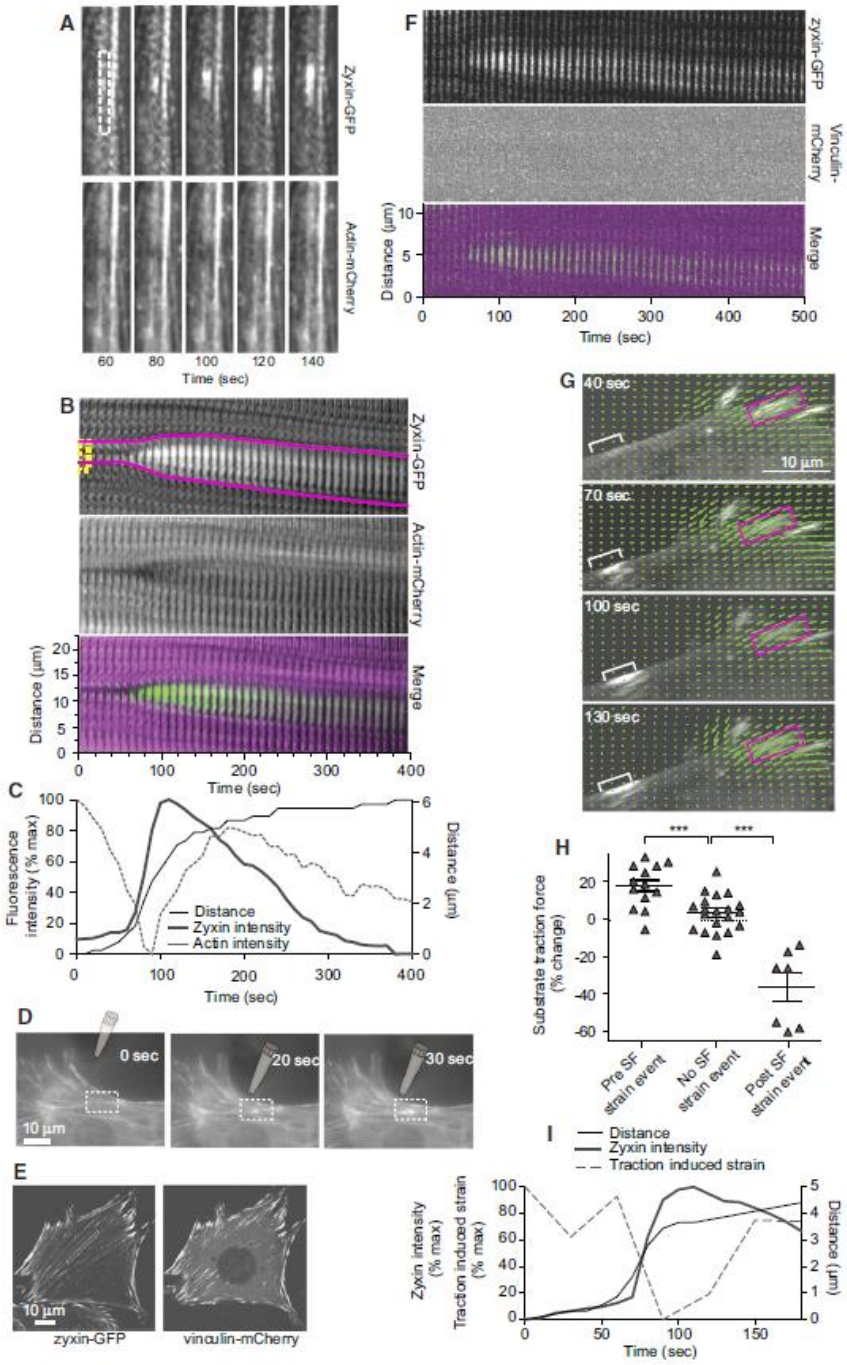

Figure 2. Zyxin Is Recruited to Sites of SF Strain

(A) Time-lapse series of zyxin-GFP, and actin-mCherry shows zyxin accumulation at a site of SF damage (see Movies S2 and S3 as an additional example).
(B) Kymograph from the dashed white box in (A) showing rapid zyxin accumulation at a region of SF strain. For merge, zyxin is green, actin is magenta.
(C) Plot from (B) of intensity over time and distance change between the fiducials highlighted with magenta lines.
(D) Images of zyxin-GFP expressing cell prodded by a micropipette. Zyxin-GFP accumulates at the site of SF inflection (white box) (see Movie S4).

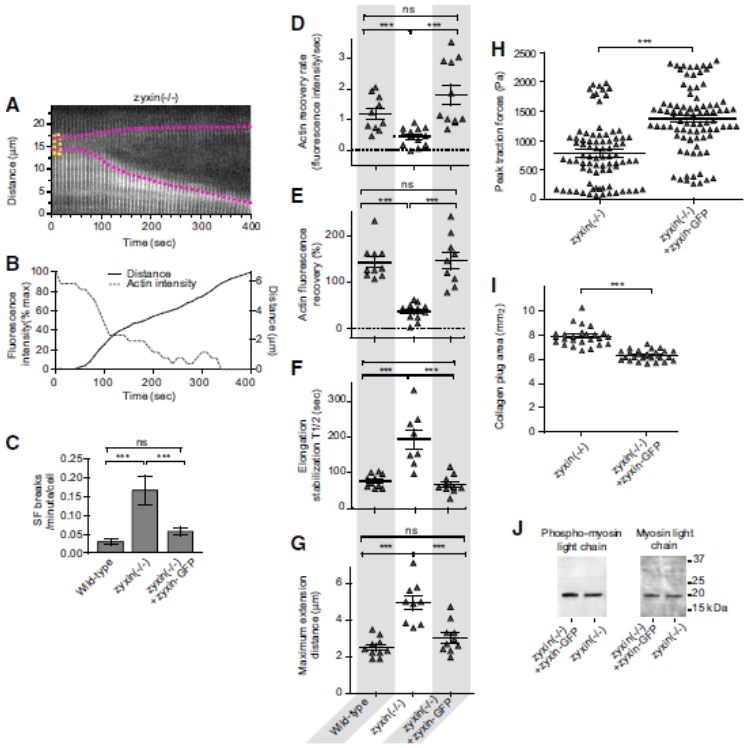

Figure 3. Stress Fiber Strain Sites Fail to Stabilize in *zyxin*$^{-/-}$ Cells

(A) Kymograph of actin-mCherry expressed in a *zyxin*$^{-/-}$ cell showing a SF strain event that fails to recover (see Movie S6).

(B) Plot from (A) of intensity over time and distance change between the fiducials highlighted with magenta dots. Lack of rise in actin fluorescence intensity and increasing distance between fiducials after ~100 s indicates lack of SF repair.

(C) Catastrophic SF break frequency in wild-type (n = 83 cells), *zyxin*$^{-/-}$ (n = 57 cells) and *zyxin*$^{-/-}$ +zyxin-GFP (n = 172 cells).

(D) Wild-type (n = 10) and rescued (n = 13) cells show enhanced rate of actin recovery at SF strain sites when compared with *zyxin*$^{-/-}$ cells (n = 13) ($p = 0.0002$).

(E) Wild-type (n = 10 events) and rescued (n = 13 events) cells show enhanced net actin recovery at SF strain sites when compared with *zyxin*$^{-/-}$ cells (n = 13 events) ($p < 0.0001$).

(F) Wild-type (n = 10 events) and rescued (n = 10 events) cells show decreased half-time to the stabilization at SF strain sites when compared with *zyxin*$^{-/-}$ cells (n = 8 events) ($p = 0.0002$).

(G) Wild-type (n = 10 events) and rescued (n = 10 events) cells show decreased maximum elongation at SF strain sites when compared with *zyxin*$^{-/-}$ cells (n = 9 events) ($p = 0.0006$).

(H) *zyxin*$^{-/-}$ cells (n = 80) showed decreased peak traction forces when compared with *zyxin*$^{-/-}$ +zyxin-GFP cells (n = 89) ($p < 0.0001$) (see also Figure S2).

(I) *zyxin*$^{-/-}$ cells (n = 25) showed decreased collagen plug contraction when compared with *zyxin*$^{-/-}$ +zyxin-GFP cells (n = 28) ($p < 0.0001$).

(J) Western blot analysis showing unchanged myosin light chain ser19 phosphorylation levels in *zyxin*$^{-/-}$ and *zyxin*$^{-/-}$ +zyxin-GFP cells (n = 3).

Plots (D–I) show mean ± SEM.

accumulation, substrate traction force at the site of associated FAs decreased by an average of 40% (Figure 2H). Kinetic analysis showed that as SF strain site length stabilized and zyxin intensity plateaued, substrate traction forces at the FA were restored (Figure 2I). We conclude that SFs undergo acute, local strain, in response to escalating stress, causing a reduction in their ability to transmit force through their associated FA to the ECM. Recruitment of zyxin to SF strain sites accompanies restoration of the cell's capacity to exert traction on the substrate.

Zyxin Null Cells Exhibit Impaired Stress Fiber Repair and Increased Stress Fiber Breakage

To determine the requirement for zyxin in the SF repair process, we characterized the SF break frequency and the recovery of actin at acute, local SF strain sites in fibroblasts derived from *zyxin*$^{-/-}$ mice (Hoffman et al., 2006). We found that *zyxin*$^{-/-}$ cells displayed a profound deficiency in their ability to restore actin levels at acute SF strain sites (Figures 3A and 3B; Movie S6) and exhibited a greater than 5-fold increase in the frequency of catastrophic SF breaks when compared with wild-type cells (Figure 3C). To confirm the increased SF breakage was directly due to the absence of zyxin, we expressed full-length zyxin-GFP in *zyxin*$^{-/-}$ cells and restored wild-type behavior (Figures 3C and S1D). Consistent with the increase in catastrophic SF breaks, *zyxin*$^{-/-}$ cells exhibited a significant drop in the rate and percentage of actin-mCherry fluorescence recovery at the strain site when compared with *zyxin*$^{-/-}$ cells expressing zyxin-GFP (Figures 3D and 3E). In addition, the half-time to cessation of elongation and the extent of SF strain were 2- to 3-fold higher in cells lacking zyxin, as compared with *zyxin*$^{-/-}$ cells expressing

(E) Micrographs showing zyxin-GFP and vinculin-mCherry expression.

(F) Kymograph made from the dashed white box in (E) showing no vinculin accumulation at the site of zyxin accumulation.

(G) Traction microscopy of zyxin-GFP expressing cell. Green vectors show the interpolated traction-induced strain map of bead positions relative to their cell-free positions (see Movie S5). Bracket highlights the local accumulation of zyxin-GFP on the SF that terminates at the FA outlined by the magenta box.

(H) When compared with quiescent SFs (n = 20), SF strain events are preceded by a net increase in traction force (n = 13) and are followed by a net decline in traction force (n = 7). Error bars show SEM.

(I) Normalized traction-induced strain integrated within the region containing the FA (magenta boxes in E). When the attached SF elongates (plotted as distance) and zyxin accumulates (normalized fluorescence intensity in the bracketed region in E), there is an acute drop in traction-induced strain at the FA.

zyxin-GFP (Figures 3F and 3G). These data demonstrate that zyxin is critical for maintaining SF integrity by detecting damage and mediating rapid SF repair.

Zyxin Null Cells Exhibit Decreased Force Generation Capacity

We postulated that zyxin's contribution to SF maintenance would be critical for the SF's ability to generate and transmit force to the substrate. By comparing whole-cell traction forces in *zyxin*$^{-/-}$ cells, with and without zyxin-GFP rescue, we found that peak forces transmitted to the substrate were significantly decreased in cells lacking zyxin (Figures 3H and S2). Collagen plug contraction assays (Grinnell, 2000) confirmed that *zyxin*$^{-/-}$ cells display compromised capacity to exert force on the extracellular matrix (Figure 3I). Since substrate adhesion is not diminished in *zyxin*$^{-/-}$ cells (Hoffman et al., 2006), zyxin's impact on force generation capacity could be due to a role in maintaining actin cytoskeletal integrity, influence on actomyosin-dependent contractility, or both. The diminished SF repair and enhanced SF break frequency observed in *zyxin*$^{-/-}$ cells supports the view that zyxin contributes directly to maintenance of cytoskeletal integrity. We detected no zyxin-dependent difference in global myosin light chain phosphorylation (Figure 3J), a surrogate marker for actomyosin-dependent contractility.

Stress Fiber Strain Sites Are Rich in Free Barbed Actin Filament Ends and Accumulate α-Actinin and VASP in a Zyxin-Dependent Manner

How does zyxin accumulation mediate restoration of actin and SF integrity in response to an acute SF strain event? The rapid restoration of SF integrity at SF strain sites raised the possibility that the strain site was rich in uncapped actin filament barbed ends that could be extended by actin polymerization. To test this hypothesis, we performed actin barbed end assays on live cells experiencing strain events. We observed that rhodamine-labeled G-actin was rapidly recruited at SF strain sites (Figure 4A; Movie S7) indicating the presence of actin barbed ends at these sites and displaying a striking correspondence with the zyxin-rich region.

Zyxin interacts directly with the F-actin crosslinking protein α-actinin (Crawford et al., 1992; Reinhard et al., 1999), as well as with the actin polymerization regulator, and actin barbed end binding protein VASP (Drees et al., 2000; Niebuhr et al., 1997). To determine whether α-actinin and/or VASP cooperate with zyxin in the SF restoration response, we examined their dynamic behaviors during acute SF strain and restoration using time-lapse imaging of fluorescently tagged zyxin and α-actinin or VASP.

α-Actinin was recruited to sites of acute SF strain with kinetics that lagged zyxin accumulation (Figures 4B–4D; Movie S8). To test whether α-actinin is dependent on zyxin for accumulation at SF strain zones, we examined the ability of α-actinin to accumulate on SFs in *zyxin*$^{-/-}$ cells. In the absence of zyxin, α-actinin displayed a typical periodic distribution on SFs (Figure 4E), illustrating that zyxin is not essential for targeting α-actinin to these structures. However, rapid accumulation of α-actinin at zones of acute SF strain that did not immediately progress to breakage was profoundly compromised in cells lacking zyxin and was restored in cells re-expressing zyxin-GFP (Figure 4F; Movie S8), demonstrating that zyxin is required, either directly or indirectly, for specific localized α-actinin recruitment to sites of acute SF strain.

In *zyxin*$^{-/-}$ cells reconstituted with zyxin-mCherry, VASP-GFP was recruited to SF strain sites with kinetics similar to that of zyxin (Figures 4D, 4G, and 4H; Movie S9) and localized to both SFs and FAs. Consistent with previous reports (Hoffman et al., 2006), VASP localization to FAs and SFs was compromised in *zyxin*$^{-/-}$ cells (Figure 4I). VASP recruitment to acute SF strain sites that did not immediately progress to breakage was also abolished in *zyxin*$^{-/-}$ cells, and restored by re-expression of zyxin-mCherry (Figure 4J; Movie S9). In pairwise comparison of the recruitment half-times, we observed that α-actinin lagged VASP by an average of 34 s ($n = 9$, $p < 0.05$) (Figure 4K). Together, these results indicate a requirement for zyxin in recruitment of the actin regulatory proteins α-actinin and VASP to sites of SF strain, and define a temporal ordering of recruitment with VASP and zyxin corecruited, followed by α-actinin.

Zyxin Recruitment to Acute Stress Fiber Strain Sites Is Not Dependent on Interactions with α-Actinin or VASP

To determine whether zyxin accumulation at SF strain sites depends on its ability to interact directly with either α-actinin or VASP, we generated GFP-tagged zyxins bearing mutations that disrupt interaction with either α-actinin or Ena/VASP family members, coexpressed them with actin-mApple in *zyxin*$^{-/-}$ cells, and imaged acute SF strain sites. To disrupt α-actinin binding to zyxin, we deleted the first 42 amino acids of zyxin to make zyxΔ1-42-GFP (Nix et al., 2001; Reinhard et al., 1999; Figure 5A). To disrupt zyxin binding to Ena/VASP family members, we mutated the phenylalanines to alanine in each of zyxin's four proline-rich (FPPP) sequences (ActA repeats) to make zyx4F > A-GFP (Drees et al., 2000; Figure 5A). Neither the FA nor SF localization of zyxin was perturbed by mutation of zyxin's α-actinin or Ena/VASP binding sites (Figure 5B). Moreover, rapid recruitment to acute SF strain sites occurred for both zyxΔ1-42-GFP (Figures 5C and 5D) and zyx4F > A-GFP (Figures 5E and 5F). Kinetic analysis revealed that zyxΔ1-42 recruitment was indistinguishable from recruitment of zyxin-GFP; however, zyx4F > A recruitment was slower (Figure 5G). These data suggest that zyxin does not depend on association with either α-actinin or Ena/VASP for localization to sites of acute SF strain. However, the rate of zyxin recruitment to SF strain sites may be increased through interaction with VASP.

α-Actinin and VASP Require Interaction with Zyxin for Recruitment to Acute Stress Fiber Strain Sites

To determine whether zyxin binding is required for localization of α-actinin or VASP to acute SF strain sites, we examined the subcellular localization of α-actinin-mCherry or VASP-mCherry in *zyxin*$^{-/-}$ cells re-expressing zyxΔ1-42-GFP or zyx4F > A-GFP to eliminate α-actinin or Ena/VASP binding, respectively. In *zyxin*$^{-/-}$ cells expressing zyxΔ1-42-GFP, α-actinin-mCherry localized to FAs and SFs (Figure 6A). However, α-actinin-mCherry failed to accumulate at sites of acute SF strain (Figures 6B–6D; cf. Figures 6B and 6C to Figures 4B and 4C). In *zyxin*$^{-/-}$ cells expressing zyx4F > A-GFP, VASP-mCherry did not localize to SFs or FAs (Figure 6E). VASP-mCherry recruitment to sites of acute SF strain was also greatly attenuated (Figures 6F–6H;

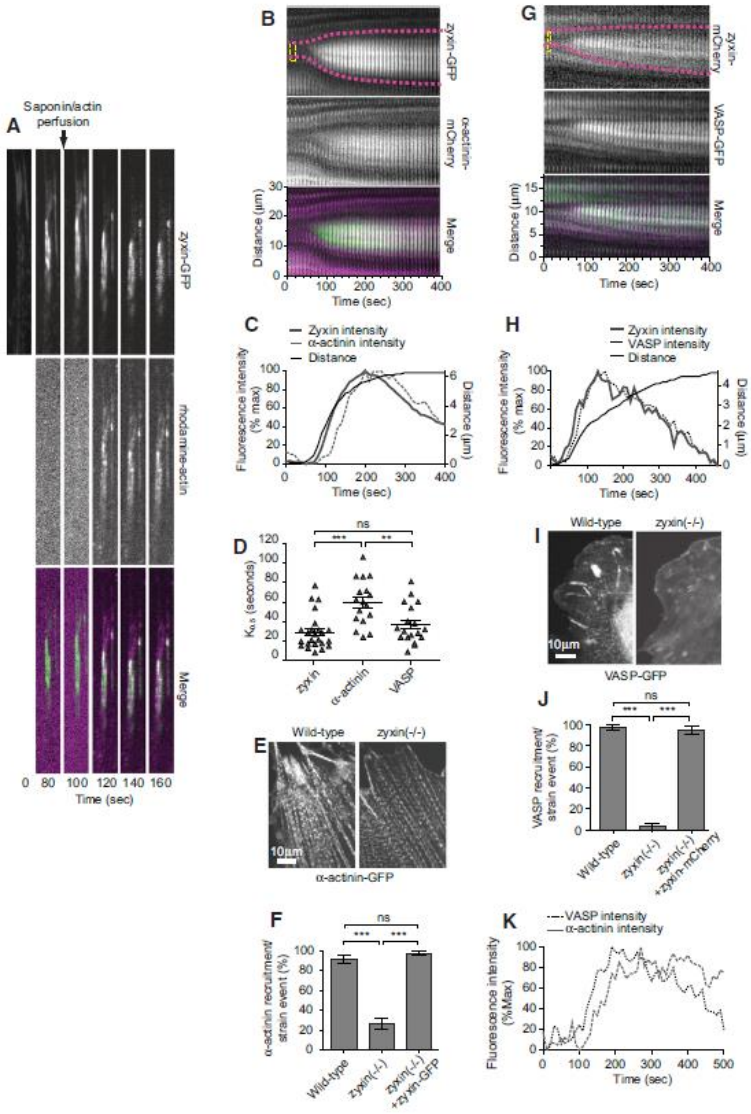

Figure 4. Stress Fiber Strain Sites Generate Free Actin Barbed Ends and Accumulate α-Actinin and VASP in a Zyxin-Dependent Manner

(A) Image sequence showing rhodamine-actin accumulation at SF strain sites (see Movie S7).

(B) Kymograph of zyxin-GFP and α-actinin-mCherry expressed in *zyxin*$^{-/-}$ cell. For merge, zyxin is green, α-actinin is magenta.

(C) Intensity and distance graph showing α-actinin accumulates at SF strain sites lagging zyxin accumulation (see Movie S8).

(D) Half-time of protein accumulation at SF strain sites shows α-actinin (n = 17) accumulation lags both zyxin (n = 24) (p = 0.0043) and VASP (n = 18) (p = 0.0133) (see also Figure S3).

(E) α-Actinin-GFP periodic distribution pattern on SF persists in *zyxin*$^{-/-}$ cells.

(F) *zyxin*$^{-/-}$ cells (n = 421) cells show a decreased percentage of α-actinin recruitment to SF strain sites when compared with wild-type (n = 233) and rescued (n = 364) cells (see Movie S8).

(G) Kymograph of VASP-GFP and zyxin-mCherry expressed in *zyxin*$^{-/-}$ cell. For merge, VASP is green, zyxin is magenta.

(H) Intensity and distance graph showing VASP accumulates at SF strain sites coincident with zyxin (see Movie S9).

(I) VASP fails to localize on SFs in *zyxin*$^{-/-}$ cells.

(J) *zyxin*$^{-/-}$ cells (n = 31) show decreased percentage of VASP recruitment to SF strain sites when compared with wild-type (n = 99) and rescued (n = 171) cells (see Movie S9).

(K) Intensity plot showing α-actinin accumulation lags VASP in a dual labeled cell. Data are shown as mean ± SEM.

compare Figures 6F and 6G with Figures 4G and 4H). Our results illustrate that compromising zyxin's ability to bind either α-actinin or VASP limits the capacity of these proteins to accumulate with zyxin at sites of local, acute SF strain, supporting the view that direct binding to zyxin contributes substantially to both α-actinin and VASP recruitment to SF strain sites.

α-Actinin and VASP Have Distinct Roles in the Stabilization of SF Strain Sites

Both α-actinin and VASP modulate actin organization and dynamics. Therefore, we tested whether the zyxin-dependent repair of acute SF strain sites required α-actinin or VASP recruitment to these sites. We examined SF strain and repair events by imaging actin-mCherry in both *zyxin*$^{-/-}$ cells expressing zyxin variants with compromised α-actinin or VASP binding functions. Quantification of actin-mCherry fluorescence at acute SF strain sites showed that expression of either zyxin-GFP or zyx4F > A-GFP in *zyxin*$^{-/-}$ cells restored both the rate and extent of actin recovery at strain sites to wild-type levels (Figures 7A and 7B). In contrast, actin recovery at SF strain sites was reduced in *zyxin*$^{-/-}$ cells whether or not they additionally expressed zyxΔ1-42-GFP (Figures 7A and 7B). Quantification of the time and distance of acute SF extension revealed that re-expression of wild-type zyxin-GFP in *zyxin*$^{-/-}$ cells was sufficient to reduce the extent of SF strain to wild-type levels, while SF strain was increased in *zyxin*$^{-/-}$ cells, whether or not they additionally expressed either zyxΔ1-42-GFP or zyx4F > A-GFP (Figures 7C and 7D). Thus, both α-actinin and VASP contribute to zyxin's ability to arrest acute, localized SF strain.

To determine how these proteins contribute to maintaining the overall integrity of actin SFs, we analyzed SF breakage frequency. This revealed that *zyxin*$^{-/-}$ cells had an increased frequency of SF breakage compared with wild-type cells,

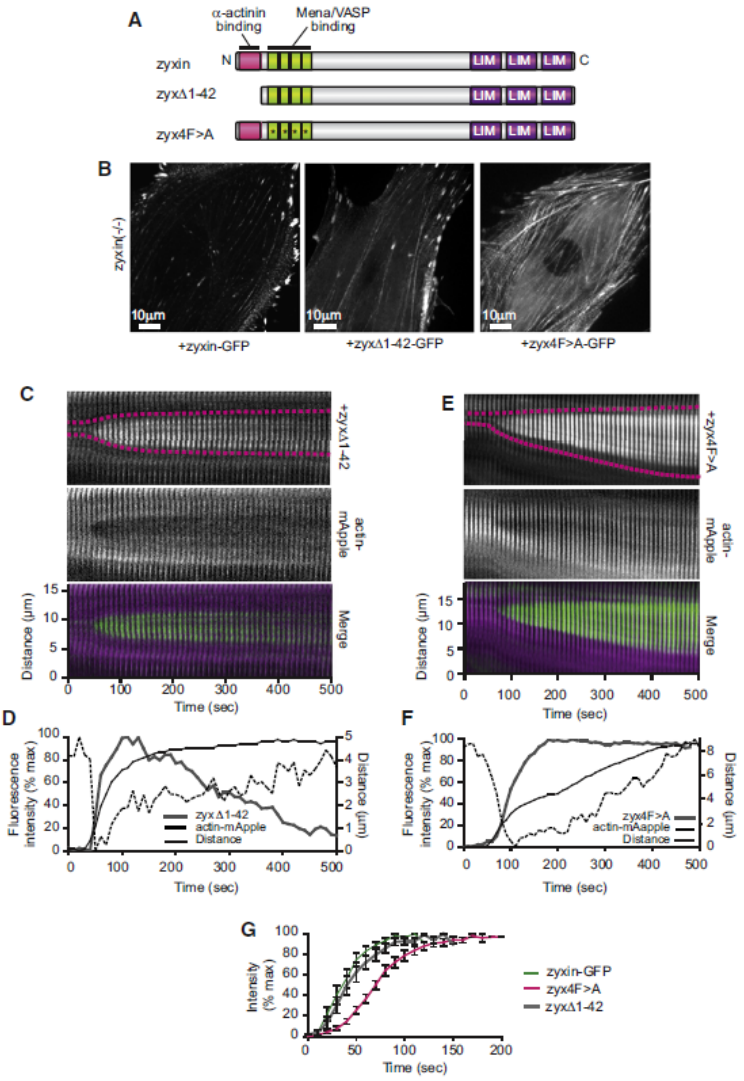

Figure 5. Zyxin Accumulation at SF Strain Sites Is Not Dependent on Zyxin's Interaction with α-Actinin, but Is Facilitated by Interaction with VASP

(A) Schematic of wild-type zyxin and zyxin mutated to interfere with α-actinin binding (zyxΔ1-42), or Mena/VASP protein binding (zyx4F > A).

(B) Mutant zyxin zyxΔ1-42 and zyx4F > A localize to SFs in *zyxin*$^{-/-}$ cells.

(C) Kymograph of zyxΔ1-42 and actin-mApple expressed in *zyxin*$^{-/-}$ cell. For merge, zyxΔ1-42 is green, actin is magenta.

(D) Intensity and distance graph showing zyxΔ1-42 accumulates at SF strain sites.

(E) Kymograph of zyx4F > A and actin-mApple expressed in *zyxin*$^{-/-}$ cell. For merge, zyx4F > A is green, actin is magenta.

(F) Intensity and distance graph showing zyx4F > A accumulates at SF strain sites.

(G) Zyx4F > A ($n = 12$) accumulation at stress fiber strain sites is slower than wild-type zyxin ($n = 13$) ($p < 0.0001$) or zyxΔ1-42 ($n = 12$) ($p = 0.0002$). Data are shown as mean ± SEM.

whether or not they were expressing zyxΔ1-42-GFP. In contrast, expression of either zyxin-GFP or zyx4F > A-GFP in *zyxin*$^{-/-}$ cells reduced the SF breakage frequency to wild-type levels (Figure 7E). Taken together, these results indicate that VASP and α-actinin have both common and distinct roles in assisting zyxin in SF repair at acute strain sites. Both α-actinin and VASP are required to stabilize elongation of local SF strain, while α-actinin has a primary role in restoring actin at the SF damage site and preventing strain events from progressing to catastrophic breaks.

DISCUSSION

By observing the dynamics of SFs in living cells, we identified novel acute, local SF damage events that occur spontaneously in response to increasing intrinsic stress within the fibers, or in response to mechanical perturbation, and defined a molecular mechanism for rapid SF repair and homeostasis of the actin cytoskeleton. SFs that exhibit acute, local strain events display a transient reduction of force transmitted through associated FAs. Zyxin rapidly accumulates at acute SF strain sites where free barbed ends of actin filaments are concentrated, and zyxin facilitates the recruitment of binding partners, VASP and α-actinin, which together comprise a repair complex that effects repair and mechanical stabilization of the SF. In the absence of zyxin, the incidence of catastrophic SF breaks is dramatically increased, and the capacity of the associated FAs to transmit forces to the substrate and retract a surrounding collagen gel is compromised (Figure 7F). The SF repair process restores the capacity of the SF to develop tension and convey traction forces to the ECM. Thus, SF strain events rapidly relieve cytoskeletal prestress, while simultaneously providing a clear target for a system that rebuilds the weakest region of the fiber, thereby enabling the cytoskeleton to tolerate dynamic increases in force load by sensing and repairing SF damage prior to failure. Without this repair system, cells exhibit a marked reduction in their ability to transmit force to remodel ECM, a process critical to tissue morphogenesis, maintenance, and repair.

Both the direct application of mechanical stimulation or conditions of elevated internal SF contractility are sufficient to induce SF strain events. The zyxin-mediated repair complex is recruited within several seconds of the local strain event, suggesting a model in which new zyxin binding sites are generated at the

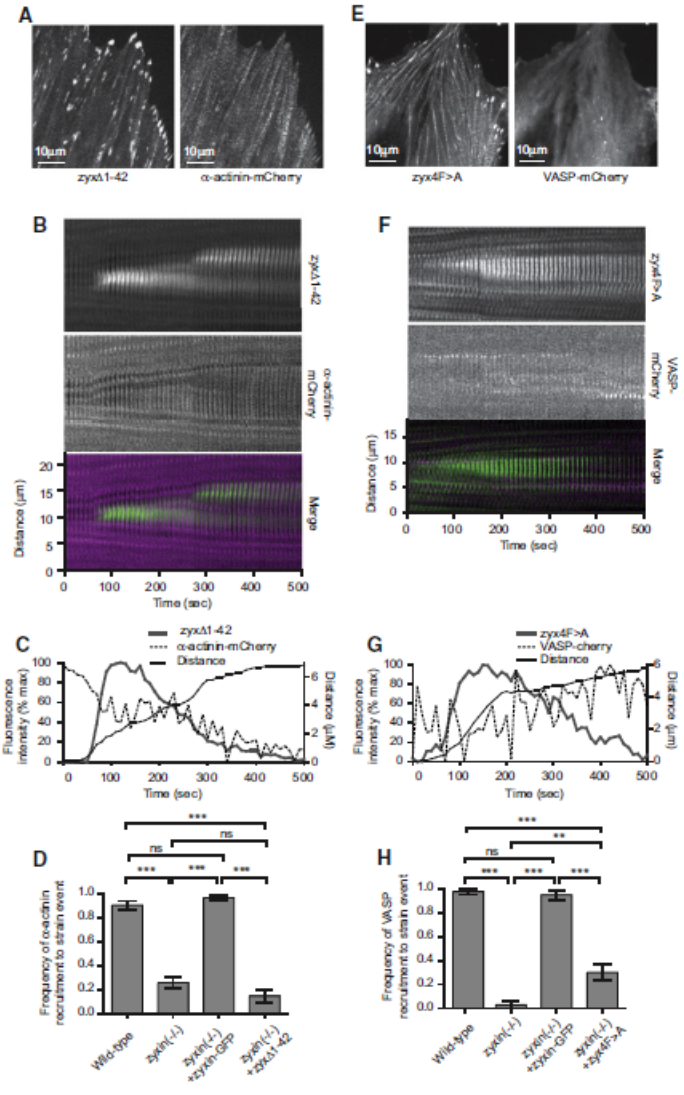

Figure 6. α-Actinin and VASP Fail to Accumulate at SF Strain Sites in *zyxin*$^{-/-}$ Cells Reconstituted with zyxΔ1-42 or zyx4F > A, Respectively

(A) α-Actinin localizes on SFs in *zyxin*$^{-/-}$ cells expressing zyxΔ1-42 transgene.

(B) Kymograph of zyxΔ1-42 and α-actinin-mCherry expressed in *zyxin*$^{-/-}$ cell. For merge, zyxΔ1-42 is green, α-actinin is magenta.

(C) Intensity and distance plot showing loss of robust α-actinin accumulation at stress fiber strain site in *zyxin*$^{-/-}$ cell expressing zyxΔ1-42.

(D) Percentage of SF strain events that recruit α-actinin in wild-type (n = 233), *zyxin*$^{-/-}$ (n = 421), *zyxin*$^{-/-}$ +zyxin-GFP (n = 364) and *zyxin*$^{-/-}$ +zyxΔ1-42 (n = 47) cells.

(E) VASP fails to localize on SFs and FAs in *zyxin*$^{-/-}$ cells expressing zyx4F > A.

(F) Kymograph of zyx4F > A and VASP-mCherry expressed in *zyxin*$^{-/-}$ cell. For merge, zyx4F > A is green, VASP is magenta.

(G) Intensity and distance graph showing loss of VASP accumulation at stress fiber strain site in *zyxin*$^{-/-}$ cell expressing zyx4F > A.

(H) Percentage of SF strain events that recruit VASP in wild-type (n = 99), *zyxin*$^{-/-}$ (n = 31), *zyxin*$^{-/-}$ +zyxin-GFP (n = 171) and *zyxin*$^{-/-}$ +zyx4F > A (n = 38) cells. Data are shown as mean ± SEM.

SF strain site. Both FRAP and photoactivation of fluorescent zyxin (data not shown) indicate that zyxin on strain sites is rapidly exchanging with a cytoplasmic pool. However, how binding sites are created is not clear. While it has been proposed previously that a conformational change in α-actinin could be responsible for stress-induced recruitment of zyxin to SFs (Colombelli et al., 2009), our data indicate that zyxin accumulation at strain sites is independent of α-actinin binding and precedes α-actinin accumulation by tens of seconds. Alternatively, it is possible that local actin filament breakage and the resultant generation of free filament barbed ends which are concentrated at SF strain sites triggers recruitment of zyxin. Indeed, zyxin is present at FAs where actin filament barbed ends are concentrated and has been shown to accumulate at sites of laser-induced SF severing (Colombelli et al., 2009). Although a direct zyxin-actin interaction has not been reported, zyxin could be recruited to free barbed ends at strain sites as a co-complex with a barbed-end capping protein. Alternatively, strain-induced changes in the actin polymer or an associated protein other than α-actinin could reveal a new docking site for zyxin on the SF. Mechanical stimulation can reveal new epitopes on cytoskeleton-associated proteins, including talin (Lee et al., 2007) and p130Cas (Sawada et al., 2006). Zyxin accumulation could also be regulated by mechanically induced local activation of kinases (Tamada et al., 2004; Wang et al., 2005), as is the movement of zyxin from FAs onto associated SF termini (Guo and Wang, 2007).

Independent of the mechanism of zyxin recruitment, our data indicate that both α-actinin and VASP participate in stabilizing elongation of acute SF strain sites. The presence of actin barbed ends throughout the SF strain site suggests that SF repair is at least in part the result of actin polymerization. Indeed, zyxin and VASP have been shown to facilitate actin polymerization (Barzik et al., 2005; Fradelizi et al., 2001; Hirata et al., 2008). However, within the sensitivity of our detection and analysis system, we did not observe a role for VASP in the restoration of actin at SF strain sites. Rather, VASP appeared to be coordinately recruited with zyxin to SF strain sites where it served to enhance the rate of zyxin accumulation, perhaps stabilizing a conformation that is compatible with its recruitment. The ability of α-actinin to crosslink actin filaments suggests that recruitment and

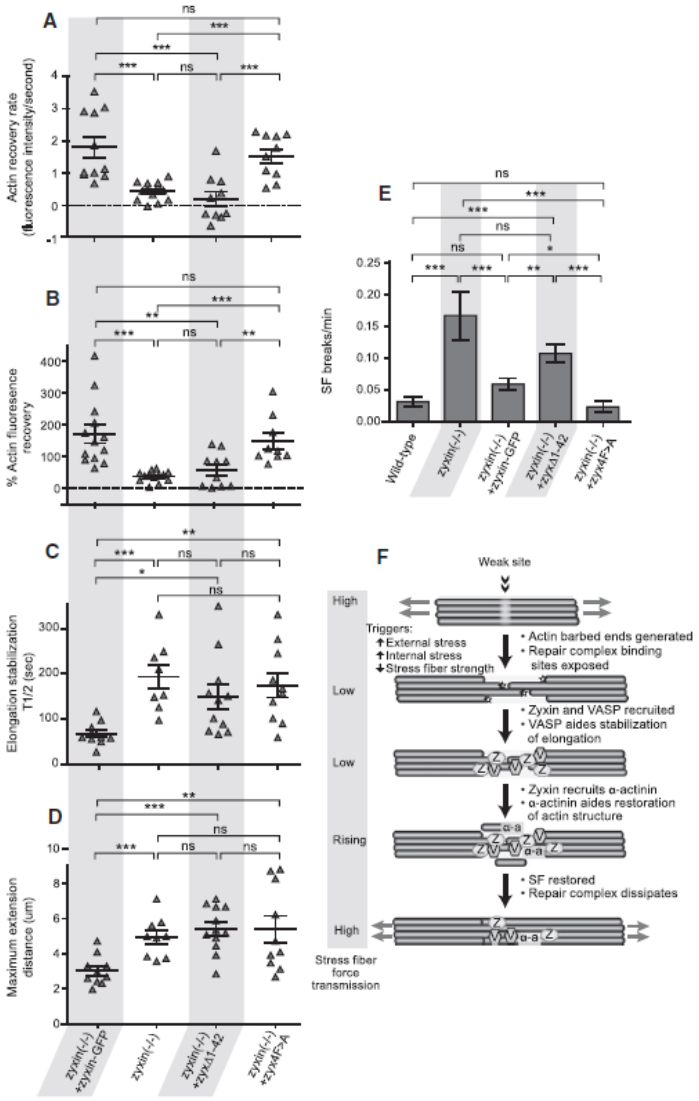

Figure 7. Zyxin Rescue Constructs Mutated to Eliminate α-Actinin or VASP Binding Fail to Rescue SF Strain Phenotypes Seen in *zyxin*$^{-/-}$ Cells

(A) Recovery rate of actin intensity immediately following thinning in *zyxin*$^{-/-}$ +zyxin-GFP (n = 13), *zyxin*$^{-/-}$ (n = 13), *zyxin*$^{-/-}$ +zyxΔ1-42 (n = 10), and *zyxin*$^{-/-}$ +zyx4F > A (n = 10) cells.

(B) Percentage of recovery of actin signal post-thinning event in *zyxin*$^{-/-}$ +zyxin-GFP (n = 13), *zyxin*$^{-/-}$ (n = 13), *zyxin*$^{-/-}$ +zyxΔ1-42 (n = 10), and *zyxin*$^{-/-}$ +zyx4F > A (n = 9) cells.

(C) Half-time to stabilization of fiber elongation during a strain event in *zyxin*$^{-/-}$ +zyxin-GFP (n = 10), *zyxin*$^{-/-}$ (n = 8), *zyxin*$^{-/-}$ +zyxΔ1-42 (n = 11), and *zyxin*$^{-/-}$ +zyx4F > A (n = 10) cells.

(D) Maximum elongation of the stress fiber region undergoing a strain event in *zyxin*$^{-/-}$ +zyxin-GFP (n = 10), *zyxin*$^{-/-}$ (n = 9), *zyxin*$^{-/-}$ +zyxΔ1-42 (n = 12), and *zyxin*$^{-/-}$ +zyx4F > A (n = 10) cells.

(E) Catastrophic stress fiber break frequency in wild-type (n = 83), *zyxin*$^{-/-}$ (n = 57), *zyxin*$^{-/-}$ +zyxin-GFP (n = 172), *zyxin*$^{-/-}$ +zyxΔ1-42 (n = 140), and *zyxin*$^{-/-}$ +zyx4F > A (n = 103) cells.

(F) Model for recruitment of a zyxin mediated repair complex to sites of SF strain. Stars indicate free actin barbed ends. Data are shown as mean ± SEM.

bundling of preexisting actin polymer from the cytoplasm may restore actin density of the SF structure to restore mechanical integrity.

Cells that lack zyxin have enhanced migration relative to their wild-type counterparts (Hoffman et al., 2006); however, the reason for this altered behavior was not understood. The loss of zyxin's contribution to the maintenance and structural stability of SFs in the knockout cells may contribute to this phenotype. In particular, it has long been appreciated that stationary cells are characterized by the presence of robust SFs, whereas migratory cells display a much less robust complement of SFs. The increased migration velocity of *zyxin*$^{-/-}$ cells may be attributable, at least in part, to the reduced stability and integrity of actin SFs in the null cells, a condition that would be expected to support enhanced migratory capacity.

Homeostasis is a central concept in animal physiology that describes the ability of living organisms to maintain constancy of their internal environment. Prior work extended this paradigm to the subcellular level, where it is evident in the maintenance of organelles such as the endoplasmic reticulum (Cox et al., 1993; Kozutsumi et al., 1988) and to macromolecular complexes such as the genetic material (Branzei and Foiani, 2008). The novel mechanism of strain recognition and repair presented here demonstrates a cellular machinery for rapid adjustment of cytoskeletal tension in response to changes in cell contractility or extrinsic forces. The demonstration that SFs display an intrinsic capacity for self-monitoring and repair in response to mechanical stress further extends the concept of homeostasis to the cytoskeleton for the regulation of both cytoarchitecture and mechanical output.

EXPERIMENTAL PROCEDURES

Materials

Cell Lines

Production and immortalization of fibroblasts derived from wild-type and zyxin null mice was described previously (Hoffman et al., 2006). Fibroblasts derived from *zyxin*$^{-/-}$ mice were stably rescued with N-terminally tagged zyxin or mutant zyxin by viral infection followed by FACS sorting to select cells expressing fluorescently tagged zyxin (Hoffman et al., 2006).

Cell Culture and Transfection

Cells were cultured in DMEM supplemented with L-glutamine, penicillin/streptomycin, sodium pyruvate, and 10% fetal bovine serum (Hyclone) and grown on coverslips coated with fibronectin (10 μg/ml). Transient transfections of DNA constructs for expression of fluorescently tagged proteins were performed using FuGENE HD transfection reagent (Roche). Time-lapse imaging of cells was performed 3–6 days after transfection.

DNA Constructs

Constructs used are described in Supplemental Experimental Procedures.

Analysis of Myosin Posphorylation

Cell lysates were harvested using SDS sample buffer and run on SDS-PAGE. Blots were probed with anti-phospho myosin light chain (ser19) (Cell Signaling Technology) then stripped and reprobed with anti-myosin light chain (Cell Signaling Technology) to control for total myosin light chain. Three independent experiments were conducted.

Collagen Gel Contraction Assay

Collagen I gels made with 0.5 × 10^5 either *zyxin*$^{-/-}$ cells or *zyxin*$^{-/-}$ +zyxin-GFP were grown in 1.5 mg/ml in 6 mm diameter glass bottom wells. The gels released from the plastic edges of the wells on day 2, and were imaged on day 7. The final gel area was determined using ImageJ.

Live-Cell Imaging for Protein Dynamic Studies

Coverslips were mounted in a closed chamber (LIS), with DMEM/F12 media (Invitrogen) supplemented with 10% fetal bovine serum. Cells were maintained at 37°C using a microscope temperature control system (LIS). Imaging was performed on an Andor spinning disk confocal on an inverted Nikon TE300 microscope with a 60× 1.4NA Nikon Plan Apochromat lens. Illumination was from solid state 488 and 568 nm lasers (Melles Griot), switched by an acousto-optic tunable filter based laser combiner (Andor Technology), and delivered by optical fiber to the Yokogawa CSU-10 scanhead. The emission light path was equipped with a dual bandpass filter (Semrock Inc). All time-lapse image sequences were captured at 10 s intervals using either Andor DV887 1024X1024 EMCCD camera, or Andor DV885 512X512 EMCCD camera (Andor Technology). Stage motions were controlled in XY with a Ludl XY stage (Ludl Electronic Products) and in Z with a Piezo stage insert (Mad City Labs). Image acquisition was performed using Andor IQ imaging software (Andor Technologies) on a PC workstation (Dell Computers).

Live Barbed Ends Assay

Cells were plated on poly-L-lysine coated coverslips and then were imaged at a 2 s frame rate until a strain event was observed. The imaging chamber was quickly perfused with saponin/rhodamine-actin solution to permeablize and label actin barbed ends. Final labeling mixture formulation was 0.005% saponin, 0.5 μM rhodamine-actin, 0.1 mM ATP, 138 nM KCl,10 mM PIPES, 3 mM EGTA, and 4 mM $MgCl_2$ (pH 6.9).

Direct Manipulation of Cells

Cells expressing zyxin-GFP for direct manipulation were plated on polyacrylamide substrates. They were prodded with a fire-polished glass pipette mounted on an Eppendorf micromanipulator. Images of this procedure were captured every 2 s using the imaging system described above.

Traction Microscopy

Methods used for traction microscopy are in Supplemental Experimental Procedures.

Image Processing and Analysis

Fluorescence Intensity and SF Elongation

Image sequences were processed, region intensity and distance measurements were collected, and movies were generated using MetaMorph software (Molecular Devices). Intensity measurements were taken as average intensity within a region of interest restricted to the site of SF elongation. Kymographs were generated using a custom macro (Ryan Littlefield) run in MetaMorph. For these, a 10 pixel wide linear region of interest along a SF was selected, the image was rotated using the nearest neighbors rotation algorithm to eliminate diagonal pixel sampling, and then each 10 pixel region was output into a montage. Distance measurements to assay SF elongation were made on the kymograph using two polylines overlaid on the kymograph flanking the site of SF extension. Each line followed a stable fluorescent intensity feature on the SF serving as a fiduciary mark. The distance change between the polylines was plotted over time. Numerical output was normalized and graphed using Prism 5 (GraphPad.)

Analysis of Actin Recovery

We tracked actin-mApple fluorescent average intensity within the strain region. Starting from the low point in the intensity plot, as the region entered the repair phase, we fit a line to the trajectory of recovery, restricted to the first 200 s of recovery, and then calculated recovery rate (fluorescence intensity/time) based on the slope of this line. Percentage actin signal recovery was calculated as the percentage that actin signal within the thinning region recovered, relative to the original signal, within the 500 s imaging period.

Analysis of Kinetics and Elongation Stabilization

For analysis of the kinetics of protein accumulation, intensity over time was fit using the Hill equation (Y = Vmax*X^h/(K^h + X^h). Analysis of dissipation was fit using the model for single phase exponential decay (Y = (Y0 − Plateau)*exp (−K*X) + Plateau). Half-time to stabilization of elongation was determined using the Hill equation fit to elongation data.

Statistical Analysis

All statistical analysis was performed using Prism 5 (GraphPad). Statistical significance for the analyses of SF breaks, changes in traction induced strain, the kinetics of fluorescence accumulation, and the kinetics of fluorescence dissipation were determined using unpaired, two-tailed t tests. Contingency analyses of actin recovery and α-actinin and VASP recruitment utilized a two-tailed Fisher's exact test. Differences were considered significant at the 95% confidence level. Statistical significance denoted as follows; ***$p < 0.001$, **$p = 0.001–0.01$, *$p = 0.01–0.05$.

SUPPLEMENTAL INFORMATION

Supplemental Information includes Experimental Procedures, two figures, one table, and 11 movies and can be found online at doi:10.1016/j.devcel.2010.08.008.

ACKNOWLEDGMENTS

We thank Frank Gertler (Massachusetts Institute of Technology), Michael Davidson (Florida State University), Carol Otey (University of North Carolina, Chapel Hill), and Ke Hu (Indiana University) for reagents. We also thank Laura Hoffman and Chris Jensen for the zyx4F>A cell line, the zyxΔ1-42 construct, and for helpful discussions, Jonathan Stricker for technical advice, and Diana Lim for graphic design. Supported by NIH RO1GM50877 (M.C.B.), the Huntsman Cancer Foundation, and shared resources from the Cancer Center Support Grant (2 P30 CA042014-21), the NIH multidisciplinary cancer research training grant (M.A.S.), the Burroughs Wellcome Career Award at the Scientific Interfaces and NIH Director's Pioneer Award 5 DP1 OD003354-02 (M.L.G), and NHLBI (C.M.W.).

Received: February 2, 2010
Revised: June 24, 2010
Accepted: July 9, 2010
Published: September 13, 2010

REFERENCES

Barzik, M., Kotova, T.I., Higgs, H.N., Hazelwood, L., Hanein, D., Gertler, F.B., and Schafer, D.A. (2005). Ena/VASP proteins enhance actin polymerization in the presence of barbed end capping proteins. J. Biol. Chem. *280*, 28653–28662.

Beningo, K.A., Lo, C.M., and Wang, Y.L. (2002). Flexible polyacrylamide substrata for the analysis of mechanical interactions at cell-substratum adhesions. Methods Cell Biol. *69*, 325–339.

Branzei, D., and Foiani, M. (2008). Regulation of DNA repair throughout the cell cycle. Nat. Rev. Mol. Cell Biol. *9*, 297–308.

Burridge, K., Fath, K., Kelly, T., Nuckolls, G., and Turner, C. (1988). Focal adhesions: transmembrane junctions between the extracellular matrix and the cytoskeleton. Annu. Rev. Cell Biol. *4*, 487–525.

Byers, H.R., White, G.E., and Fujiwara, K. (1984). Organization and function of stress fibers in cells in vitro and in situ. A review. Cell Muscle Motil. *5*, 83–137.

Chrzanowska-Wodnicka, M., and Burridge, K. (1996). Rho-stimulated contractility drives the formation of stress fibers and focal adhesions. J. Cell Biol. *133*, 1403–1415.

Clark, E.A., Golub, T.R., Lander, E.S., and Hynes, R.O. (2000). Genomic analysis of metastasis reveals an essential role for RhoC. Nature *406*, 532–535.

Colombelli, J., Besser, A., Kress, H., Reynaud, E.G., Girard, P., Caussinus, E., Haselmann, U., Small, J.V., Schwarz, U.S., and Stelzer, E.H. (2009). Mechanosensing in actin stress fibers revealed by a close correlation between force and protein localization. J. Cell Sci. *122*, 1665–1679.

Cox, J.S., Shamu, C.E., and Walter, P. (1993). Transcriptional induction of genes encoding endoplasmic reticulum resident proteins requires a transmembrane protein kinase. Cell *73*, 1197–1206.

Crawford, A.W., Michelsen, J.W., and Beckerle, M.C. (1992). An interaction between zyxin and alpha-actinin. J. Cell Biol. *116*, 1381–1393.

Drees, B., Friederich, E., Fradelizi, J., Louvard, D., Beckerle, M.C., and Golsteyn, R.M. (2000). Characterization of the interaction between zyxin and members of the Ena/vasodilator-stimulated phosphoprotein family of proteins. J. Biol. Chem. *275*, 22503–22511.

Farge, E. (2003). Mechanical induction of Twist in the Drosophila foregut/stomodeal primordium. Curr. Biol. *13*, 1365–1377.

Fradelizi, J., Noireaux, V., Plastino, J., Menichi, B., Louvard, D., Sykes, C., Golsteyn, R.M., and Friederich, E. (2001). ActA and human zyxin harbour Arp2/3-independent actin-polymerization activity. Nat. Cell Biol. *3*, 699–707.

Gardel, M.L., Sabass, B., Ji, L., Danuser, G., Schwarz, U.S., and Waterman, C.M. (2008). Traction stress in focal adhesions correlates biphasically with actin retrograde flow speed. J. Cell Biol. *183*, 999–1005.

Grinnell, F. (2000). Fibroblast-collagen-matrix contraction: growth-factor signalling and mechanical loading. Trends Cell Biol. *10*, 362–365.

Guo, W.H., and Wang, Y.L. (2007). Retrograde fluxes of focal adhesion proteins in response to cell migration and mechanical signals. Mol. Biol. Cell *18*, 4519–4527.

Harris, A.K., Wild, P., and Stopak, D. (1980). Silicone rubber substrata: a new wrinkle in the study of cell locomotion. Science *208*, 177–179.

Heydemann, A., and McNally, E.M. (2007). Consequences of disrupting the dystrophin-sarcoglycan complex in cardiac and skeletal myopathy. Trends Cardiovasc. Med. *17*, 55–59.

Hirata, H., Tatsumi, H., and Sokabe, M. (2008). Mechanical forces facilitate actin polymerization at focal adhesions in a zyxin-dependent manner. J. Cell Sci. *121*, 2795–2804.

Hoffman, L.M., Jensen, C.C., Kloeker, S., Wang, C.L., Yoshigi, M., and Beckerle, M.C. (2006). Genetic ablation of zyxin causes Mena/VASP mislocalization, increased motility, and deficits in actin remodeling. J. Cell Biol. *172*, 771–782.

Hutson, M.S., Tokutake, Y., Chang, M.S., Bloor, J.W., Venakides, S., Kiehart, D.P., and Edwards, G.S. (2003). Forces for morphogenesis investigated with laser microsurgery and quantitative modeling. Science *300*, 145–149.

Iba, T., and Sumpio, B.E. (1991). Morphological response of human endothelial cells subjected to cyclic strain in vitro. Microvasc. Res. *42*, 245–254.

Iwamoto, H., Nakamuta, M., Tada, S., Sugimoto, R., Enjoji, M., and Nawata, H. (2000). A p160ROCK-specific inhibitor, Y-27632, attenuates rat hepatic stellate cell growth. J. Hepatol. *32*, 762–770.

Kozutsumi, Y., Segal, M., Normington, K., Gething, M.J., and Sambrook, J. (1988). The presence of malfolded proteins in the endoplasmic reticulum signals the induction of glucose-regulated proteins. Nature *332*, 462–464.

Krieg, M., Arboleda-Estudillo, Y., Puech, P.H., Kafer, J., Graner, F., Muller, D.J., and Heisenberg, C.P. (2008). Tensile forces govern germ-layer organization in zebrafish. Nat. Cell Biol. *10*, 429–436.

Kumar, S., Maxwell, I.Z., Heisterkamp, A., Polte, T.R., Lele, T.P., Salanga, M., Mazur, E., and Ingber, D.E. (2006). Viscoelastic retraction of single living stress fibers and its impact on cell shape, cytoskeletal organization, and extracellular matrix mechanics. Biophys. J. *90*, 3762–3773.

Langanger, G., Moeremans, M., Daneels, G., Sobieszek, A., De Brabander, M., and De Mey, J. (1986). The molecular organization of myosin in stress fibers of cultured cells. J. Cell Biol. *102*, 200–209.

Lauffenburger, D.A., and Horwitz, A.F. (1996). Cell migration: a physically integrated molecular process. Cell *84*, 359–369.

Lazarides, E., and Burridge, K. (1975). Alpha-actinin: immunofluorescent localization of a muscle structural protein in nonmuscle cells. Cell *6*, 289–298.

Lee, S.E., Kamm, R.D., and Mofrad, M.R. (2007). Force-induced activation of talin and its possible role in focal adhesion mechanotransduction. J. Biomech. *40*, 2096–2106.

Lele, T.P., Pendse, J., Kumar, S., Salanga, M., Karavitis, J., and Ingber, D.E. (2006). Mechanical forces alter zyxin unbinding kinetics within focal adhesions of living cells. J. Cell. Physiol. *207*, 187–194.

Lo, C.M., Buxton, D.B., Chua, G.C., Dembo, M., Adelstein, R.S., and Wang, Y.L. (2004). Nonmuscle myosin IIb is involved in the guidance of fibroblast migration. Mol. Biol. Cell *15*, 982–989.

McBeath, R., Pirone, D.M., Nelson, C.M., Bhadriraju, K., and Chen, C.S. (2004). Cell shape, cytoskeletal tension, and RhoA regulate stem cell lineage commitment. Dev. Cell *6*, 483–495.

Niebuhr, K., Ebel, F., Frank, R., Reinhard, M., Domann, E., Carl, U.D., Walter, U., Gertler, F.B., Wehland, J., and Chakraborty, T. (1997). A novel proline-rich motif present in ActA of Listeria monocytogenes and cytoskeletal proteins is the ligand for the EVH1 domain, a protein module present in the Ena/VASP family. EMBO J. *16*, 5433–5444.

Nix, D.A., Fradelizi, J., Bockholt, S., Menichi, B., Louvard, D., Friederich, E., and Beckerle, M.C. (2001). Targeting of zyxin to sites of actin membrane interaction and to the nucleus. J. Biol. Chem. *276*, 34759–34767.

Palmer, B.M. (2005). Thick filament proteins and performance in human heart failure. Heart Fail. Rev. *10*, 187–197.

Paszek, M.J., and Weaver, V.M. (2004). The tension mounts: mechanics meets morphogenesis and malignancy. J. Mammary Gland Biol. Neoplasia *9*, 325–342.

Peterson, L.J., Rajfur, Z., Maddox, A.S., Freel, C.D., Chen, Y., Edlund, M., Otey, C., and Burridge, K. (2004). Simultaneous stretching and contraction of stress fibers in vivo. Mol. Biol. Cell *15*, 3497–3508.

Peyton, S.R., Raub, C.B., Keschrumrus, V.P., and Putnam, A.J. (2006). The use of poly(ethylene glycol) hydrogels to investigate the impact of ECM chemistry and mechanics on smooth muscle cells. Biomaterials *27*, 4881–4893.

Reinhard, M., Zumbrunn, J., Jaquemar, D., Kuhn, M., Walter, U., and Trueb, B. (1999). An alpha-actinin binding site of zyxin is essential for subcellular zyxin localization and alpha-actinin recruitment. J. Biol. Chem. *274*, 13410–13418.

Sabass, B., Gardel, M.L., Waterman, C.M., and Schwarz, U.S. (2008). High resolution traction force microscopy based on experimental and computational advances. Biophys. J. *94*, 207–220.

Sadoshima, J., and Izumo, S. (1997). The cellular and molecular response of cardiac myocytes to mechanical stress. Annu. Rev. Physiol. *59*, 551–571.

Sawada, Y., Tamada, M., Dubin-Thaler, B.J., Cherniavskaya, O., Sakai, R., Tanaka, S., and Sheetz, M.P. (2006). Force sensing by mechanical extension of the Src family kinase substrate p130Cas. Cell *127*, 1015–1026.

Tamada, M., Sheetz, M.P., and Sawada, Y. (2004). Activation of a signaling cascade by cytoskeleton stretch. Dev. Cell *7*, 709–718.

Wang, N., Butler, J.P., and Ingber, D.E. (1993). Mechanotransduction across the cell surface and through the cytoskeleton. Science *260*, 1124–1127.

Wang, Y., Botvinick, E.L., Zhao, Y., Berns, M.W., Usami, S., Tsien, R.Y., and Chien, S. (2005). Visualizing the mechanical activation of Src. Nature *434*, 1040–1045.

Wozniak, M.A., and Chen, C.S. (2009). Mechanotransduction in development: a growing role for contractility. Nat. Rev. Mol. Cell Biol. *10*, 34–43.

Yoshigi, M., Hoffman, L.M., Jensen, C.C., Yost, H.J., and Beckerle, M.C. (2005). Mechanical force mobilizes zyxin from focal adhesions to actin filaments and regulates cytoskeletal reinforcement. J. Cell Biol. *171*, 209–215.

Zamir, E., and Geiger, B. (2001). Molecular complexity and dynamics of cell-matrix adhesions. J. Cell Sci. *114*, 3583–3590.

Developmental Cell *19*

Supplemental Information

A Zyxin-Mediated Mechanism for Actin Stress Fiber Maintenance and Repair

Mark A. Smith, Elizabeth Blankman, Margaret L. Gardel, Laura Luettjohann, Clare M. Waterman, and Mary C. Beckerle

Table S1.

Frequency of breaks	0.03 +/-0.01 breaks/minute/cell (n=83 cells, 1100 minutes of observation)
Frequency of strain events	0.18 +/-0.03 events/minute/cell (n=83 cells, 1100 minutes of observation)
Mean recovery rate of actin fluorescence signal	1.20 +/- 0.18 fluorescence intensity units/second (n=10)
Percent recovery	142.6 +/- 12% (n=11)
Average maximum elongation distance	2.5 +/- 0.2μm (n=10)
Elongation rate	4.0 +/- 1.4 μm/min; (n=10)
Half-time to cessation of elongation	77 +/- 6 seconds (n=10)
Strain event recovery/break	82%/18%

Figure S1
Associated with Figure 2

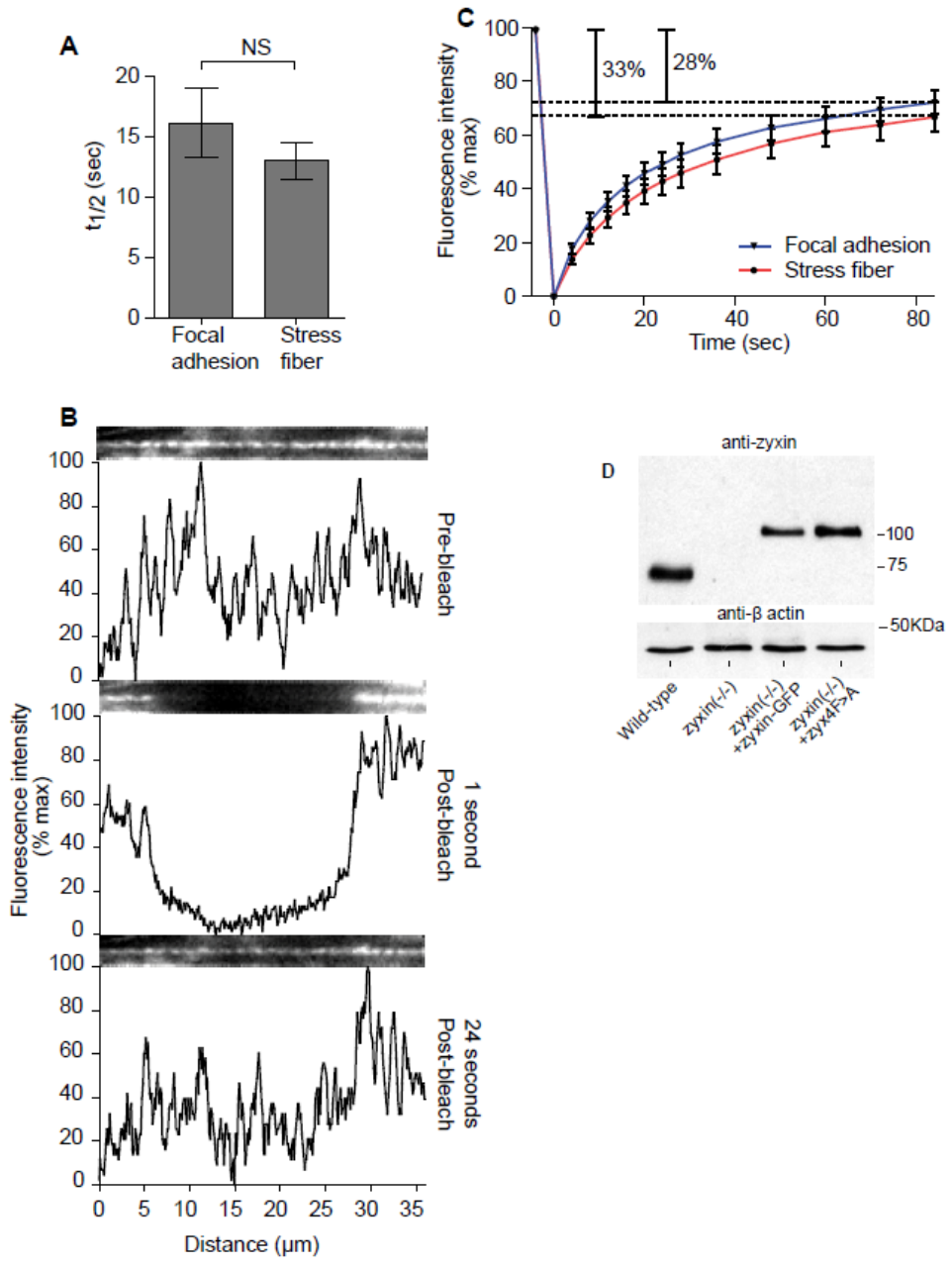

Figure S1. Recovery of zyxin-GFP is rapid and not significantly different in SF and FA
(A) Zyxin-GFP FRAP recovery t1/2 for FA (n=78) and SF (n=61) are not significantly different (P=0.3716).
(B) Example SF FRAP showing micrograph of SF with linescan of fluorescence intensity plotted below.
(C) Pooled FA and SF recovery curves.
(D) Western blot showing population levels of rescue constructs in stable cell lines.

Figure S2
Associated with Figure 3

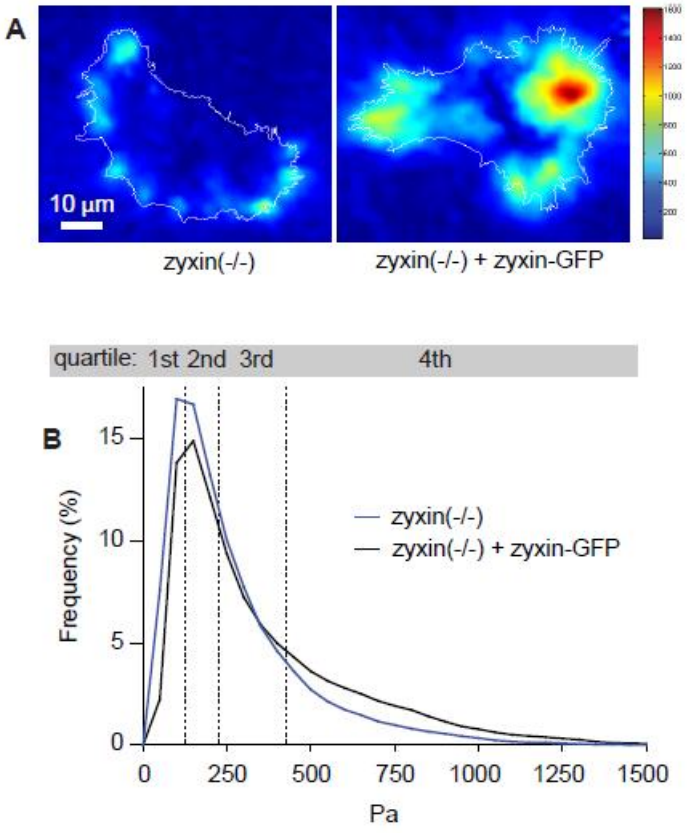

Figure S2. Peak traction forces are lower in zyxin (-/-) cells than zyxin (-/-) cells expressing zyxin-GFP

(A) Color-mapped traction force images, with cell outline overlaid, showing higher peak forces in the rescued cell.

(B) Graph of binned force vector frequencies showing quartile divisions.

SUPPLEMENTAL EXPERIMENTAL PROCEDURES

DNA constructs

pZyx-mCherry- The mCherry coding sequence (Shaner et al., 2004) was PCR amplified to add BamHI and NotI restriction sites. The PCR products were digested in BamHI and NotI and then ligated into pEGFP-zyxin, replacing the EGFP coding sequence.

pcDNA3 α-actinin-mCherry- HindIII/XbaI EGFP fragment of pCDNA3 α-actinin: EGFP was replaced with a PCR product of mCherry with HindIII and XbaI sites. mCherry was amplified from pZyx-Cherry.

pmCherry-actin- The mCherry coding sequence was amplified from pRSET-B-mCherry, digested with AgeI and BglII and ligated in place of GFP in pEGFP-actin (Clontech, cat# PT3265-5).

pZyx4F>A Using site directed mutagenesis the phenylalanines were mutated to alanine in each of zyxin's four proline-rich (FPPP) sequences (ActA repeats). This was cloned into the pLINX viral transformation vector.

pZyxΔ1-42 This N-terminal truncation of zyxin was generated using a PCR based approach, then cloned into the Tol2 Gateway transformation vector.

Other plasmids were generous gifts from; Dr. Michael Davidson (Florida State University): pActin:mApple; Dr. Frank Gertler (Massachusetts Institute of Technology): pVASP:GFP; Dr. Carol Otey (University of North Carolina, Chapel Hill): α-actinin-GFP.

Traction Microscopy

Preparation of polyacrylamide (PAA) substrates and live cell traction microscopy

Fibronectin-coated PAA substrates containing 40nm fluorescent spheres were prepared on glass coverslips (Gardel et al., 2008; Sabass et al., 2008) using a 7.5% acrylamide/0.1% bis-acrylamide gel, with a shear elastic modulus, *G'*, of 12,000 Pa. Fibronectin was covalently attached to the top surface of the PAA gel by utilizing the bifunctional cross-linker sulfo-SANPAH (Pierce).

Coverslips containing cells bound to PAA substrates were mounted in a perfusion chamber (Warner) in F12 media supplemented with 30 μL/1 mL Oxyrase (Oxyrase Enzyme system, EC0050). Cells were imaged on a spinning disk confocal microscope that consisted of a 2.5 W water-cooled Coherent Innova 70c Krypton/Argon ion laser with the 488 and 647 nm lines selected via a polychromatic acousto-optical modulator (PCAOM, Neos Technologies), Yokogawa CSU-10 scanhead mounted on a Nikon TE-2000E automated inverted microscope equipped with a Perfect Focus system (Nikon) and a linearly encoded robotic stage (Applied Scientific Instruments). Temperature control was maintained using an air curtain incubator (Nevtek). Images were generated with a 60x 1.2 NA Plan Apo water immersion objective lens (Nikon) using a 1.5X optovar. Zyxin-GFP images were captured at 10 sec intervals, and latex spheres were captured at 30 sec intervals using a Roper HQ 2 camera equipped with an interline transfer CCD (6.4 um pixel size). Following imaging, cells were perfused with 2 mL of 0.5% trypsin to release them from the PAA substrate, and an image of beads in the unstrained substrate was taken in the 647 channel.

Image Analysis

Time-lapse bead images were aligned to the reference frame with pixel accuracy, either using MetaMorph software or using custom algorithms in Matlab (Ji and Danuser, 2005). For detection of bead displacement, a series of beads were tracked using cross-correlation tracking (Ji and Danuser, 2005). Template sizes were adaptively chosen between 11x11 and 25x25 pixels (1 pixel=0.067 mm) depending on the local image contrast. This corresponds to 1.3-3 times the diameter of a diffraction-limited image region created by the beads. Templates were placed on the positions of significant beads (Crocker and Grier, 1996). We typically obtained 1000-3000 vectors of bead displacements for each image frame of our movie.

Regions around sites of cell adhesion to the extracellular matrix were drawn based on the zyxin-GFP localization to FAs and the strain field was interpolated using a Gaussian-weighted kernel onto the centroid of the drawn region. We found this measurement to be insensitive to small variations in region geometry or location and showed similar variation as measuring the 90% of max strain within the region. The magnitude of local deformation in the compliant matrix provides a robust approximation of the magnitude and direction of the force generated by the cell at FAs.

Whole-cell traction force analysis

To isolate stress vectors within the whole cell area, a binary mask was created by thresholding intensity of zyxin-GFP or α-actinin-GFP in the zyxin (-/-) cells. Some force is propagated through the PAA gel outward from the cell edge. The whole-cell binary mask underwent circular dilation (80-pixel diameter) to extend its edge to include these force vectors. Vector magnitudes outside the cell were defined as background forces and only vectors whose magnitudes were greater than background were included in whole-cell traction force analysis.

Vector magnitude frequency from each frame was plotted on a histogram. Traction stress was binned in 50 Pascal increments on the x-axis. The frequency data was averaged using all frames and using both zyxin (-/-) cells and zyxin (-/-) +zyxin-GFP in order to find a general distribution of quartiles. The area under the curve was found for each quartile in each frame and plotted as a single point in a scatter plot. The area underneath the curves in the fourth quartile—representing the uppermost forces exerted by a cell at one time point—was found to be significantly greater in the cells containing zyxin.

CHAPTER 3

LATERAL COMMUNICATION BETWEEN STRESS FIBER SARCOMERES FACILITATES A LOCAL REMODELING RESPONSE

Reprinted with permission from *Biophysical Journal*.
Chapin, L.M., Blankman, E.; Smith, M.A.; Shiu Y.; Beckerle M.C. 2012. Lateral communication between stress fiber sarcomeres facilitates a local remodeling response. *Biophysical Journal* 103: 2082-2092.

2082 Biophysical Journal Volume 103 November 2012 2082–2092

Lateral Communication between Stress Fiber Sarcomeres Facilitates a Local Remodeling Response

Laura M. Chapin,[†] Elizabeth Blankman,[†] Mark A. Smith,[†] Yan-Ting Shiu,[‡*] and Mary C. Beckerle[†*]
[†]Huntsman Cancer Institute, Departments of Biology and Oncological Sciences, Salt Lake City, Utah; and [‡]Division of Nephrology and Hypertension, Department of Medicine, University of Utah, Salt Lake City, Utah

ABSTRACT Actin stress fibers (SFs) are load-bearing and mechanosensitive structures. To our knowledge, the mechanisms that enable SFs to sense and respond to strain have not been fully defined. Acute local strain events can involve a twofold extension of a single SF sarcomere, but how these dramatic local events affect the overall SF architecture is not believed to be understood. Here we have investigated how SF architecture adjusts to episodes of local strain that occur in the cell center. Using fluorescently tagged zyxin to track the borders of sarcomeres, we characterize the dynamics of resting sarcomeres and strain-site sarcomeres. We find that sarcomeres flanking a strain site undergo rapid shortening that directly compensates for the strain-site extension, illustrating lateral communication of mechanical information along the length of a stress fiber. When a strain-site sarcomere extends asymmetrically, its adjacent sarcomeres exhibit a parallel asymmetric shortening response, illustrating that flanking sarcomeres respond to strain magnitude. After extension, strain-site sarcomeres become locations of new sarcomere addition, highlighting mechanical strain as a trigger of sarcomere addition and revealing a, to our knowledge, novel type of SF remodeling. Our findings provide evidence to suggest SF sarcomeres act as strain sensors and are interconnected to support communication of mechanical information.

INTRODUCTION

Cells are constantly exposed to mechanical stimuli from their environment. They interact with the environment via focal adhesions that are linked to an internal actomyosin cytoskeleton. Actomyosin structures support cell shape determination and cell contractility, and are required for many cell functions including cell adhesion, cell division, and migration. Cells can use the actin cytoskeleton not only to sense changes in internal mechanics but also to remodel the cytoskeleton in response to mechanical and chemical changes in their environment (1–4). The ways in which actin structures remodel in response to mechanical changes are not, to our knowledge, fully understood.

One way that cells regulate their shape and contractility is by remodeling actin stress fibers (SFs) (5,6). Actin SFs are made up of sarcomeric units in series along their lengths, similar to striated muscle fibers. Like muscle sarcomeres, the SF sarcomeres are thought to be contractile subunits and their boundaries are defined by proteins such as α-actinin and zyxin (7–10). Fluorescently labeled α-actinin and zyxin have been commonly used to track SF dynamics in living cells (11–16). The tracking of changes in SF sarcomeres has facilitated understanding of the structural architecture of the actin cytoskeleton and how it plays a role in SF mechanics.

The creation and elimination of sarcomeres in SFs is more dynamic than what occurs in myofibrils of muscle. In nonmuscle cells, SFs can form new sarcomeres at the junction of the SF and the focal adhesion, where there is a concentration of proteins involved in actin polymerization (12,15,17,18). In addition to creating new sarcomeres, SFs have also been reported to eliminate sarcomeres at "sinks" along the SF, which are often located at SF bifurcations (15). The ability to add and remove single sarcomeric units along the length of a stress fiber has been suggested to allow for constant maintenance of a very dynamic actin cytoskeleton, though it remains controversial how the addition and elimination of sarcomeres relate to fiber mechanics.

SF dynamics and mechanical properties can be influenced by exposure of cells to a variety of pharmacological agents (19,20). For example, Peterson et al. (13) described regional variation in sarcomere length change when cells were treated with calyculin A, a phosphatase inhibitor that induces myosin II activation. Regions of the SF closest to focal adhesions exhibit sarcomeric shortening in response to calyculin A, whereas the center regions of the same fiber simultaneously undergo lengthening. Thus, large-scale compensatory behavior across an entire SF has been described, though the level at which compensatory changes occur across adjacent individual sarcomeres has not been reported.

SF dynamics have also been studied in response to various physical perturbations. One method used to characterize single SF mechanics is laser severing, in which individual SFs are cut with a laser nanoscissor (11,21,22). Sarcomeric recoil can be analyzed after a severing event to characterize physical properties of actin SFs and the impact of the cytoplasm on dynamic behavior. Specifically, after severing, the trajectory of the SF during recoil demonstrated that SFs are viscoelastic structures and also experience viscoelastic forces from the cytoplasm (21).

Submitted June 17, 2012, and accepted for publication September 19, 2012.

*Correspondence: mary.beckerle@hci.utah.edu or y.shiu@hsc.utah.edu

Editor: Douglas Robinson.

0006-3495/12/11/2082/11 $2.00

http://dx.doi.org/10.1016/j.bpj.2012.09.038

Although analysis of retracting SFs provides a way to study certain physical characteristics of actin SFs, it is unknown whether intact SFs share properties with SFs that are severed experimentally.

In recent work, direct inspection of SF behavior in living and undisturbed cells revealed the spontaneous occurrence of acute, local strain events where single SF sarcomeres undergo rapid actin SF thinning and elongation (16). Despite significant local strain (up to twofold extension), the majority of SFs remain intact and the strain events do not escalate to catastrophic breaks (16). Zyxin was identified as a key player for recruitment of additional proteins to accomplish localized actin repair of the strain sites and subsequent mechanical restoration. The strain events occur when there is elevated tension along a stress fiber as indicated by elevated traction strain measured at the focal adhesion site where the SF ends. Traction decreases upon rapid elongation of a sarcomere, suggesting that sarcomere elongation provides a mechanism by which cells can respond to changes in force without undergoing complete SF breakage. As of this writing, it is not known why certain sarcomeres experience strain events whereas their neighboring sarcomeres do not. It is also not well understood how the dramatic lengthening in a single sarcomere is managed by the neighboring sarcomeres in the rest of the fiber. Acute local strain events provide us with a unique opportunity to analyze dynamics of single SFs without being physically invasive. Furthermore, these strain events happen spontaneously and are not induced by drug treatment, allowing us to study SFs in a more biologically relevant context.

Here we have sought to address several gaps in our understanding of SF sarcomere dynamics. We find that SFs display a range of sarcomere dynamics in unstimulated fibers:

1. resting SF sarcomeres exhibit length fluctuations over time,
2. certain sarcomeres (called "strain-site sarcomeres") exhibit local strain,
3. strain sites can develop new sarcomeres even in the center of a stress fiber, and
4. there is a highly local compensatory sarcomeric shortening response by adjacent sarcomeres flanking the strain-site sarcomeres.

Taken together, our results demonstrate actin SFs use a local compensatory response to accommodate sudden lengthening in individual sarcomeres.

MATERIALS AND METHODS

Cell culture

Fibroblasts derived from a zyxin −/− mouse were rescued with a stably expressing zyxin-GFP (23). Cells were cultured in Dulbecco's Modified Eagle Media (DMEM) with 10% fetal bovine serum (Hyclone, Logan, Utah), sodium pyruvate, penicillin/streptomycin, and L-glutamine. Cells were plated on glass coverslips coated with fibronectin (10 μm/mL) and imaged 3–6 days later.

Live cell microscopy

Imaging conditions were the same as previously described in Smith et al. (16). Cells were plated in Delta TPG culture dishes (Bioptechs, Butler, PA) and were imaged in DMEM/F12 media (Invitrogen, Carlsbad, CA) with 10% fetal bovine serum. A spinning disk confocal (Andor Technology, Belfast, Northern Ireland) on an inverted TE300 microscope (Nikon, Melville, NY) was used for all imaging. A 60× 1.4 NA Plan Apochromat lens (Nikon) was used. All time-lapse image sequences were captured at 10-s intervals, unless the imaging interval was otherwise indicated to be 30 s, using either model No. DV887 1024 or No. DV885 512 × 512 electron-multiplying charge-coupled device cameras (Andor Technology).

Data acquisition and image analysis

Image analysis was carried out using MetaMorph software (Molecular Devices, Eugene, OR). Kymographs were created using a macro written for use in MetaMorph, and fluorescent intensity data were collected using the linescan feature. The linescan parameters were set to collect a 3-pixel-wide average intensity, and intensity data were recorded using the software Excel (Microsoft, Redmond, WA). Intensity data were then analyzed using code written for the software MATLAB (The MathWorks Natick, MA) to smooth data (5 × 5 filter) and track local maxima of intensity over time. MATLAB output included pixel locations and intensity values. The length of a sarcomere is the length between two consecutive zyxin striations, and measured from the point of maximal intensity. Images that clearly show SFs in the plane of focus were used, thus ensuring the features that are tracked are not due to changes in focus. The software Excel was used for all other analysis, except statistical analysis that was carried out using Prism 5 (Graphpad Software, San Diego, CA). Differences were determined using unpaired two-tailed *t*-tests.

RESULTS

Fluctuations of stress fiber sarcomeres in vivo maintain stress fiber homeostasis

To assess sarcomere dynamics in resting SFs, cells expressing zyxin-GFP were imaged with 10-s intervals and each zyxin striation was tracked over time (Fig. 1 *A*). Linescans were made from intensity data, which were used to find the peak intensity values of each striation for each time point (Fig. 1 *B*, *white lines* on the *intensity heatmap kymograph*). Each zyxin puncta identifies the border between two adjacent sarcomeres; the distance between adjacent zyxin striations represents the length of one sarcomere. The average length of resting sarcomeres in the center of SFs was 1.6 ± 0.063 μm (mean ± SE). We found that within a single SF, individual sarcomeres undergo different degrees of length change relative to the initial sarcomere length measured at the start of the imaging period. From measurement of 58 sarcomeres over 10 min, we determined that ~40% of the sarcomeres experienced little or no change in length (ranging from 0 ± 0.18 μm) whereas the remaining sarcomeres experienced either lengthening or shortening of up to 1.0 μm (Fig. 1 *C*). These adjustments represent

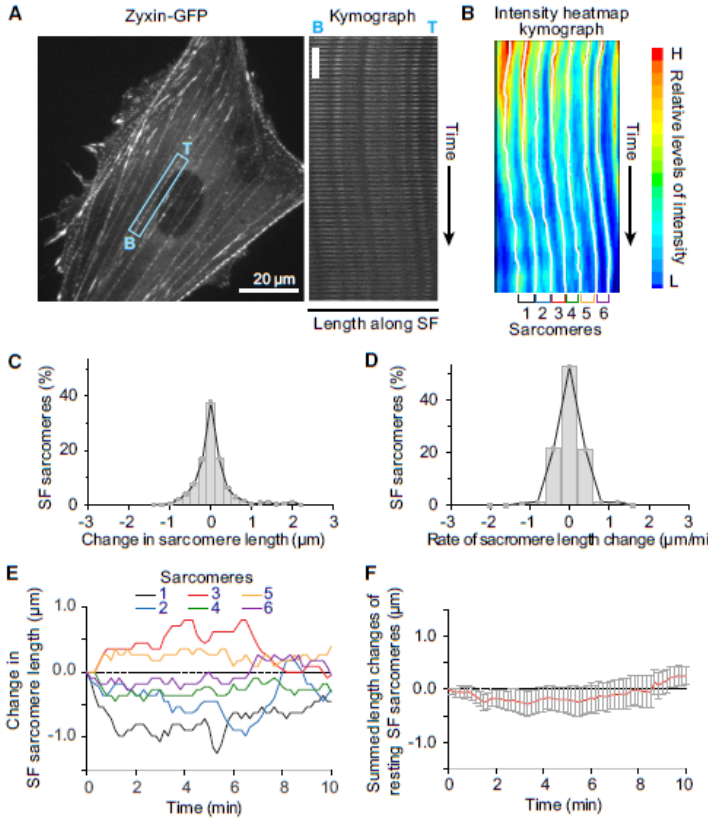

FIGURE 1 Fluctuations of stress fiber sarcomeres in vivo maintain stress fiber homeostasis. (*A*) Using mouse embryonic fibroblasts stably expressing zyxin-GFP, the centers of resting stress fibers were imaged over time and represented using a kymograph. Top and bottom of the region is labeled in the image and kymograph (*blue T* and *B*). (*Vertical shaded bar*) 1 min on the kymograph. (*B*) Fluorescent intensity linescan data were analyzed by tracking peak intensity values over time (*open lines*) and shown as an intensity heatmap kymograph. Colors in heatmap indicate relative level of fluorescent intensity. (*C*) Frequency distribution of sarcomere length change from the first frame. $n = 9$ SFs, 7 cells, 58 sarcomeres, and 3458 total points. The frequency distribution has binning of 0.2 μm, which satisfies the Nyquist sampling criteria. (*D*) Frequency distribution of the rates of sarcomere length change. (*E*) One example of sarcomere length changes over time for the SF shown in panels *A* and *B*. The color of the line pairs with the same color markings of labeled sarcomeres in panel *B*. (*F*) The net change in sarcomere length for adjacent sarcomeres, and the mean of nine SFs is shown. Error bars represent SE.

changes in sarcomere length of up to 50% compared to the initial sarcomere length.

In addition to sarcomere length change, we also determined how rapidly a SF sarcomere lengthens or shortens, and also how the length changes in individual sarcomeres may contribute to the overall change in length of 4–10 sarcomeres in series. Rates of sarcomere length change were calculated for each sarcomere, and individual sarcomeres exhibited shortening or elongation rates of 1.3 μm/min when observed during 10-s intervals. However, the average rate of change is zero for a 10-min image sequence, indicating balanced fluctuations in sarcomere length with no net length change (Fig. 1 *D*).

We next asked how the changes in sarcomere length were distributed across the SF, and whether some sarcomeres changed more than others or if there were equal changes in all sarcomeres. When length change of individual sarcomeres in a six-sarcomere unit length in a stress fiber is plotted over time for 10 min, we observe sarcomeric length fluctuations in which single sarcomeres lengthen or shorten, and generally return to their initial resting length (Fig. 1 *E*). Among all of the sarcomeres that changed their length (regardless of whether they returned to their initial length), ~74% returned to their original length within 2.5 ± 0.2 min (mean ± SE, data not shown). Approximately 26% of the sarcomeres do not return to the original sarcomere length during the average fluctuation cycle. Additionally, cycles of sarcomere length change were not all alternating cycles of lengthening and shortening. We observed many sarcomeres to have consecutive episodes of lengthening or shortening and return to the initial sarcomere length between these two cycles.

To test whether these sarcomere length changes contributed to overall shortening or lengthening of all sarcomeres in series, we calculated the net length change of the sarcomeres in series (Fig. 1 *F*). Despite individual sarcomeres undergoing episodes of shortening or lengthening, there was very little overall change in length across multiple sarcomeres. This illustrates that whereas individual sarcomeres undergo a range of positive and negative length changes as illustrated in Fig. 1 *E*, a SF segment of six sarcomeric units can retain its overall length—an indication of local compensation for the elongation or contraction of individual sarcomeric units.

Strain events in individual sarcomeres introduce dramatic regional structural change to the stress fiber

A strain event is identified as elongation of a single sarcomere that, on average, exceeds elongation speed that is observed in resting SF sarcomeres by 0.5 μm/min, and can be easily identified in zyxin-GFP-expressing cells because zyxin accumulates at the strain sites (Fig. 2 *A*, *white arrowhead*; image of whole cell included in Fig. S1 in the Supporting Material). Zyxin-GFP puncta were identified and the peak fluorescence intensity was tracked over time and the length of the strain-site sarcomere was calculated (Fig. 2, *A* and *B*). The time frame of each strain event was determined by fitting a Gaussian curve to smoothed derivative data and time boundaries were determined where the Gaussian fit line approached zero (see Fig. S2, *A* and *B*).

Using this method, we found that a strain event is sustained for an average of 5.5 $\pm$ 0.6 min (mean $\pm$ SE; see Fig. S2 *C*). In comparison to dynamics of resting SF sarcomeres, it was found that strain events can be associated with significant sarcomere lengthening that, in our samples, reached a maximum of 5.5 μm, accounting for a 275% increase in sarcomere length ($p < 0.0001$, Fig. 2 *C*), with an average maximum net elongation of 2.7 $\pm$ 0.4 μm, or 125.0 $\pm$ 20.2%. Additionally, the rate at which strain sites extend is significantly faster than sarcomere length changes in resting SFs ($p < 0.0001$, Fig. 2 *D*).

We next sought to identify features that could be used to predict where in the SF a strain event might occur. To test whether the SF strain events happen in longer, presumably weaker units, the initial length of the future strain-site sarcomere was compared to the initial lengths of its neighboring sarcomeres (i.e., within the four closest sarcomeres on each side of the strain-site sarcomere). At the beginning of the strain event, the length of future strain-site sarcomeres is significantly longer than neighboring sarcomeres, as well as the resting SF sarcomeres (Fig. 1 and $p < 0.005$, $p = 0.0009$, Fig. 2 *E*); further, neighboring sarcomeres are

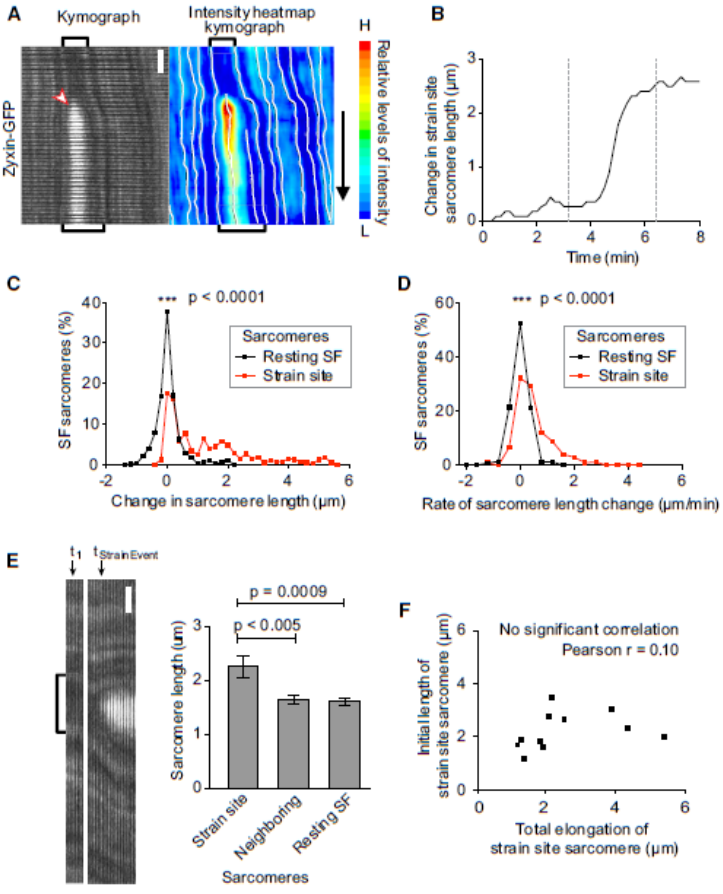

FIGURE 2 Strain events in individual sarcomeres introduce dramatic structural change to the stress fiber. (*A*) Strain events can be identified as acute, local elongation of a single sarcomere with recruitment of zyxin (*white arrowhead*) to central regions of SFs. Elongation of the strain-site sarcomere and its neighboring sarcomeres is visualized using zyxin-GFP-expressing cells, and peaks in fluorescence intensity are tracked over time (*white lines on intensity heatmap kymograph*). Images were taken at 10-s intervals. (*Vertical gray bar*) 1 min. (*B*) The strain-site sarcomere elongates over time. A specific time span was determined for each strain site (*dotted lines*; see Fig. S2 in the Supporting Material) with an average time frame of 5.5 $\pm$ 0.6 min. (*C*) Frequency distribution of the changes in sarcomere length from the first frame of the imaging period in resting SFs (*gray line*, Fig. 1 *C*) and strain-site sarcomeres (*red line*). $n = 13$ SFs, 11 cells, and 13 strain-site sarcomeres. (*D*) Frequency distribution of the rate of sarcomere length change in resting SFs (*black line*, from Fig. 1 *D*) and strain-site sarcomeres (*red line*). (*E*) Sarcomeres were identified as a future strain-site sarcomere (*black bracket*, and as indicated by zyxin accumulation at $t_{StrainEvent}$) or neighboring sarcomeres. Sarcomere lengths were measured in the first frame of the strain event (t_1). Sarcomere lengths of the future strain site were compared to the neighboring sarcomere lengths and lengths of sarcomeres in resting SFs. There was a significant difference between the future strain-site sarcomere length and lengths of sarcomeres adjacent to strain sites. $n = 11$ future strain-site sarcomeres, 98 neighboring sarcomeres, and 87 resting sarcomeres reported on in Fig. 1. (*F*) The length of the future strain-site sarcomere compared to its final amount of elongation.

similar to resting SF sarcomeres in length ($p = 0.7128$, Fig. 2 *E*). This significant difference between sarcomere lengths may point to a structural deficiency that makes a single sarcomere less able to withstand sudden changes in tension within a stress fiber.

We then sought to determine whether the initial length of the strain-site sarcomere may be related to the extent to which the strain site elongates. One possibility is sarcomeres that are initially longer may lead to strain sites that elongate more than others. We found that initial sarcomere length was not a factor in the final strain-site sarcomere extension length (Pearson's $r = 0.31$, Fig. 2 *F*). These data suggest the starting length of future strain-site sarcomeres does not dictate the final extension length.

Strain events become sites of new sarcomere addition in central regions of SFs

It has been shown that strain events result in actin repair and enhanced mechanical stability of the SF (16), though the long-term restoration of SF homeostasis has not been characterized in detail. Many groups have described the addition of new sarcomeres at the SF-focal adhesion junction (12,15,17), but sarcomere addition in other regions of a stress fiber has not been reported. Here we asked whether the elongated strain-site sarcomere remodels to form nascent sarcomeres within its boundaries. By imaging live cells, we found that the rapid zyxin accumulation at acute strain sites resolves into new distinct zyxin-rich dense bodies in 12.2 ± 1.5 min (Fig. 3 *A*, *white arrowheads*; image of whole cell included in Fig. S3 and Fig. S4 *A*).

Most strain-site sarcomeres grow from one sarcomere into three sarcomeres separated by two newly formed zyxin striations (see Fig. S4 *B*), though the addition of more than three sarcomeres has also been observed (such as the example in Fig. 3 *A*). The appearance of these newly formed zyxin-rich dense bodies occurred while the rest of the SF remained in focus, and persisted for the entire imaging period. Once new sarcomeres have been established, their lengths are similar to sarcomere lengths in resting SFs (Fig. 3 *B*). Within the time of strain-site remodeling and new sarcomere formation, there can also be remodeling of the neighboring sarcomeres where single or multiple neighboring sarcomeres shorten, then disappear (see Fig. S4 *C*). The regions of shortening sarcomeres flanking the strain site may be locations of sinks, which were described previously (15). A more detailed explanation of image analysis of new sarcomere establishment is included in Fig. S5.

Sarcomeres that neighbor the strain site undergo rapid changes to compensate for strain-site elongation

The progression of a strain event involves acute, local elongation within a single sarcomere. How do neighboring sarcomeres respond to such rapid, local strain events?

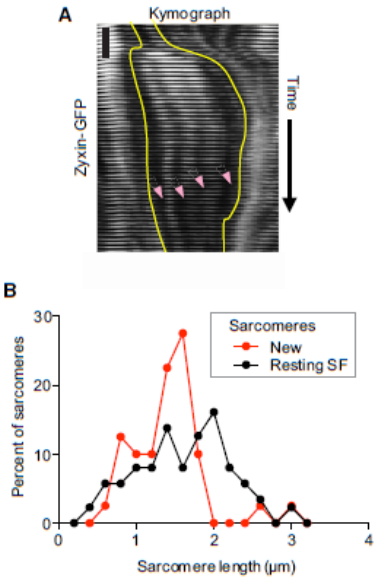

FIGURE 3 Strain events become sites of new sarcomere addition in central regions of SFs. (*A*) A kymograph of a strain site in a zyxin-GFP-expressing cell. From the initial site of zyxin recruitment, new sarcomeres form (*white arrowheads*) as indicated by distinct borders of adjacent sarcomeres. Images were taken at 30-s intervals, for 60 min. (*Vertical black bar*) 4 min. (*B*) The lengths of newly formed sarcomeres after a strain event (*gray line* in print, *red line* online, $n = 40$ sarcomeres) are not significantly different than the lengths of resting SF sarcomeres ($p = 0.11$) (*black line*, $n = 87$).

Based on our analysis of resting SF sarcomeres (specifically, local compensation for the elongation or contraction of individual sarcomeric units), we postulated that there would be a collective shortening of SF sarcomeres in response to an acute strain event. To address this question of local compensation, neighboring sarcomeres were paired to each other based on their proximity to the strain site, and their sarcomere length changes during the strain event were collected (Fig. 4 *A*; SF is shown in context of the whole cell in Fig. S1). When changes in the first four pairs of sarcomeres were added together to determine a net change over time, compared to the sarcomere length in the initial frame, it was found that neighboring sarcomeres shorten to account for the strain-site extension (Fig. 4 *B*). We then asked whether each pair of sarcomeres contributes equally to the shortening response, or whether there is a gradient of shortening along the SF. At the end of the strain event, total compensatory shortening for each pair of neighboring sarcomeres was plotted as a percent of the strain-site elongation. There are statistically similar amounts of percent compensatory shortening between the first four closest pairs of sarcomeres, ranging between 20.1 and 34.1% (Fig. 4 *C*). When

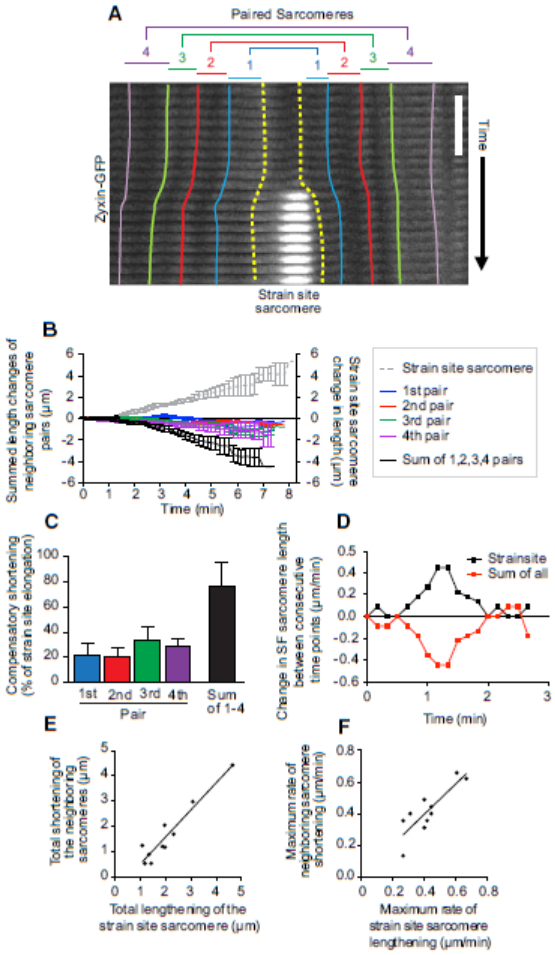

FIGURE 4 Sarcomeres that neighbor the strain site undergo rapid changes to compensate for strain-site elongation. (*A*) Sarcomeres were labeled according to their proximity to the strain-site sarcomere (at *top*, number labels; *colored lines* show sarcomere borders). Images were taken at 10-s intervals. (*Vertical gray bar*) 1 min. (*B*) Plot of changes in sarcomere length over time, starting with the initial frame of the strain event. The graph includes the mean and SE of the strain-site sarcomere (*dotted gray line*), neighboring pairs of sarcomeres 1–4 (*blue*, *red*, *green*, and *purple lines*, respectively) and the net distance change of all neighboring sarcomeres 1–4 (*black line*). (*C*) The amount of neighboring sarcomere shortening as it compares to strain-site lengthening, as a percent. $n = 9$ SFs, 8 cells, 9 strain sites, and the neighboring sarcomeres. (*D*) Plot of derivatives over time. The change in sarcomere length between consecutive time points shown for the strain-site sarcomere (*black line*) and as many of the neighboring sarcomeres as included in the original image (4–6 sarcomeres on one or both sides, *red line*). (*E*) The total shortening of the four closest pairs of neighbors were compared to the total lengthening of the strain-site sarcomere. $n = 10$ SFs, 8 cells, 10 strain sites, and the neighboring sarcomeres. (*F*) The maximum rate of sarcomere length change was plotted for paired strain sites and neighboring sarcomeres. If the strain site elongates at a high rate, the neighbors shorten at a similar rate.

taken together, the mean percent of compensatory shortening of the first four sarcomere pairs was 76.8 ± 18.5% of the strain-site lengthening (mean ± SE, Fig. 4 *C*). These data indicate there is a similar shortening response of the four closest pairs of sarcomeres, with an average net shortening comparable to nearly 80% of the extension that occurs in the strain-site sarcomere.

We next compared the rate of neighboring sarcomere length changes with that of the strain site itself. In particular, we analyzed changes in neighboring and strain-site sarcomere length between consecutive time points (10 s) during the window of time when the strain site is undergoing the greatest amount of continuous lengthening, which was found to be 1.8 ± 0.3 min (Fig. 4 *D*). Analyzing the rate of sarcomere length change in this way emphasized that the period of rapid strain-site lengthening (Fig. 4 *D*, *black line*) was accompanied by a parallel shortening response of the neighboring sarcomeres (Fig. 4 *D*, *red line*). When the four closest sarcomeres on each side of the strain site were analyzed during this shorter window of rapid change, it was found there is a striking correlation between total amount of shortening and the amount of strain-site lengthening (Pearson's $r = 0.95$, Fig. 4 *E*). When the maximum rate of strain-site lengthening was compared to the maximum rate of neighbor sarcomere shortening, there was also a correlative relationship, suggesting the changes in the neighboring sarcomeres occur on a similar timescale as the strain-site elongation (Pearson's $r = 0.84$, Fig. 4 *F*).

Strain-site and neighboring sarcomeres show similar "sidedness"

Many groups have focused on mechanosensitivity of regions of the SF. Specifically the junction of the SF and the focal adhesion has been studied as a location of SF extension and actin polymerization (12,15,17), illustrating some polarity in the response to strain. We wondered about the symmetry of the strain events and whether the shortening of sarcomeres adjacent to the strain site mirrored the symmetry (or lack thereof) at the strain site. To answer this question, we took advantage of the observation that some strain events elongate equally on each side, whereas others display an asymmetric extension of the strain site (Fig. 5, *A* and *B*). The location of the SF within the cell does not seem to be a factor in either occurrence of strain events or their asymmetric lengthening, and images of the SFs in context of the whole cell are included in Fig. S6, *A* and *B*.

Neighboring sarcomeres were analyzed for shortening trends on either side of the strain event. The net change in sarcomere length was determined for each side, then compared to the total response and was reported as a percentage (Fig. 5, *C* and *D*). To investigate the relationship of "sidedness" of the strain site and the neighboring sarcomeres, we compared the contribution of each side of

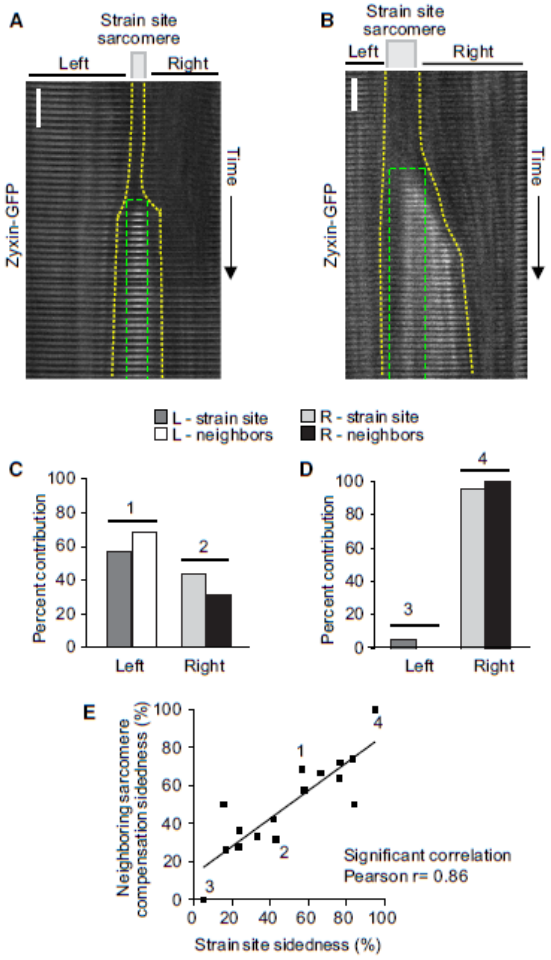

FIGURE 5 Strain-site and neighboring sarcomeres show similar sidedness. (*A* and *B*) The strain-site sarcomere was identified (*thick dotted lines toward the edges*) and compared over time to the initial boundaries of the strain-site sarcomere (*thin dashed lines near the centers*). (*Vertical gray bar*) 1 min. (*C* and *D*) The summed contributions of each side during strain-site elongation and neighboring sarcomere shortening. Left- and right-side contributions are shown of each example in panels *A* and *B*. (*E*) The amount of extension from the initial borders of the sarcomere (as shown in *A* and *B*) were compared to the net changes in neighboring sarcomere length (as shown in *C* and *D*). The percent strain-site elongation in one direction was paired with the percent shortening of neighboring sarcomeres on the same side. Each strain event has two data points on the graph, which represent information from each side of the strain site (*scatter points* from examples 1–4 are indicated). $n = 16$, 8 SFs, 8 strain-site sarcomeres, and the neighboring sarcomeres.

the strain site with the percent contribution of the corresponding side of neighboring sarcomeres in a scatter plot, including the examples in *C* and *D* as labeled points (1–4, Fig. 5 *E*). There is a significant correlation (Pearson's $r = 0.86$) and suggests there is some ability for the strain-site sarcomere neighbors to adjust the amount of sarcomeric shortening according to the amount of strain-site extension that occurs within a half-sarcomere.

DISCUSSION

SFs are contractile actomyosin structures that are tension-bearing and producing elements within cells. Although SFs were recognized as major cytoskeletal elements more than 35 years ago (24,25), much remains to be learned about their structural organization and behavior. Here we have used high-resolution live-cell imaging to visualize strain dynamics in intact SFs within living cells that were not disturbed by any chemical or physical manipulation. We have tracked fluctuations in individual sarcomere lengths using zyxin-GFP to monitor the lateral borders of sarcomeric units within a stress fiber. By this approach, we have been able to track sarcomeric strain dynamics along the length of a stress fiber at higher resolution than has been achieved using methods such as photobleaching where SF segments can be examined, but analysis at the level of individual sarcomeres is not possible (26). By monitoring the behavior of individual contiguous sarcomeres within a stress fiber segment, we have found evidence for dynamic fluctuations of sarcomere length in resting SFs. Individual sarcomeres shorten and lengthen over time, whereas a stable overall SF length is maintained.

We have previously reported that SFs experience stochastic local strain events that are revealed by dramatic single sarcomere extension (16). In our study, by analyzing the behavior of sarcomeres that surround sites of acute strain, we found evidence for lateral *trans*-sarcomeric communication along the length of the SF with compensatory shortening observed in adjacent sarcomeres. These observations highlight the existence of a SF-resident mechanism for tensional homeostasis (Fig. 6) that relies on bidirectional lateral communication of mechanical information along the length of a stress fiber. Moreover, we have determined that sarcomeres that undergo extreme strain, as evidenced by an increase in length that exceeds twofold, are remodeled to generate multiple new sarcomeres. These findings illustrate the ability of strain to trigger sarcomere addition, and highlight what is believed to be a novel mechanism for incorporating additional structural units in response to mechanical cues. Our results also provide pioneering evidence of the ability of a stress fiber to establish new sarcomeres along its length, and not just at its focal adhesion-tethered ends.

Stress fiber sarcomeres display dynamic length fluctuations in living cells

Our analysis of sarcomere dynamics in resting SFs that were not disturbed illustrates the occurrence of random positive and negative changes in individual sarcomeric length of

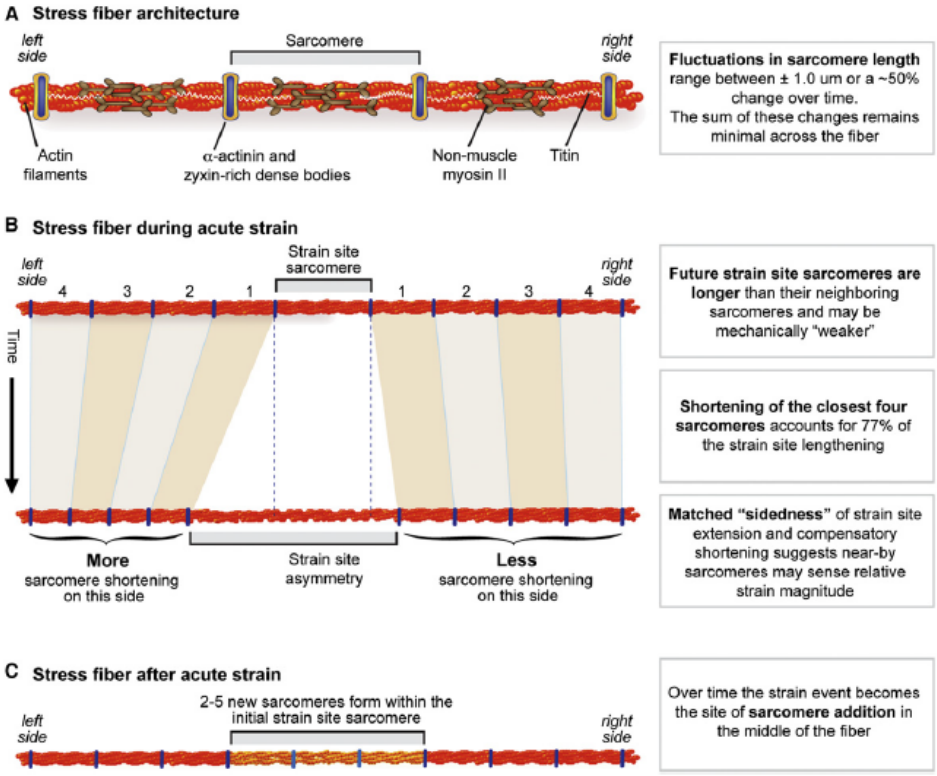

FIGURE 6 Actin stress fiber dynamics work to maintain structural homeostasis.

up to 1.0 μm. This extension and shortening of sarcomeres represents changes in sarcomere length up to 50% of the initial measured end-to-end distance. Sarcomere lengthening, relative to baseline, is an indicator of positive strain. Sarcomere shortening, indicative of negative strain. We have tracked the net change in SF length in a series of sarcomeres and observed that, despite the significant length changes that can occur in individual sarcomeres, little net change in total length occurs when including a number of sarcomeres in series. These findings suggest the existence of a SF-resident mechanism for maintaining tensional homeostasis.

Longer sarcomeres are predisposed to becoming sites of acute strain

Local SF strain events occur spontaneously in cultured cells (16) and are evident as rapid elongation of zyxin-labeled individual sarcomeric units. Here we report that the sarcomeres, which go on to become the sites of acute local lengthening, tend to be longer than sarcomeres adjacent to strain sites. Of the 58 sarcomeres on different SF segments that we observed, the majority of the future strain-sites sarcomeres were longer than neighboring sarcomeres. Nonhomogeneous sarcomere lengths have been previously described in unstimulated cells (26); our observations provide evidence for a mechanical consequence to the structural variation in a stress fiber, in which longer sarcomeres tend to be sites of potential weakness.

The underlying molecular features that might predispose a sarcomere to strain are not completely understood. Differences in the amount of cross-linking proteins like α-actinin, which have been shown to alter the stiffness of actin networks (27,28), could occur and lead to heterogeneous mechanical properties of individual sarcomeres. Analysis of skeletal muscle sarcomere dynamics has led to a proposed "popping sarcomere" theory where an individual muscle fiber sarcomere can suddenly extend to a length that is greater than the cross-bridge would normally allow (29). These events are postulated to occur in weak muscle-fiber sarcomeres, which are defined as sarcomeres that have greater lengths than their neighbors (29).

Conversely, strong muscle-fiber sarcomeres are characterized as having shorter lengths. In the SF setting, if there

is less actin filament overlap in longer SF sarcomeres, there would be less exposure to sliding frictional force compared to shorter sarcomeres. When there was an increase in tension across the SF, it is possible that the sarcomere with less resistance to sliding frictional forces might be predisposed to undergo a strain event. Local differences in actin SF elasticity has been reported (30,31), and single skeletal muscle fiber sarcomeres have been shown to have varying amount of actin thin filaments and bound myosin (32). This, or other types of underlying molecular heterogeneity, may account for mechanical differences among adjacent sarcomeres.

New sarcomeres can be added in the middle of the stress fiber

Many groups have described the addition of new sarcomeres at the focal adhesion-SF junction where actin SFs assemble and move along the SF away from the focal adhesion (12,15,17,18). The addition of new sarcomeres is largely thought to be tension-dependent, where greater tensile stress leads to faster addition of sarcomeric units (12,17). Here we have reported that sarcomere addition is not limited to the SF-focal adhesion junction, and can occur in the central region after acute local strain events at the same location. It is worth noting that, even though the locations of new sarcomeres are different, what triggers the formation of new sarcomeres seems to be the same: increases in tension. The formation of new sarcomeres after a strain event occurs under tension (16), like the addition of sarcomeres at the focal adhesion-SF junction (12,17), though the direct link between tension and rate of formation or number of new sarcomeres in the center of the SF has not been examined.

Although no significant difference between mean lengths of the resting SF sarcomeres and the new sarcomeres was observed, the length distributions for old versus new sarcomeres were distinct. Almost 20% of resting SF sarcomeres displayed lengths >2.0 μm, whereas only 5% of newly formed sarcomeres were longer than 2.0 μm. The predominance of shorter sarcomeres may indicate a change in load-bearing potential along the SF after a strain event.

Sarcomeres flanking the strain site shorten to accommodate acute local lengthening

We have directly measured the dynamic behavior of the four closest sets of sarcomeres flanking the strain site as the strain site elongates. It has been previously reported that SFs have regional compensatory behavior along their length (13). Here we have described a highly localized process of compensatory sarcomeric shortening in response to acute strain events. As the strain site extends, the closest four sets of neighboring sarcomeres shorten to account for nearly 80% of the elongation. Each pair shortens roughly the same amount, which would mean the entire strain event could theoretically be accounted for by compensatory shortening of the five or six closest sarcomere pairs. Technical challenges made it difficult to reliably track >9–10 sarcomeres in series along SFs in living cells; thus, the lateral range of the compensatory response outside of the sarcomeres that are directly visualized can only be inferred. Nonetheless, it was clear from our analysis that cumulative amount of compensatory shortening of the strain-site neighboring sarcomeres varies depending on the total elongation of the strain event, and the rate of shortening correlates with the rate of strain-site lengthening.

Focal adhesions have long been recognized as locations where mechanical information is transmitted (33,34); however, more recently, the actin cytoskeleton itself has been shown to be mechanosensitive (35,36). For example, cytoskeletal stiffness increases as fibroblasts experience stiffer gel substrates (37), indicating the ability to sense mechanical stimuli and undergo a matched global cytoskeletal response. Although the amount of actin cytoskeletal remodeling can be linked to differences in mechanical stimuli, the exact mechanisms of actin cytoskeletal sensitivity to changes in force magnitude are not yet well characterized (38). Here we present another example of a highly localized strain-sensitive mechanoresponse by the actin cytoskeleton.

Strain-site elongation and the compensatory shortening of neighboring sarcomeres occur in the same time domain and suggest the possibility of multiple cause-effect relationships. For example, increased contractility in neighboring sarcomeres may drive the elongation of the single strain-site sarcomere. Alternatively, as the strain site elongates, the flanking sarcomeres may passively shorten due to increased slack in the system. A combination of these factors may also be present. Although the source of increased tension across the SF is not yet believed known, our discovery of the localized compensatory shortening response that occurs at the same time a single sarcomere experiences significant positive strain is, to our knowledge, novel.

Several groups have reported that release of SF tension induces buckling of the fibers and subsequent actin remodeling (39–42). For example, after an instantaneous 26% shortening of an elastic substrate where cells were cultured, SFs of these cells deform and disassemble, via a process that ultimately restores prerelease architecture (39). Our findings show an instantaneous shortening response by sarcomeres that reside adjacent to a strained sarcomere. The lack of evidence of SF buckling in our system illustrates that dramatic deformation of the SF is not required to induce a compensatory contractile response. The SF appears to be exquisitely sensitive to even highly localized mechanical stress.

Trans-sarcomeric communication allows for a strain-sensitive shortening response

Sarcomeric shortening responses are often asymmetric, and the amount of neighboring sarcomere shortening correlates

with the asymmetry of strain-site elongation. Asymmetric sarcomere lengthening has been observed in striated muscle fibers (32). One protein that associates with both Z- and M-lines is titin, which has been shown to respond to different magnitudes of stretch (43,44). Titin itself, as well as other proteins associated with the Z-line, is thought to engage in signaling events not only in cardiac muscle fibers but also actin SF sarcomeres (43,45). Additionally, titin filaments are hypothesized to become stiffer when overstretched and have been implicated as a cause of half-sarcomere nonuniformity in striated muscle fibers (32). Differences in titin stiffness or some other underlying molecular heterogeneity, such as variable elasticity or actin and myosin content (30–32), could explain the strain-site asymmetry in actin SFs. Additionally, molecular heterogeneity may occur across a single SF that is experiencing changes in mechanical properties, just as molecular heterogeneity can occur between SFs experiencing changes in mechanical properties in different locations in the cell (46,47).

CONCLUSIONS

Pioneering work has revealed the importance of the SF-focal adhesion junction in mechanosensing and force-dependent sarcomere addition to SFs (12,17). The data presented here show that sarcomeres have the capacity to sense mechanical changes and undergo sarcomere addition at locations far distant from the ends of the SF, indicating that mechanosensitivity is not limited to the ends of SFs as previously hypothesized (48). Additionally, the actin SF mechanoresponse can be highly localized to only a few sarcomeres along the length of an intact SF, allowing for rapid and efficient maintenance of the actin cytoskeleton.

SUPPORTING MATERIAL

Six figures are available at http://www.biophysj.org/biophysj/supplemental/S0006-3495(12)01080-6.

We thank the software developers Ryan Littlefield and Keith Carney for the kymograph journal in MetaMorph and "xtrack" code in MATLAB, respectively. We thank Diana Lim for graphic design.

This work was supported in part by grants from the National Institutes of Health (No. R01GM50877), the Huntsman Cancer Foundation, and shared resources from the Cancer Center Support Grant (No. 2 P30 CA42014-21) to M.C.B. Y.-T.S. is supported by grants from the National Institutes of Health (Nos. R01HL67646 and R01DK088777).

REFERENCES

1. Discher, D. E., P. Janmey, and Y. L. Wang. 2005. Tissue cells feel and respond to the stiffness of their substrate. *Science.* 310:1139–1143.
2. Hall, A. 1998. Rho GTPases and the actin cytoskeleton. *Science.* 279:509–514.
3. Jaffe, A. B., and A. Hall. 2005. Rho GTPases: biochemistry and biology. *Annu. Rev. Cell Dev. Biol.* 21:247–269.
4. Vogel, V., and M. Sheetz. 2006. Local force and geometry sensing regulate cell functions. *Nat. Rev. Mol. Cell Biol.* 7:265–275.
5. Friedrich, B. M., A. Buxboim, …, S. A. Safran. 2011. Striated actomyosin fibers can reorganize and register in response to elastic interactions with the matrix. *Biophys. J.* 100:2706–2715.
6. O'Neill, G. M. 2009. The coordination between actin filaments and adhesion in mesenchymal migration. *Cell Adhes. Migr.* 3:355–357.
7. Isenberg, G., P. C. Rathke, …, K. E. Wohlfarth-Bottermann. 1976. Cytoplasmic actomyosin fibrils in tissue culture cells: direct proof of contractility by visualization of ATP-induced contraction in fibrils isolated by laser micro-beam dissection. *Cell Tissue Res.* 166:427–443.
8. Katoh, K., Y. Kano, …, K. Fujiwara. 1998. Isolation and contraction of the stress fiber. *Mol. Biol. Cell.* 9:1919–1938.
9. Lazarides, E., and K. Burridge. 1975. Alpha-actinin: immunofluorescent localization of a muscle structural protein in nonmuscle cells. *Cell.* 6:289–298.
10. Weber, K., and U. Groeschel-Stewart. 1974. Antibody to myosin: the specific visualization of myosin-containing filaments in nonmuscle cells. *Proc. Natl. Acad. Sci. USA.* 71:4561–4564.
11. Colombelli, J., A. Besser, …, E. H. Stelzer. 2009. Mechanosensing in actin stress fibers revealed by a close correlation between force and protein localization. *J. Cell Sci.* 122:1665–1679.
12. Endlich, N., C. A. Otey, …, K. Endlich. 2007. Movement of stress fibers away from focal adhesions identifies focal adhesions as sites of stress fiber assembly in stationary cells. *Cell Motil. Cytoskeleton.* 64:966–976.
13. Peterson, L. J., Z. Rajfur, …, K. Burridge. 2004. Simultaneous stretching and contraction of stress fibers in vivo. *Mol. Biol. Cell.* 15:3497–3508.
14. Rossier, O. M., N. Gauthier, …, M. P. Sheetz. 2010. Force generated by actomyosin contraction builds bridges between adhesive contacts. *EMBO J.* 29:1055–1068.
15. Russell, B., M. W. Curtis, …, A. M. Samarel. 2010. Mechanical stress-induced sarcomere assembly for cardiac muscle growth in length and width. *J. Mol. Cell. Cardiol.* 48:817–823.
16. Smith, M. A., E. Blankman, …, M. C. Beckerle. 2010. A zyxin-mediated mechanism for actin stress fiber maintenance and repair. *Dev. Cell.* 19:365–376.
17. Guo, W. H., and Y. L. Wang. 2007. Retrograde fluxes of focal adhesion proteins in response to cell migration and mechanical signals. *Mol. Biol. Cell.* 18:4519–4527.
18. Hotulainen, P., and P. Lappalainen. 2006. Stress fibers are generated by two distinct actin assembly mechanisms in motile cells. *J. Cell Biol.* 173:383–394.
19. Usui, T. 2007. Actin- and microtubule-targeting bioprobes: their binding sites and inhibitory mechanisms. *Biosci. Biotechnol. Biochem.* 71:300–308.
20. Deguchi, S., and M. Sato. 2009. Biomechanical properties of actin stress fibers of non-motile cells. *Biorheology.* 46:93–105.
21. Kumar, S., I. Z. Maxwell, …, D. E. Ingber. 2006. Viscoelastic retraction of single living stress fibers and its impact on cell shape, cytoskeletal organization, and extracellular matrix mechanics. *Biophys. J.* 90:3762–3773.
22. Russell, R. J., S. L. Xia, …, T. P. Lele. 2009. Sarcomere mechanics in capillary endothelial cells. *Biophys. J.* 97:1578–1585.
23. Hoffman, L. M., C. C. Jensen, …, M. C. Beckerle. 2006. Genetic ablation of zyxin causes Mena/VASP mislocalization, increased motility, and deficits in actin remodeling. *J. Cell Biol.* 172:771–782.
24. Bragina, E. E., J. M. Vasiliev, and I. M. Gelfand. 1976. Formation of bundles of microfilaments during spreading of fibroblasts on the substrate. *Exp. Cell Res.* 97:241–248.
25. Burridge, K. 1981. Are stress fibers contractile? *Nature.* 294:691–692.

26. Guolla, L., M. Bertrand, …, A. E. Pelling. 2012. Force transduction and strain dynamics in actin stress fibers in response to nanoNewton forces. *J. Cell Sci.* 125:603–613.

27. Esue, O., Y. Tseng, and D. Wirtz. 2009. Alpha-actinin and filamin cooperatively enhance the stiffness of actin filament networks. *PLoS ONE.* 4:e4411.

28. Burridge, K., and J. R. Feramisco. 1981. Non-muscle α-actinins are calcium-sensitive actin-binding proteins. *Nature*. 294:565–567.

29. Morgan, D. L. 1990. New insights into the behavior of muscle during active lengthening. *Biophys. J.* 57:209–221.

30. Charras, G. T., and M. A. Horton. 2002. Determination of cellular strains by combined atomic force microscopy and finite element modeling. *Biophys. J.* 83:858–879.

31. Haga, H., S. Sasaki, …, T. Sambongi. 2000. Elasticity mapping of living fibroblasts by AFM and immunofluorescence observation of the cytoskeleton. *Ultramicroscopy.* 82:253–258.

32. Rassier, D. E. 2012. The mechanisms of the residual force enhancement after stretch of skeletal muscle: non-uniformity in half-sarcomeres and stiffness of titin. *Proc. Biol. Sci. R. Soc. B.*. http://dx.doi.org/10.1098/rspb.2012.0467.

33. Balaban, N. Q., U. S. Schwarz, …, B. Geiger. 2001. Force and focal adhesion assembly: a close relationship studied using elastic micropatterned substrates. *Nat. Cell Biol.* 3:466–472.

34. Riveline, D., E. Zamir, …, A. D. Bershadsky. 2001. Focal contacts as mechanosensors: externally applied local mechanical force induces growth of focal contacts by an mDia1-dependent and ROCK-independent mechanism. *J. Cell Biol.* 153:1175–1186.

35. Galkin, V. E., A. Orlova, and E. H. Egelman. 2012. Actin filaments as tension sensors. *Curr. Biol.* 22:R96–R101.

36. Sawada, Y., and M. P. Sheetz. 2002. Force transduction by Triton cytoskeletons. *J. Cell Biol.* 156:609–615.

37. Solon, J., I. Levental, …, P. A. Janmey. 2007. Fibroblast adaptation and stiffness matching to soft elastic substrates. *Biophys. J.* 93:4453–4461.

38. Hoffman, B. D., C. Grashoff, and M. A. Schwartz. 2011. Dynamic molecular processes mediate cellular mechanotransduction. *Nature*. 475:316–323.

39. Costa, K. D., W. J. Hucker, and F. C. Yin. 2002. Buckling of actin stress fibers: a new wrinkle in the cytoskeletal tapestry. *Cell Motil. Cytoskeleton*. 52:266–274.

40. Deguchi, S., T. S. Matsui, and M. Sato. 2012. Simultaneous contraction and buckling of stress fibers in individual cells. *J. Cell. Biochem.* 113:824–832.

41. Lu, L., S. J. Oswald, …, F. C. Yin. 2008. Mechanical properties of actin stress fibers in living cells. *Biophys. J.* 95:6060–6071.

42. Sato, K., T. Adachi, …, Y. Tomita. 2005. Quantitative evaluation of threshold fiber strain that induces reorganization of cytoskeletal actin fiber structure in osteoblastic cells. *J. Biomech.* 38:1895–1901.

43. Cavnar, P. J., S. G. Olenych, and T. C. Keller, 3rd. 2007. Molecular identification and localization of cellular titin, a novel titin isoform in the fibroblast stress fiber. *Cell Motil. Cytoskeleton.* 64:418–433.

44. Gautel, M. 2011. Cytoskeletal protein kinases: titin and its relations in mechanosensing. *Pflugers Archiv. Eur. J. Physiol.* 462:119–134.

45. Frank, D., and N. Frey. 2011. Cardiac Z-disc signaling network. *J. Biol. Chem.* 286:9897–9904.

46. Tanner, K., A. Boudreau, …, S. Kumar. 2010. Dissecting regional variations in stress fiber mechanics in living cells with laser nanosurgery. *Biophys. J.* 99:2775–2783.

47. Totsukawa, G., Y. Wu, …, F. Matsumura. 2004. Distinct roles of MLCK and ROCK in the regulation of membrane protrusions and focal adhesion dynamics during cell migration of fibroblasts. *J. Cell Biol.* 164:427–439.

48. Kirchenbuchler, D., S. Born, …, R. Merkel. 2010. Substrate, focal adhesions, and actin filaments: a mechanical unit with a weak spot for mechanosensitive proteins. *J. Phys. Cond. Matter.* 22:194109.

Supplementary Information for the manuscript entitled: **"Lateral communication between stress fiber sarcomeres facilitates a local remodeling response"**

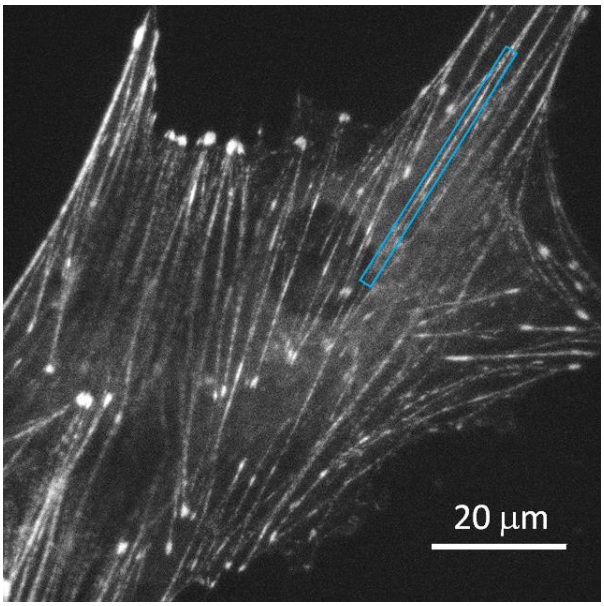

Supplementary Figure S1: The cell in which the stress fiber in Figure 2A was imaged. The stress fiber shown in Figure 2A is outlined in the *blue box*.

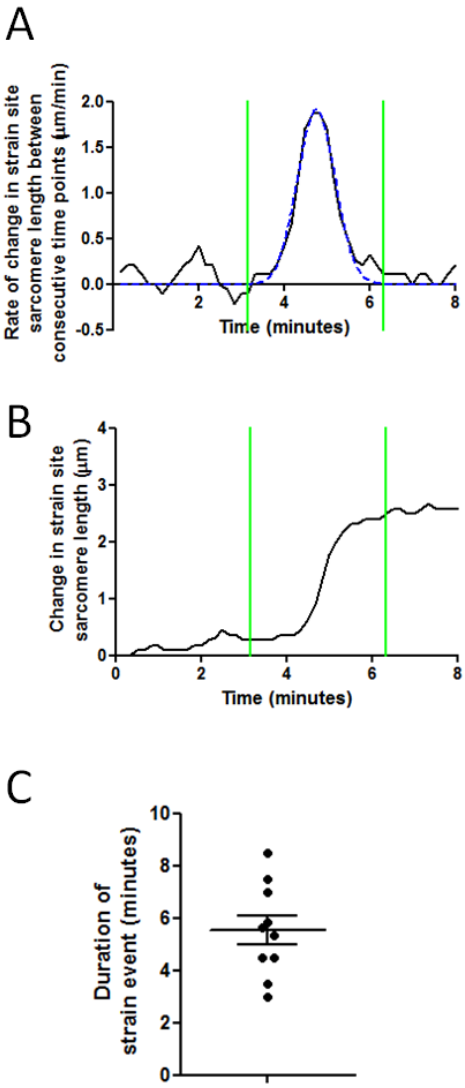

Supplementary Figure S2: Determining the duration of a strain event. *(A)* Starting with the data showing a change in strain site sarcomere length, the derivatives were found for each time point. The derivatives underwent smoothing (*black line*) before being fit with a Gaussian curve (*blue line*). The time of the event was determined by identifying where the Gaussian line approached zero (*vertical green lines*). *(B)* Application of the time frame to the change in strain site sarcomere length data. This was done for each strain event to consistently apply a set time range used during analysis. *(C)* The average duration of a strain event using this method is 5.5 ± 0.6 minutes.

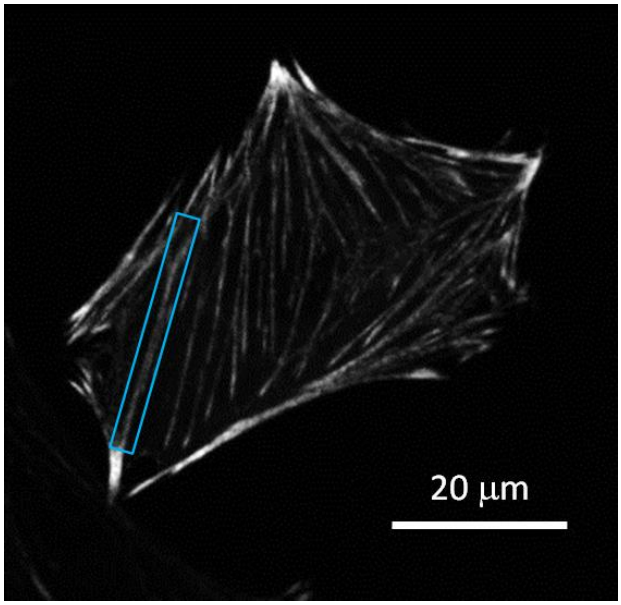

Supplementary Figure S3: The cell in which the stress fiber in Figure 3A was imaged. The stress fiber shown in Figure 3A is outlined in the *blue box.*

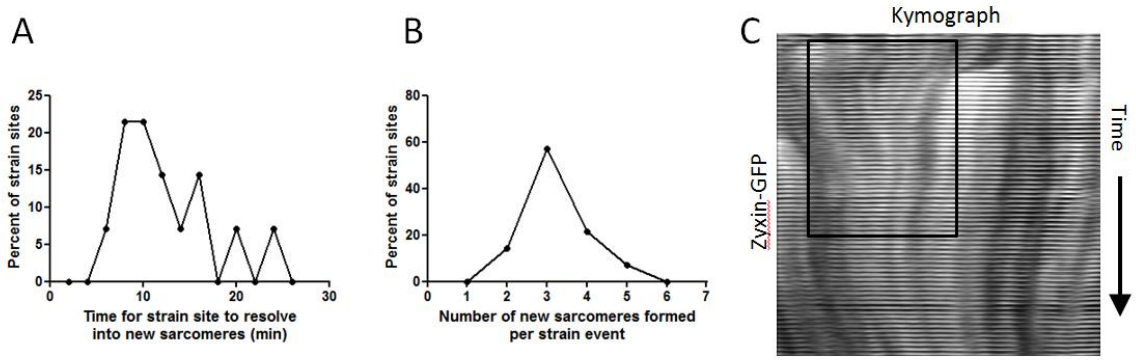

Supplementary Figure S4: Sarcomeres neighboring strain sites condense and some can be eliminated. *(A)* Frequency distribution of the time it takes for a strain site to remodel to form nascent sarcomeres from the initial zyxin recruitment at the strain site. *(B)* Frequency distribution of the number of new sarcomeres that are formed following a strain event. *(C)* Sarcomeres flanking a strain site sarcomere undergo shortening. Over time, it is possible the condensing sarcomeres go on to become completely removed from the SF (*black box*).

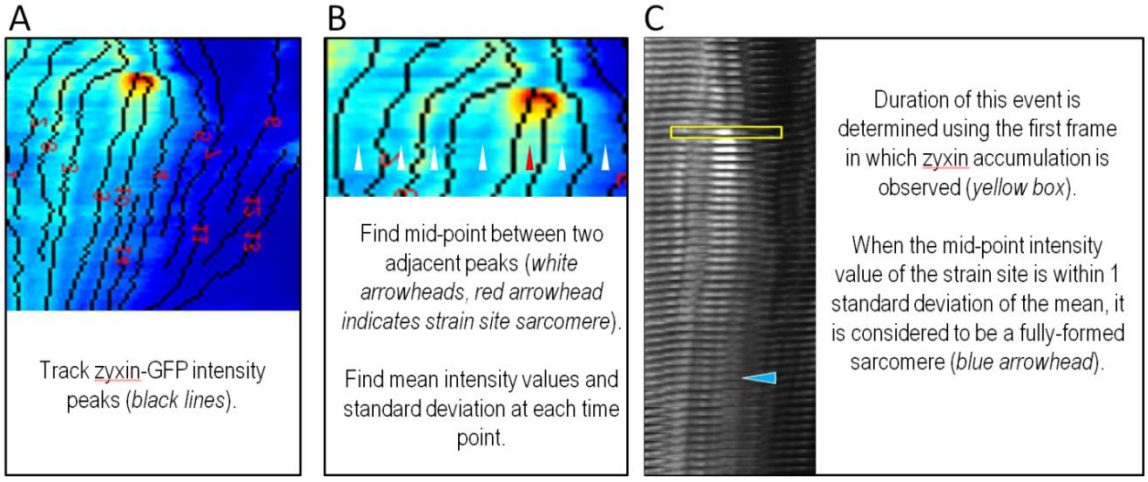

Supplementary Figure S5: Determining when the strain site remodels into distinct new sarcomeres. *(A-C)* Sequential steps of image analysis used to determine when the dissipating zyxin-GFP intensity resolves into new sarcomeres.

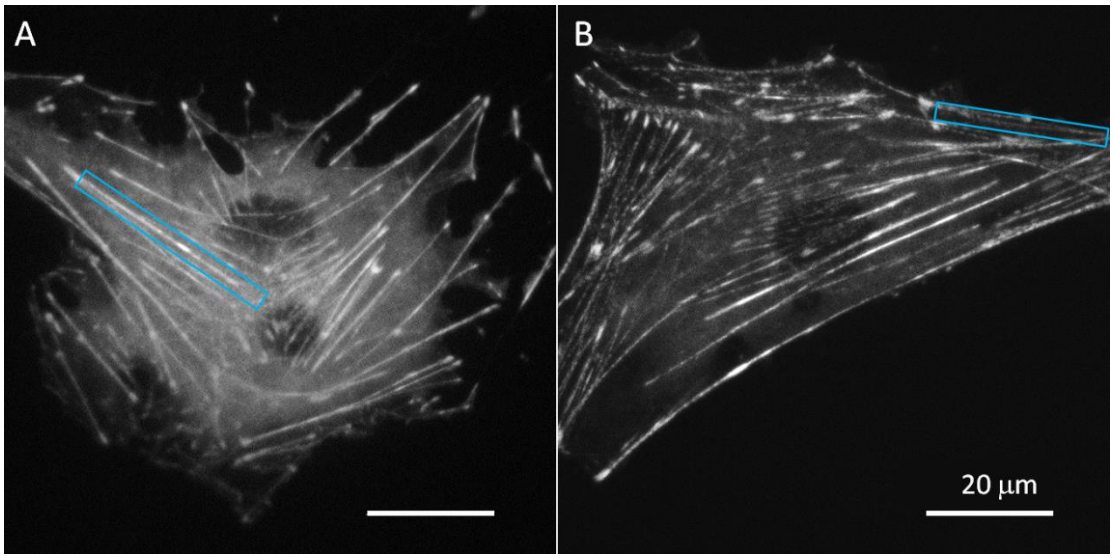

Supplementary Figure S6: The cells in which the stress fibers in Figure 5 were imaged.
(A) The stress fiber shown in Figure 5A is outlined in the *blue box. (B)* The stress fiber shown in Figure 5B is outlined in the *blue box*.

CHAPTER 4

MATHEMATICAL MODELING OF THE DYNAMIC MECHANICAL BEHAVIOR OF NEIGHBORING SARCOMERES IN ACTIN STRESS FIBERS

Chapin, L.M.ǂ, Edgar, L.T.ǂ, Blankman, E., Beckerle, M.C. and Shiu, YT

ǂ These authors contributed equally

4.1 Abstract

Actin stress fibers (SFs) in live cells consist of series of dynamic individual sarcomeric units. Within a group of consecutive SF sarcomeres, individual sarcomeres can spontaneously shorten or lengthen without changing the overall length of this group, but the underlying mechanism is unclear. We used a computational model to test our hypothesis that this dynamic behavior is inherent to the heterogeneous mechanical properties of the sarcomeres and the cytoplasmic viscosity. Each sarcomere was modeled as a discrete element consisting of an elastic spring, a viscous dashpot and an active contractile unit all connected in parallel, and experiences forces as a result of actin filament elastic stiffness, myosin II contractility, internal viscoelasticity, or cytoplasmic drag. When all four types of forces are considered, the simulated dynamic behavior closely resembles the experimental observations, which include a low-frequency fluctuation in individual sarcomere length and compensatory lengthening and shortening of adjacent sarcomeres. Our results suggest that heterogeneous stiffness and viscoelasticity of actin fibers, heterogeneous myosin II contractility, and the cytoplasmic drag are sufficient to cause

spontaneous fluctuations in SF sarcomere length. Our results shed new light to the dynamic behavior of SF and help design experiments to further our understanding of SF dynamics.

4.2 Introduction

Anchorage-dependent cells exist in a state of isometric tension and are constantly subjected to mechanical cues from their environment. External mechanical signals can be sensed through focal adhesions, sites that connect and transmit forces between the actin-myosin cytoskeleton and the extracellular matrix (1, 2). The actin-myosin cytoskeleton is the primary intracellular structure generating cellular contractile force and bearing tension. Cells can also remodel the cytoskeleton in response to mechanical and chemical cues in their surroundings (3-6). The mechanisms in which actin structures remodel in response to mechanical changes are not fully understood.

Actin SFs are pre-stressed linear polymers made up of a series of sarcomeric subunits that extend along the axial length of the SF. SF pre-stress originates from myosin-based contractility and the boundary conditions tethering the filaments at one or both ends (1, 2). Similar to muscle sarcomeres, SF sarcomeres are thought to be contractile units and are identified by proteins such as α-actinin and zyxin, which make up their borders akin to the Z-line the muscle sarcomeres (7-10). Fluorescently labeled α-actinin and zyxin have been used to track sarcomere dynamics in living cells (11-16) and subsequently have led to better understanding of the dynamic structural changes that occur within SFs. These experiments provide a new opportunity for deeper investigation of SF biomechanics.

Recently we (17) and others (15, 18) reported fluctuations in SF sarcomere lengths in steady state, resting SFs. In our investigations we used mouse embryonic fibroblasts due to their robust actin cytoskeleton. We found the most changes in length occurred between 1.0 μm shortening and lengthening from the initial sarcomere length (17). We aim to develop a

mathematical model using what is known about the mechanical environment of actin SFs in order to explain the dynamics of SF sarcomeres we observed in the lab. Another goal of this model is to help design experiments needed in the future to more fully define the mechanical determinants behind sarcomere remodeling in actin SFs.

Although actin SFs have many molecular components, we focus on actin and myosin because they are the most abundant proteins in sarcomeres and likely predominate the mechanical properties and behavior of the SF sarcomeres. Nearly 75% of the dry mass of a single sarcomere isolated from *Sarcophaga bullata* flight muscle is made up of myosin and actin (19), indicating many of the structural and mechanical changes of sarcomeres may be largely due to those two proteins. Here we use our mathematical model to investigate the role of actin viscoelasticity and contractile forces from myosin as the major players responsible for sarcomere length fluctuations in resting SFs.

The mechanical properties likely vary between adjacent sarcomeres due to molecular heterogeneity that exists along these structures. In terms of actin, many computational models used to describe SF dynamics have assumed that actin stiffness is homogeneous along the length of a SF (11, 20, 21). However, there is experimental evidence suggesting SFs have local variations in actin stiffness across the cell (22, 23). The changes in actin stiffness along a single SF may result in stiffness differences amongst neighboring sarcomeres, and therefore regulate the amount of spontaneous lengthening or shortening that occurs. Our model will test the hypothesis that this variability of actin stiffness between individual sarcomeres, which varies over time, may be a major factor driving fluctuations in sarcomere length.

In addition to actin, heterogeneity of myosin-driven contractility may also contribute to the changes in sarcomere length between adjacent SF regions. Myosin II molecules arrange themselves in periodic spacing along the lengths of SFs (10). Increased myosin contractility has been hypothesized to contribute to shortening of sarcomeres in NIH3T3 mouse fibroblasts (18), though this hypothesis has not been verified by experimental testing. In laser severing induced SF

retraction assays, cells treated with myosin inhibitors (Y27632, ML7, or blebbistatin) failed to retract its actin SFs following laser severing, suggesting that the retraction of pre-stressed SFs requires myosin activity (1, 24). In contrast, SFs within cells treated with calyculin A, which stimulates continual myosin activation, exhibited simultaneous shortening of sarcomeres near focal adhesions and lengthening of sarcomeres in the center regions of the same SFs (13). Such regional variation in the sarcomeric response suggests that, in different regions of a single SF, groups of myosin motors may act independently and have different magnitudes of contraction.

Another key factor in the mechanical behavior of SFs suggested by the retraction studies was the presence of cytoplasmic drag forces (1, 25, 26). As the SF retracted through the cytoplasm, the sarcomeres near to the severed end shortened faster and by a greater amount than sarcomeres further away. The damping occurring along the length of the retracting SF suggests the presence of an external viscous force. Our model will consider for cytoplasmic drag forces acting on the actin SFs.

In summary, we hypothesized the fluctuations in sarcomere lengths in steady state, resting SFs are driven by the dynamic heterogeneity of stiffness and myosin II contraction along the length of the SF. To test this hypothesis, we designed a mathematical model of an actin SF. The mechanical determinants within our model were actin viscoelasticity, active myosin II contraction, and cytoplasmic drag forces. The model made valid predictions of a retracting SF when simulating a laser severance experiment. When random dynamic fluctuations in stiffness and myosin II contractility were added to generate dynamic heterogeneity, sarcomeres within our model exhibited spontaneous length fluctuations similar to what has been seen in vivo.

4.3 Materials and methods

4.3.1 Cell culture

Mouse embryonic fibroblasts (MEFs) from a zyxin -/- mouse, stably expressing zyxin-green fluorescent protein (GFP), were used for live cell microscopy. MEFs were cultured in

Dulbecco's Modified Eagle Media with 10% fetal bovine serum (Hyclone, Logan, UT), sodium pyruvate, penicillin/streptomycin, and L-glutamine. MEFs were plated on fibronectin-coated glass coverslips (10 μL/mL), and imaged 3-6 days after they were plated. Additional details of these methods have been previously published (16, 17, 27).

4.3.2 Imaging and data analysis

MEFs were plated in Delta TPG culture dishes (Bioptechs, Butler, PA) and were imaged in Dulbecco's Modified Eagle Media/F12 media (Invitrogen, Carlsbad, CA) with 10% fetal bovine serum. Live cell imaging was done using a spinning disk confocal (Andor Technology, Belfast, Northern Ireland) on an inverted TI300 microscope (Nikon, Melville, NY). The imaging time interval was 10 seconds during an imaging period of 10 minutes. A 60x 1.4 NA Plan Apochromat lens (Nikon) was used, along with a DV887 1024 x 1024 or DV885 512 x 512 electron-multiplying charge-coupled device cameras (Andor Technology). A more detailed description can be found in Smith et al. (16).

4.3.3 Sarcomeric model of a stress fiber

A SF was modeled using a one-dimensional series of discrete elements. Each discrete element represented a single sarcomere and consisted of a linear elastic spring, a linear viscous dashpot, and an active contractile unit all connected in parallel (Figure 4.1A). The SF was represented as N_{sarc} elements arranged end-to-end and had N_{nodes} nodes ($N_{nodes} = N_{sarc} + 1$). The length of each sarcomere was randomly assigned based on the distribution of lengths reported by Chapin et al. 2012 (17). The dynamic model ran from time $t = t_0$ to $t = t_f$ with a step size in time of t_d. The values of N_{sarc}, N_{nodes}, t_0, t_f and t_d are given in Table 4.1. For each time step, the displacement of each node was calculated by balancing all forces acting on the node from its left (L) and right (R) neighboring sarcomeres (Figure 4.1B): elastic force (f_{spring}), myosin contractile force ($f_{contract}$), internal viscous force ($f_{visc,int}$), external drag force (f_{drag}), and external load ($f_{external}$).

For all nodes numbered $i = 1$ to $i = N_{nodes}$ from left to right (positive direction points to the right), the force balance for a node i at time $t = n$ was:

Elastic force from right + Contractile force from right + Internal viscous force from right

– Elastic force from left – Contractile force from left – Internal viscous force from left

– External drag force from cytoplasm + Applied external load

= mass times acceleration

$$f^n_{springR} + f^n_{contractR} + f^n_{visc,intR} - f^n_{springL} - f^n_{contractL} - f^n_{visc,intL} - f^n_{drag} + f^n_{external} = ma^n_i \qquad \text{(Eqn. 1)}$$

In Eqn. 1, the forces acting on node i are grouped on the left, and the inertial term involving the nodal mass (m) and acceleration (a_i) are on the right. L indicates forces acting on the node from the sarcomere to the left, while R indicates forces due to the sarcomere on the right. The mass of a sarcomere was calculated from the mass of dried insect flight muscle (19) and half the sarcomere mass was projected to each node to determine nodal mass (m).

Any external force applied to the sarcomere was represented with $f_{external}$ and was considered nonzero only at the far-right node (i.e., $i = N_{nodes}$). Elastic forces were calculated using Hooke's Law, and therefore were dependent on the current length of the sarcomere and a linear stiffness (also called spring constant) k such that

$$f^n_{springL} = k_{sarcL}\Delta L_L = k_{sarcL}\left(u^n_i - u^n_{i-1}\right), \; f^n_{springR} = k_{sarcR}\Delta L_R = k_{sarcR}\left(u^n_{i+1} - u^n_i\right), \qquad \text{(Eqn. 2)}$$

where L is the sarcomere length and u_i is the displacement of node i. The stiffness of each sarcomere was set in a way so that the bulk stiffness of the SF, k_B, matched the results from ex vivo tensile testing of SFs dissected from bovine smooth muscle cells (25). Linear regression was performed on force vs. change in SF length data from Deguchi et al. to calculate k_B (k_B = 4.14 nN/μm, R^2 = 0.992). Simulations of uniaxial extension with external loads ($f_{external}$) varying from 0 to 50 nN were used to obtain a force-strain plot for our SF model when only considering passive elasticity to compare with ex vivo results from Deguchi et al. (Figure 4.1D).

The dashpot within each discrete element represented the internal viscoelasticity within the molecular structure of the SF sarcomere. The dissipative force from the dashpot component was calculated from the rate of change of length of the sarcomere and a damping parameter γ such that

$$f^{n}_{visc,intL} = \gamma \frac{d}{dt}\Delta L_L = \gamma\left(v^{n}_{i} - v^{n}_{i-1}\right),\ f^{n}_{visc,intR} = \gamma \frac{d}{dt}\Delta L_R = \gamma\left(v^{n}_{i+1} - v^{n}_{i}\right), \qquad \text{(Eqn. 3)}$$

where v_i is the velocity of node *i*.

We also considered an external viscous force (i.e., drag force) due to drag from the surrounding cytoplasm. The drag force for node *i* was calculated using the velocity of the node and a damping parameter η such that

$$f^{n}_{drag} = \eta v^{n}_{i}. \qquad \text{(Eqn. 4)}$$

Nonmuscle myosin II causes active contraction of the sarcomere. The magnitude of active contraction within each sarcomere was calculated using a force function, $h(L)$ such that

$$f^{n}_{contractL} = h(L_L),\ f^{n}_{contractR} = h(L_R), \qquad \text{(Eqn. 5)}$$

where the function $h(L)$ depends on the current length of the sarcomere (see "Myosin Contraction Model" below).

A backward difference was used to cast velocity (v) and acceleration (a) into terms involving nodal displacement:

$$v^{n}_{i} = \frac{1}{t_d}\left(u^{n}_{i} - u^{n-1}_{i}\right),\ a^{n}_{i} = \frac{1}{t_d}\left(v^{n}_{i} - v^{n-1}_{i}\right) = \frac{1}{t_d^{\,2}}\left(u^{n}_{i} - u^{n-1}_{i}\right) - \frac{1}{t_d}v^{n-1}_{i}. \qquad \text{(Eqn. 6)}$$

After substituting all the force representations (Eqns. 2-5) and numerical derivatives (Eqn. 6) into Eqn. 1, we are left with an equation consisting of nodal displacements at time points *n* and *n-1* as well as various parameters. After arranging all unknowns (nodal displacement at $t = n$) to the left

side of the equation and all knowns (nodal displacement at $t = n\text{-}1$, parameters) to the right side, we obtain the following equation for each node:

$$\left(k^*_{sarcL}+\frac{1}{t_d}\gamma^*\right)u^n_{i-1}-\left(k^*_{sarcL}+k^*_{sarcR}+\frac{2}{t_d}\gamma^*+\frac{1}{t_d}\eta^*+\frac{1}{t_d{}^2}\right)u^n_i+\left(k^*_{sarcR}+\frac{1}{t_d}\gamma^*\right)u^n_{i+1}=$$
$$\left(\frac{1}{t_d}\gamma^*\right)u^{n-1}_{i-1}-\left(\frac{2}{t_d}\gamma^*+\frac{1}{t_d}\eta^*+\frac{1}{t_d{}^2}\right)u^{n-1}_i+\left(\frac{1}{t_d}\gamma^*\right)u^{n-1}_{i+1}-\frac{1}{t_d}v^{n-1}_i+h^*(L_L)-h^*(L_R)-f^{*n}_{external}$$

(Eqn. 7)

The ()* notation denotes any quantity that has been mass normalized, such that for an arbitrary scalar x,

$$x^*=\frac{x}{m}. \qquad \text{(Eqn. 8)}$$

During each time step, we simultaneously calculate nodal displacement by assembling the force balance equations for each node into a matrix problem,

$$\left[K^n\right]\left\{u^n\right\}=\left\{f^n\right\}, \qquad \text{(Eqn. 9)}$$

where $[K^n]$ is a square matrix ($N_{nodes} \times N_{nodes}$) and contains coefficients from the unknown terms on left-hand side of Eqn. 7, $\{u^n\}$ is a column vector containing the unknown nodal displacements, $\{u\} = \{u_1, u_2, u_3, \ldots, u_{Nnodes}\}^T$, and $\{f^n\}$ is a $N_{nodes} \times 1$ column vector containing the known terms found on the right hand side of Eqn. 7. Displacement was constrained at the left end of the SF ($u_1 = 0$). When constructing the force balance for the far right node ($i = N_{nodes}$), all the terms in Eqn. 1 related to the right sarcomere (R) were ignored. In some simulations as specified in the text, an external load $f_{external}$ was applied to the right end of the SF. In other simulations also as specified in the text, displacement was constrained for the far right node ($u_{Nnodes} = 0$).

Solving Eqn. 9 for $\{u^n\}$ by inverting $[K^n]$ gives us nodal displacements and therefore the position of the nodes in the current configuration. We then calculate $[K^{n+1}]$ and $\{f^{n+1}\}$ to calculate displacement at the next time point and continue this process until the simulation ends.

Myosin contraction model. Nonmuscle myosin II drives sarcomeres to contract. This contractile force was represented using an overlap model derived from filament overlap theory describing tension in skeletal muscle fibers (26, 28). For this myosin representation, contractile force depends on the length of the sarcomere as the current length of the sarcomere determines the degree of overlap between interacting myosin and actin filaments. The contraction force function $h(L)$ was a piece-wise function that generated contractile force based on sarcomere length (Figure 4.1C).

$$f_{contract}^{n} = h(L^{n-1}). \qquad \text{(Eqn. 10)}$$

To simplify formulation of our mathematical model and keep the force function $h(L)$ out of the sparse matrix $[K]$, we made the myosin II contractile force to be dependent on the sarcomere length at the previous time step ($t = n\text{-}1$) as opposed to the current time step ($t = n$). Error due to this assumption should be negligible as long as the time step t_d stays sufficiently small.

Random fluctuations in time. We first investigated whether the fluctuation of sarcomere lengths in resting-state SFs was merely due to the length-force relationship of myosin II and the heterogeneous distribution of sarcomere lengths seen in vivo [17]. However, we observed that sarcomeres within our simulations of resting-state SFs did not exhibit the low-frequency fluctuations as seen in vivo. To add dynamic heterogeneity, we implemented additional time-dependency into certain mechanisms within our math model. These time-dependencies would need to be oscillatory in nature and have a low natural frequency compared to the sampling window in order to replicate the behavior of in vivo sarcomeres. To accomplish this, we created a random fluctuation function, $y(t)$. Fluctuations due to $y(t)$ were designed to be sinusoidal in

nature and represent cycles of recruitment/de-recruitment of actin and myosin molecules within each sarcomere. Each sarcomere was assigned a random sinusoidal wave of the form

$$y(t) = a\sin\left(\frac{2\pi t}{T} + \phi\right), \qquad \text{(Eqn. 11)}$$

where a was the amplitude of the sinusoid and determined the amount of scaling, T was the period of the wave (i.e., the amount of time the wave takes to complete one cycle), and ϕ was the phase shift that determined at which point during its cycle the wave is at when t = 0. The use of a sinusoid function when constructing the random fluctuations ensured that fluctuations were unsteady yet not divergent. For each sarcomere, a, T, and ϕ were assigned random values based on normal distributions.

Each fluctuation function has a randomly generated amplitude, frequency, and phase shift (see Table 1). Each sarcomere was assigned a random sinusoid wave based on Eqn. 11 for actin ($y_{actin}(t)$) and myosin ($y_{myosin}(t)$). The result was significant heterogeneity amongst the random fluctuations from sarcomere to sarcomere. The actin fluctuation function, $y_{actin}(t)$, was used to vary the stiffness of the sarcomere, k_{sarc}, throughout time. The myosin fluctuation function, $y_{myosin}(t)$, was used to vary the magnitude of myosin contraction, $h(L_{sarc})$, over time. To determine if fluctuations in actin and myosin could produce sarcomere length fluctuations, we performed simulations of resting-state SFs with actin fluctuations only, with myosin fluctuations only, and with both actin and myosin fluctuations.

4.4 Results

Our research group recently tracked SF sarcomere dynamics over time and quantitatively described how the lengths of neighboring SF sarcomeres fluctuate in a compensatory manner (17). These results (summarized in Table 1) laid the foundation of formulating a mathematical

model presented in this study in order to give us insight of these phenomena and help design future experiments. In addition to these published experimental results (17), we also performed additional analysis especially for this model. As previously described (17), SF sarcomere dynamics were tracked using high-resolution fluorescent light microscopy and cells stably expressing zyxin-GFP, a common SF sarcomere border protein. Figure 4.2 shows scatter plots of all sarcomere length change for each minute of the imaging session. There is no significant difference between any imaging session during the 10-minute imagine period. Additionally, the magnitude of change in sarcomere length is consistent regardless of the starting sarcomere length (data not shown). We have used this and previously published data in our model.

A mechanical model was constructed and implemented in order to describe the sarcomere length fluctuation data from the experiments (17). The computational implementation of this model was verified by comparing simulation results to the analytical solution to a single sarcomere formulation of Eqn. 7 with a constant myosin contractile force (data not shown). To validate our model, we simulated a severed SF and the resulting retraction. Laser severing experiments have been used to understand the mechanical environment of a SF as it retracts through the cytosol (1, 24). Upon severance of the SF, sarcomeres closest to the cut site shorten the most while sarcomeres farthest from the cut site shorten the least (Figure 4.3A) (11). Our validation benchmarks were determined from Colombelli et al. 2009 (11) who found that SFs retracted an average of 8 μm upon severance. They also found that this shortening was highly nonlinear, and the majority of length change occurred within the first 20 seconds following severance. We optimized the remaining parameters within the model so that results of our severed SF simulation matched with the behavior described by Colombelli et al. 2009 (11). Parameters that varied during the optimization were the myosin contraction magnitude (f_c, see Figure 4.1C), the internal viscoelasticity damping parameter (γ), and the cytoplasmic drag force damping parameter (η). The values of the parameters determined by the validation exercise are given in

Table 1. Our simulated edge retraction matches the length change and decays with a time constant as reported by Colombelli et al. 2009 (Figures 4.3A-B).We also compared our simulation results (Supplemental Figure 4.S1A) with the work of Stachowiak and O'Shaugnessey 2009 (29) for additional validation (Supplemental Figure 4.S1B).

The parameters in Table 1 were used in the simulations of sarcomeres within resting-state SFs. Parameter values were prescribed by the user, determined from a literature source, or determined during the validation exercise. Unless otherwise mentioned, all the parameters in Table 1 remained constant throughout all simulations in Figures4. 4-6 (see below), with the exception of initial sarcomere length which is randomly generated from a normal distribution and varies between each simulation.

Our first simulations considered random fluctuations in sarcomere stiffness only. We implemented heterogeneous stiffness by assigning each sarcomere a random fluctuation function that oscillated the sarcomere stiffness, k_{sarc}, over time (Figure 4.4). Assigning each sarcomere a fluctuation function with a randomly generated amplitude, period, and phases resulted in each sarcomere having a different stiffness value at each point in time. In these simulations, each sarcomere's length simply oscillated around the value determined by the myosin contractile force. Sarcomeres showed periodic lengthening and shortening but did not return to the initial length.

The next round of simulations involved fluctuations in myosin contractility only. In these simulations, actin stiffness was kept uniform and constant while the force applied by myosin varied between sarcomeres and over time. We found that sarcomeres with varying myosin activity produced regular sinusoidal changes in length (Figure 4.5). The regular sinusoidal nature of these length changes meant that sarcomeres regularly returned to their original length but did not stay at any one length value for long. These results showed no persistence in sarcomere length.

In the last round of simulations, we assigned fluctuations to both actin stiffness and myosin activity (Figure 4.6). Sarcomeres in these simulations exhibited highly irregular changes

in length (up to 1 μm) and persisted at or around this new length before returning to the initial sarcomere length (average of 2.5 minutes). In these simulations, most sarcomeres did not change length by more than ~20% at any point in time. However in each simulation, at least one (usually several) sarcomeres experienced length changes greater than 50%. These results suggested that heterogeneous actin stiffness and myosin contractility are sufficient to cause realistic length fluctuations of individual sarcomeres as well as induce large changes in length in neighboring sarcomeres.

Lastly, we collected distributions of length changes and rate of length changes amongst sarcomeres from seven simulations to compare with data collected from live cells (Figure 4.7). Each simulation represented a different SF in different cells, similar to the experimental conditions (17). The distribution of length changes from all the simulations was centered around 0 μm (Figure 4.7A). Almost all length changes in the distribution were less than 1 μm, and approximately 75% of length changes were less than 0.4 μm. The distribution of rate of length changes was also centered around 0 μm/min, with approximately 90% of the rates less than 0.4 μm/min (Figure 4.7B). The experimental and simulated data for sarcomere change in length and rate of change in length were not significantly different by t-test.

4.5 Discussion

In previous experiments we observed changes in SF sarcomere length in live cells over time (17). In this work we present a mathematical model to help shed light into the mechanisms behind this dynamic behavior. Our mathematical model included force contributions from actin stiffness, myosin contraction, internal viscoelasticity, and cytoplasmic drag. We found that by including local fluctuations in actin stiffness and myosin activity between adjacent sarcomeres our mathematical model was able to simulate sarcomeres with "breathing"-like fluctuation behavior that closely resembled our experimental data.

Our findings suggest these factors are sufficient to cause sarcomere length fluctuations. Fluctuating myosin II contractility seems to have the most profound effect, however the best results were obtained when both actin and myosin were allowed to fluctuate. Although the mechanics regulate the behavior of neighboring sarcomeres, we need to consider dynamic changes in the mechanical properties that may result from other processes within the cell such as actin polymerization/de-polymerization and myosin recruitment/de-recruitment. We demonstrated that certain in vivo behaviors of the cytoskeleton could only be simulated when the mechanical determinants of the system were allowed to vary dynamically.

The validation exercise involving the simulation of a retracting SF (Figure 4.3) was used to assign values to the myosin contractile force (f_c), the internal viscoelasticity damping parameter (γ), and the cytoplasmic drag damping parameter (η). In the retraction simulation, f_c determined the final retraction distance while γ and η determined the rate of retraction. If γ and η are both set to zero, then the retraction of the SF was purely elastic and the SF instantaneously 'snapped' to its retracted state. Increasing the damping parameters caused the retracting end to move slower and increased the decay time of retraction distance vs. time. During this exercise, we found that increasing the cytoplasmic drag damping parameter, η, produced much more realistic results than increasing internal viscoelasticity damping parameter, γ (data not shown). Increasing either parameter resulted in increased motion damping. However in simulations that involved increasing γ only, all sarcomeres within the SF retracted at the same rate. Conversely, increasing η caused sarcomeres near the retraction site to shorten quicker than sarcomeres further away. Many studies involving retraction SFs have seen sarcomeres near the severance site shorten at a higher rate compared to sarcomeres further away, forming a 'collapsed cap' [1, 11, 30]. Our model suggests that cytoplasmic drag force is the main cause of this behavior and plays a significant role in determining the mechanical behavior of SFs. Stachowiak and O'Shaugnessey 2009 made similar observations in that external viscosity due to the cytoplasm was necessary for

nonuniform sarcomere shortening and formation of the collapsed cap in SF retraction simulations (29).

Many mathematical models of actin SFs represent myosin contraction based on A.V. Hill's model of skeleton muscles (30). The Hill model involves a hyperbolic relationship between contractile force and velocity of isometric sarcomere shortening. Mathematical models of actin SFs using the Hill model have successfully predicted SF retraction in simulations of laser severance (11, 28, 31). In this work, we venture away from the classic Hill model and developed our myosin II model based on sliding filament overlap theory. Data suggest a relationship between sarcomere length and contractile force which we adapted for use in our SF model [28, 29]. This myosin representation suggests an 'optimal' sarcomere length that generates a maximum amount of contraction force (f_c, peak of the curve in Figure 4.1C). When the sarcomere becomes extended past this length, overlap between actin and myosin decreases and myosin-driven contractility cannot occur as efficiently. Likewise, if sarcomeres shorten past this optimal length, myosin-driven contractility loses effectiveness due to structural hindrance and force decreases. Our SF model was able to accurately simulate a retracting SF using this sliding filament model for myosin II and make predictions similar to other SF models [11, 30]. We also were able to extend this formulation to generate realistic fluctuations of sarcomere lengths over time. With our mathematical formulation, we found that cytoplasmic drag played a more important role in SF behavior than internal viscoelasticity (i.e., $\eta >> \gamma$). Previous SF models using the Hill model for myosin II contraction found that external and internal sources of friction and viscous damping played approximately equal roles. Arguably these differences can simply be attributed to differences in the mathematical formulations between these models. At the very least, our results suggest there may be multiple mathematical formulations that accurately predict actin SF behavior.

We designed our SF model using a force vs. sarcomere length relationship for myosin II as we initially hypothesized that heterogeneity in myosin II contraction along the SF due to nonuniform sarcomere lengths caused the length fluctuations we observed in vivo. However, this formulation of the model was not able to realistically predict these length fluctuations. We were not able to produce realistic length fluctuations until we allowed for both heterogeneity along the SF and dynamic changes in these properties via our random fluctuation functions. Actin polymerization/de-polymerization may contribute to sarcomere length changes, either by producing a 'pushing' force that extends or retracts the sarcomere or by changing the stiffness of the sarcomere under myosin contraction. Fluorescently-labeled actin monomers have been shown to incorporate into SFs at sarcomere edges (32-34), and many proteins involved in actin polymerization localize at sarcomere borders (16, 35), though these factors have not been examined in the context of SF sarcomere length fluctuations.. Myosin has been shown to vary between individual sarcomeres in striated muscle fibers (36). There have also been reports of different levels of myosin II isoforms and sites of myosin light chain phosphorylation that differ across a SF (13, 37), suggesting levels of myosin-driven contractility may also differ along the length of a single SF. The dynamic changes in molecular motors and the cytoskeleton have been discussed in other publications (38) and demonstrate the importance of molecular dynamics when considering SF mechanics. In our model, we represent the molecular dynamics of actin and myosin II using random fluctuations functions. We assume that the fluctuations in actin and myosin activity within SFs are cyclic in our choice of a sine function, but do not claim that the sine functions accurately describes the dynamics and myosin within live cells. Rather, these functions demonstrate that dynamic changes in mechanical properties are necessary to fully describe the mechanical behavior of SFs.

Several improvements could be made to our model in order to further elucidate the mechanism behind sarcomere length fluctuations in live cells. Our model was one-dimensional and assumed uniform properties through the thickness of the SF. Most likely the properties of the

SF are heterogeneous throughout the thickness as well as along the length of the fiber, and including this heterogeneity may improve accuracy of our simulations. Additionally, we used a random process to fluctuate the levels of actin and myosin activity within the SFs. However, these processes could be explicitly modeled using molecular dynamics which would provide deterministic mechanisms for changes in actin and myosin over time. This process will be difficult as relationships between molecular concentration of actin and myosin and the mechanical properties of the SF sarcomeres need to be established. Additionally, there may be other molecules that contribute to the mechanical behavior of the SF such as α-actinin (39, 40), zxyin (16), or titin (41-43). Our mathematical set out to represent the overall activity of all these molecules and the consequences for SF mechanics using our fluctuation functions and we made no attempt to explicitly model the contribution of individual molecule types. SF sarcomeres showed greater standard deviation in their length fluctuations when force was applied to the cytoskeleton at the focal adhesion (18). In the future as the link between SF sarcomere structure and force transmission becomes clearer, our model may be used to describe how forces travel from the extracellular environment into the cell through the cytoskeleton and estimate forces within the cytoskeleton of live cells.

In conclusion, we designed a mathematical model to show that the spontaneous sarcomere length fluctuations in resting, steady-state SFs can be driven by heterogeneous properties between neighboring SFs and dynamic changes in stiffness and contractility over time. Understanding how these factors play a role in SF sarcomere maintenance and repair will lead to a better knowledge of actin SF mechanics in live cells. Hypotheses regarding actin SF dynamics in live cells can be difficult to test experimentally. Computational modeling allows us to test hypotheses despite this lack of experimental options. Such models allow us to test our current understanding of SF dynamics and help us understand the ways in which cells respond to forces in their environment. Additional, our simulations can also help guide future experiments in actin SF mechanics.

4.6 Acknowledgments

This work was supported in part by grants from the National Institutes of Health (R01GM50877), the Huntsman Cancer Foundation, and shared resources from the Cancer Center Support Grant (2 P30 CA42014-21) to MCB. YTS is supported by grants from the National Institutes of Health (R01HL67646 and R01DK088777).

Table 4.1: Parameters used in mathematical model

Parameter*	**Description**	**Value**	**Notes or Sources**
N_{sarc}	Number of sarcomeres	8	-
N_{nodes}	Number of nodes	9	$N_{nodes} = N_{sarc} + 1$
L_{sarc}	Length of sarcomere	1.6 ± 0.063 μm (mean ± standard error)	Randomly generated using a normal distribution [17]
t_0	Start time	0 seconds	[17]
t_f	End time	600 seconds	[17]
t_d	Time step	10 seconds	[17]
k_{sarc}	Sarcomere stiffness	33.1 nN/μm	[27]
m	Sarcomere mass	8.25 μg	[19]
γ	Dampening parameter of internal viscoelasticity	0.01 nN-s/μm	Validation exercise
η	Dampening parameter of cytoplasmic drag	6.5 nN-s/μm	Validation exercise
f_c	Maximal myosin contractile force (i.e., maximal $f_{contract}$)	32.7 nN	Validation exercise
a	Amplitude of fluctuation function, $y(t)$	$0 < a \leq 1$	Randomly generated using an uniform distribution
T	Period of fluctuation function, $y(t)$	10 ± 10% minutes for myosin. 4 ± 10% minutes for actin.	Randomly generated using a normal distribution
ϕ	Phase shift of fluctuation function, $y(t)$	$-\pi \leq \phi \leq \pi$	Randomly generated using an uniform distribution

***:** Unless otherwise mentioned in the text, all the parameters remain constant throughout all simulations, with the exception of L_{sarc}, which is generated from a normal distribution.

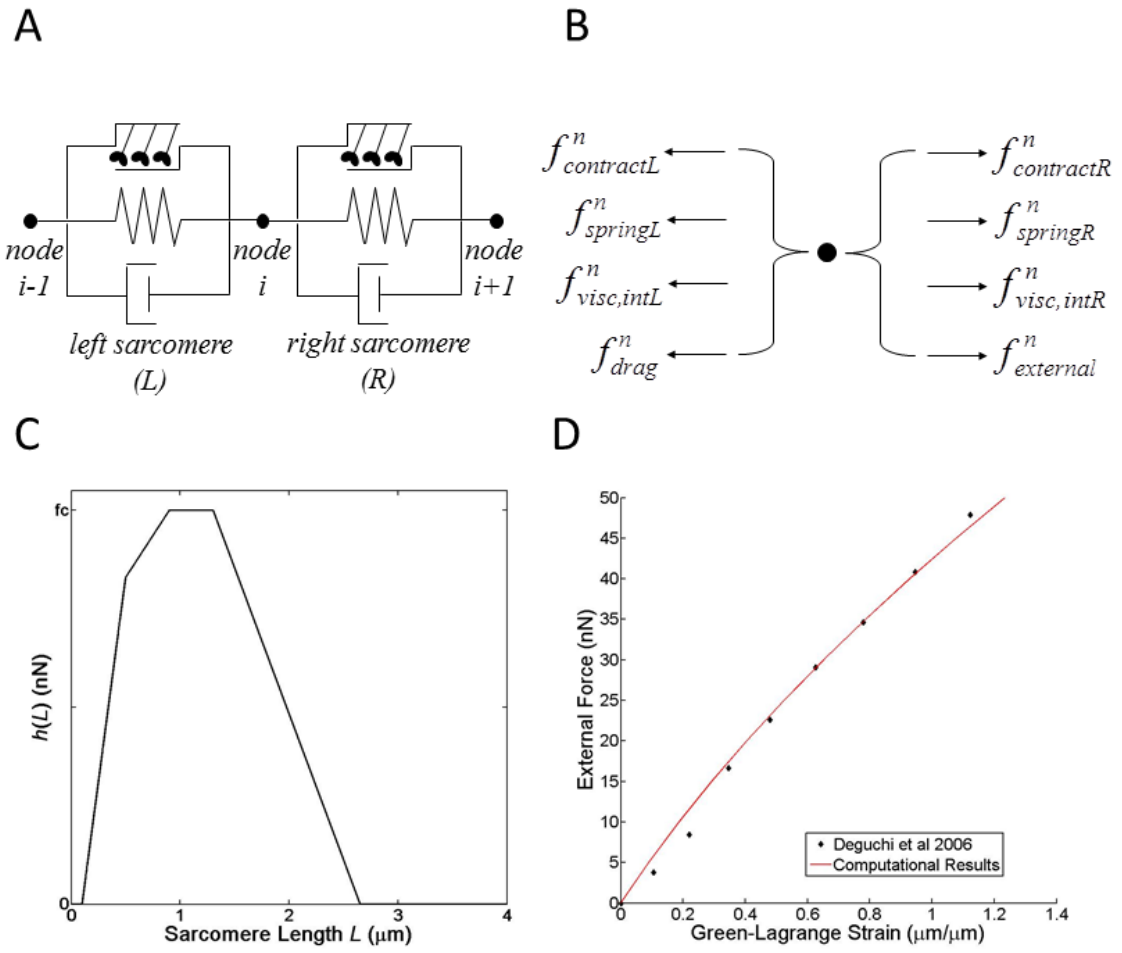

Figure 4.1: Formulation of the mathematical model

(A) Each stress fiber is depicted as a discrete element consisting of an active contractile unit (top), a linear elastic spring (middle), and a linear viscous dashpot (bottom) connected in parallel. (B) Forces at a node *i* (shown in panel A) at each time point ($t = n$). f_{spring}, = *elastic force;* $f_{contract}$, = *contractile force;* $f_{visc,int}$, = *internal viscous force;* f_{drag}, = *external drag force;* $f_{external}$ = *external load.* (C) The simulated sarcomere length-force relationship. *h(L)* = force function. f_c = maximum $f_{contract}$. (D) Applied external force vs. Green-Lagrange strain from simulation of uniaxial extension. Simulated data are presented in red, experimental data from Deguchi et al., 2006, *Journal of Biomechanics*, is presented in black points.

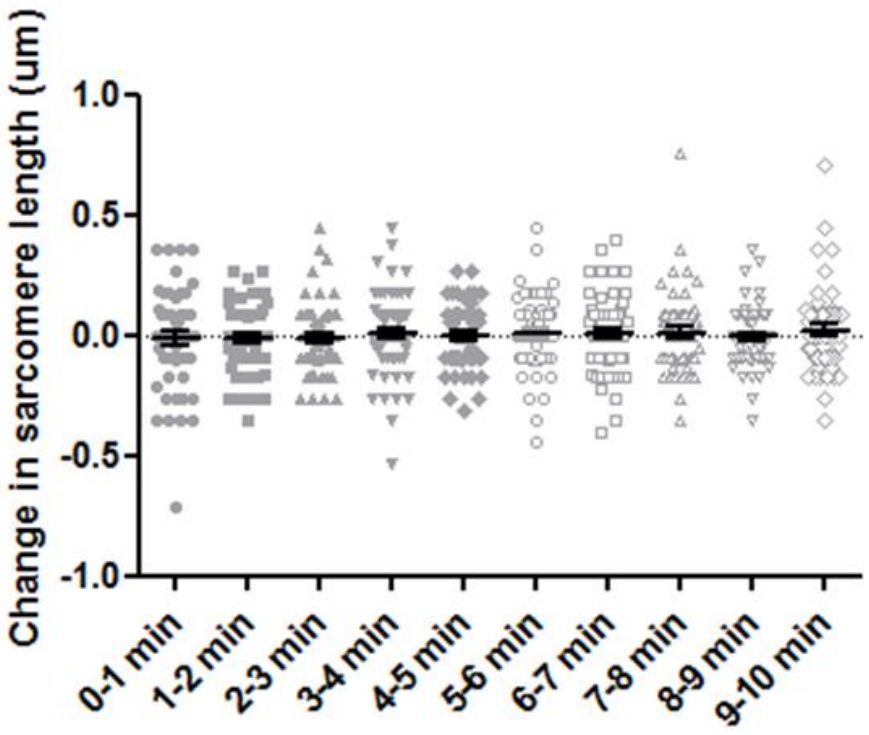

Figure 4.2: Stress fiber sarcomeres have consistent fluctuations in length
Solid and outlined gray points indicate the change in sarcomere length compared to the initial sarcomere length, shown for each minute of a 10-minute imaging sequence. The black lines indicate mean and standard error. n = 53 to 58 sarcomeres, per time category.

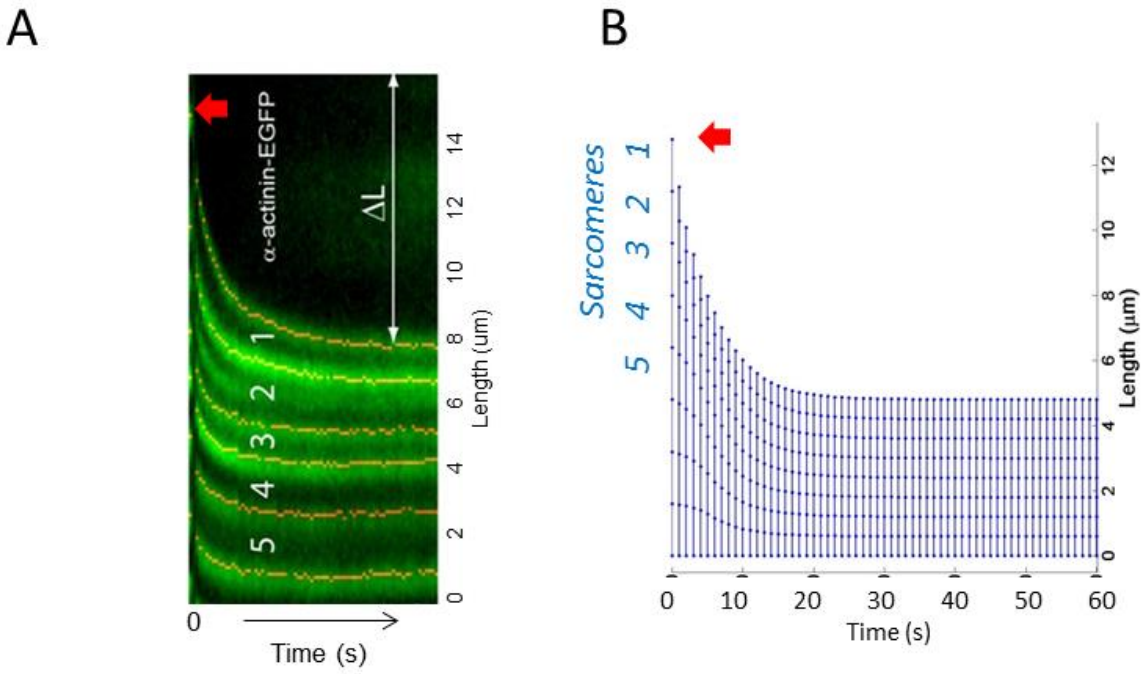

Figure 4.3: Computational model is validated using experimental results
(A) Colombelli et al. tracked α-actinin-EGFP in laser cut SFs. Sarcomere 1 is closest to the cut site (red arrow), and 5 is the farthest sarcomere in this particular stress fiber. The change in length of the retracting fiber is shown by ΔL. Reproduced with permission from *Journal of Cell Science* (11). (B) Using parameters based on experimental results from our work, and others (e.g., Colombelli et al., 2009, *Journal of Cell Science*, in (A)), our simulated results look similar in the way sarcomeres 1-5 retract and shorten.

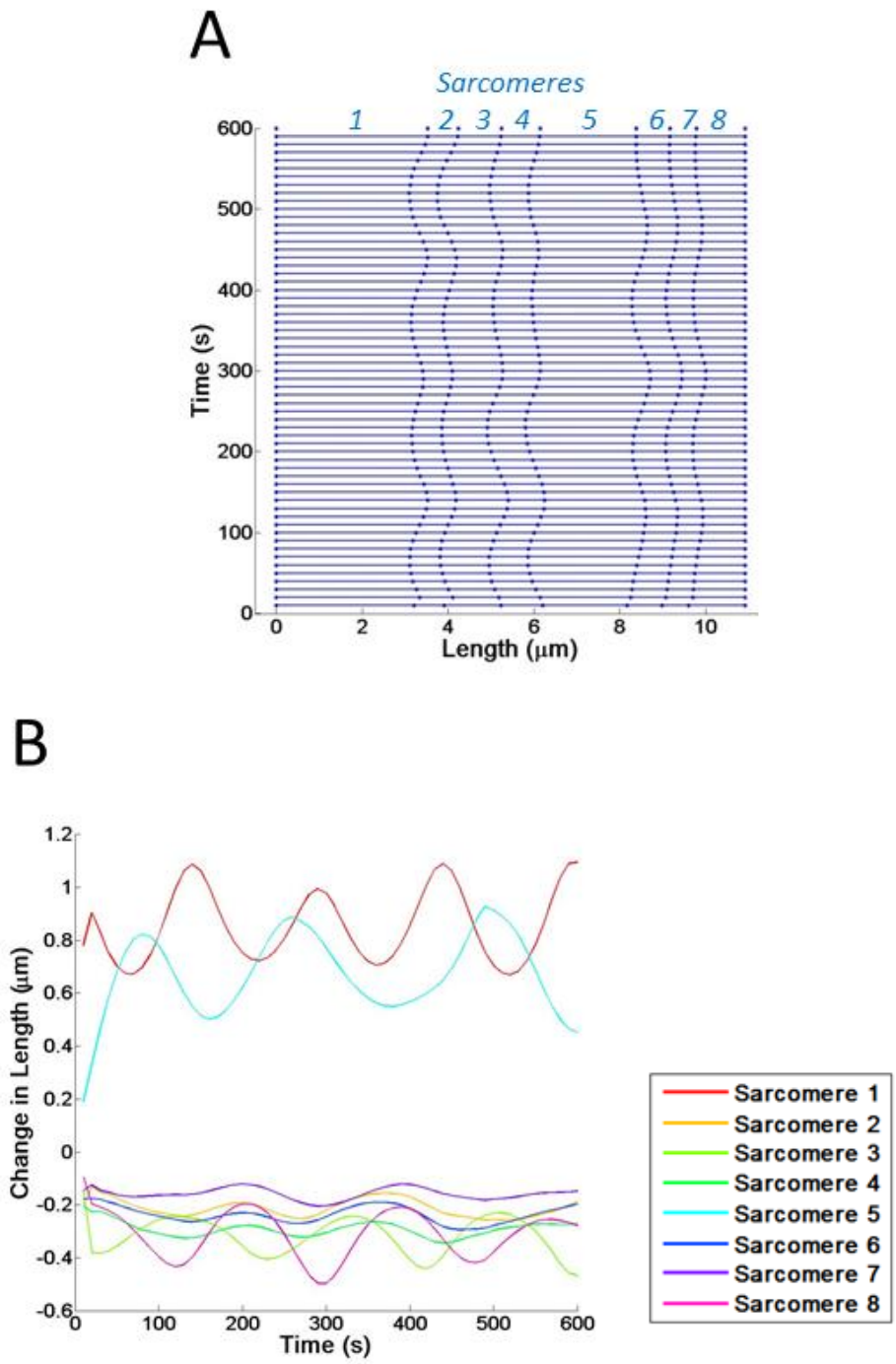

Figure 4.4: Introducing variable actin stiffness
(A) Kymograph showing changes in sarcomere length over time. Sarcomeres 1-8 are indicated. (B) The changes in length of each sarcomere is shown with a colored line, corresponding to the sarcomere number.

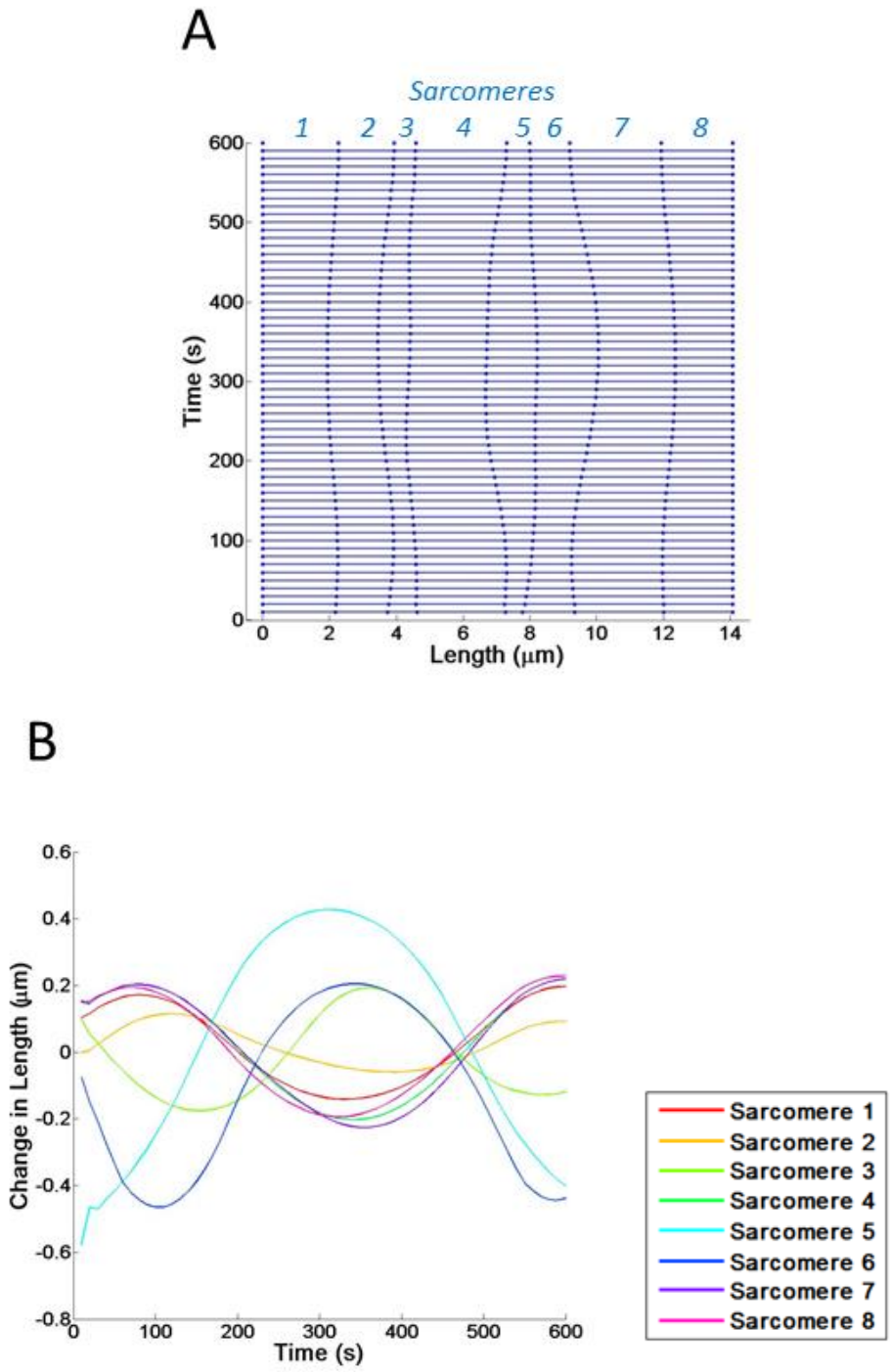

Figure 4.5: Introducing variable myosin activity
(A) Kymograph showing changes in sarcomere length over time. Sarcomeres 1-8 are indicated in italicized blue font on the right y axis. (B) The changes in length of each sarcomere is shown with a colored line, corresponding to the sarcomere number.

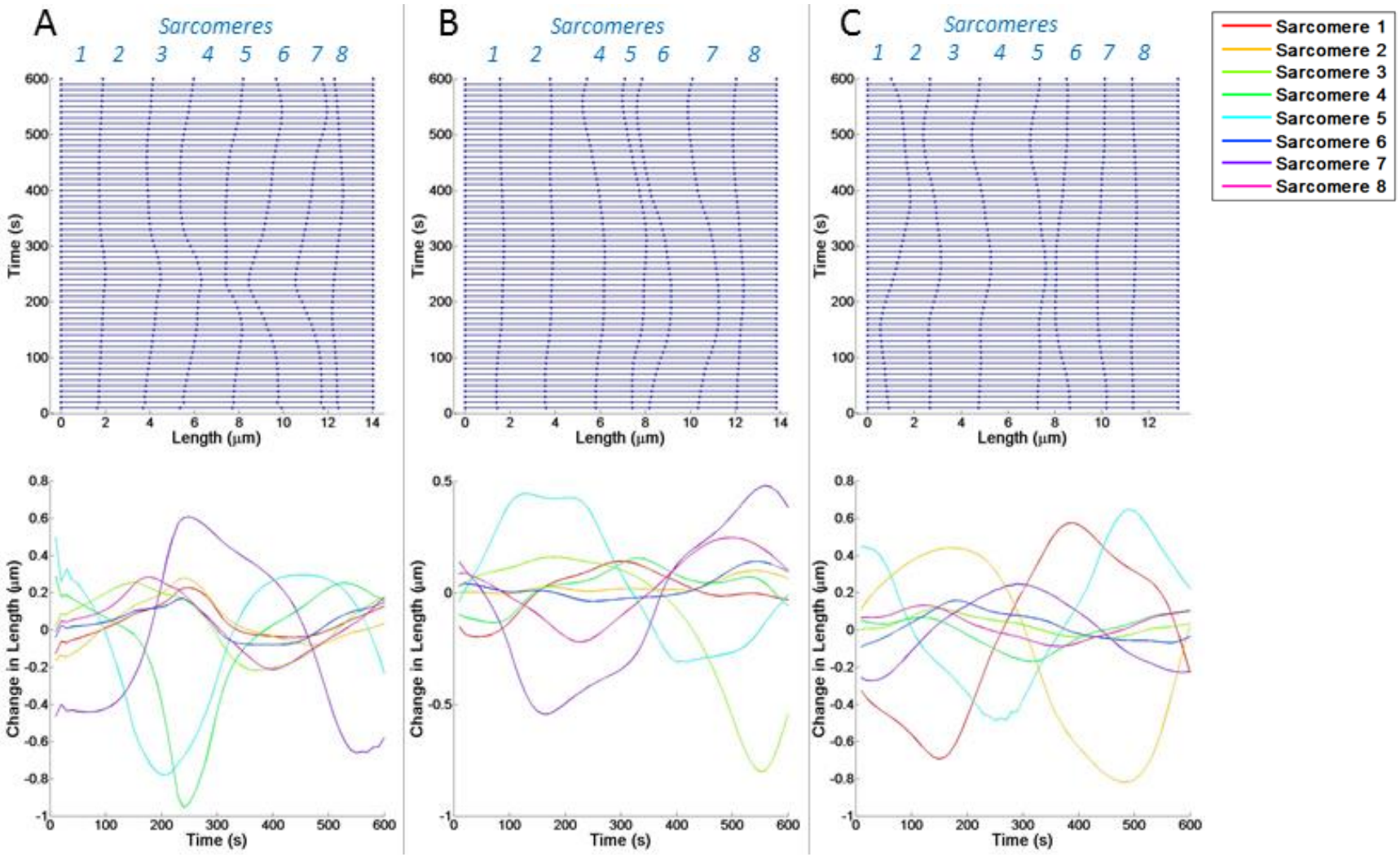

Figure 4.6: Introducing variable actin stiffness and myosin activity

Kymographs showing changes in sarcomere length over time. Sarcomeres 1-8 are indicated in blue italicized font on the right y axis. The changes in length of each sarcomere are shown with colored lines, corresponding to the sarcomere number. Three simulations (A-C) are shown.

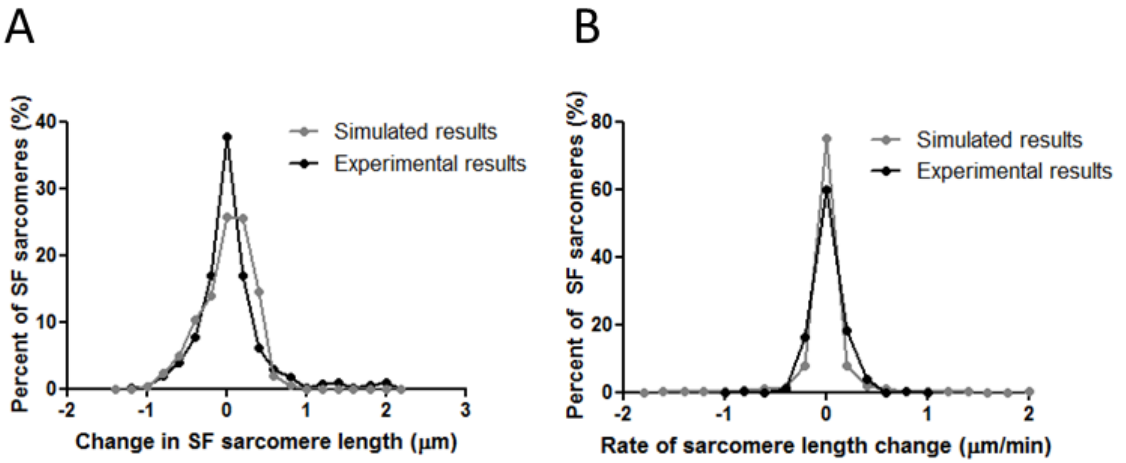

Figure 4.7: Statistical comparison between experimental and simulated data
(A) Frequency distribution of changes in sarcomere length in live cells. Black line is experimental data (previously reported in Chapin et al 2012 *Biophysical Journal*). Gray line is simulated data. (B) Frequency distribution of rates of sarcomere length change in live cells. Black line is experimental data (previously reported in Chapin et al 2012 *Biophysical Journal*). Gray line is simulated data. Data were compared using a t-test, and no significant difference was reported for either group.

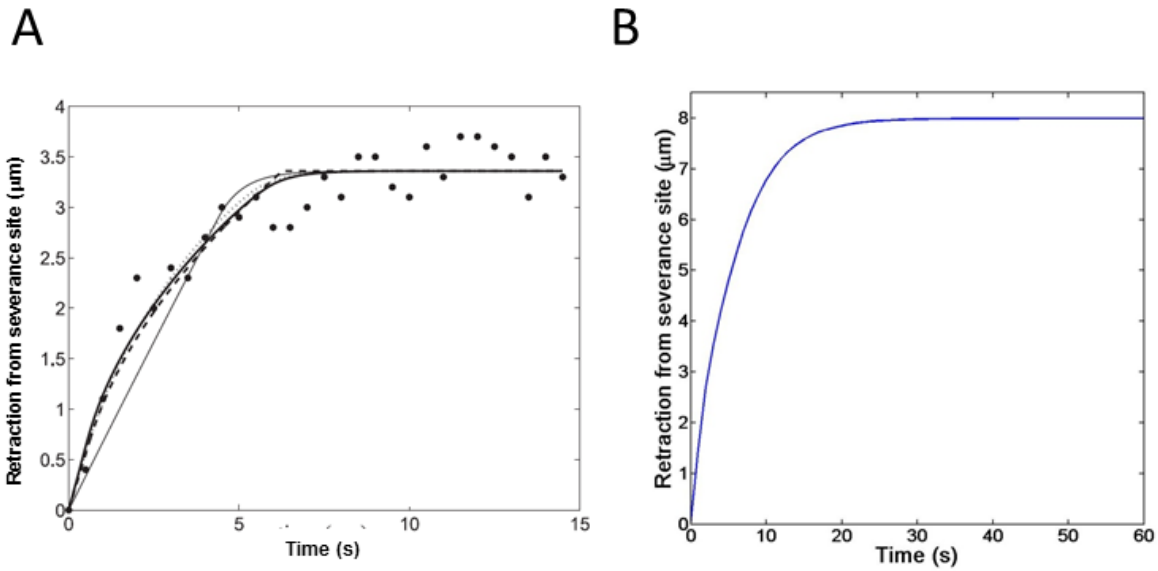

Figure 4.S1: Computational model is validated using experimental results
(A) Stress fiber end retraction following laser severing. Black points indicate experimental data from Kumar et al. 2006. The solid line, dotted line, and dashed line all represent simulated results using various parameters. Figure adapted with permission from Stachowiak and O'Shaugnessey 2009 *Biophysical Journal*. (B) Our model simulates edge retraction data. Compare to black dots in (A).

4.7 References

1. Kumar S, *et al.* (2006) Viscoelastic retraction of single living stress fibers and its impact on cell shape, cytoskeletal organization, and extracellular matrix mechanics. *Biophysical journal* 90(10):3762-3773.

2. Wang N, *et al.* (2001) Mechanical behavior in living cells consistent with the tensegrity model. *Proceedings of the National Academy of Sciences of the United States of America* 98(14):7765-7770.

3. Discher DE, Janmey P, & Wang YL (2005) Tissue cells feel and respond to the stiffness of their substrate. *Science* 310(5751):1139-1143.

4. Hall A (1998) Rho GTPases and the actin cytoskeleton. *Science* 279(5350):509-514.

5. Jaffe AB & Hall A (2005) Rho GTPases: biochemistry and biology. *Annual review of cell and developmental biology* 21:247-269.

6. Vogel V & Sheetz M (2006) Local force and geometry sensing regulate cell functions. *Nature reviews. Molecular cell biology* 7(4):265-275.

7. Isenberg G, Rathke PC, Hulsmann N, Franke WW, & Wohlfarth-Bottermann KE (1976) Cytoplasmic actomyosin fibrils in tissue culture cells: direct proof of contractility by visualization of ATP-induced contraction in fibrils isolated by laser micro-beam dissection. *Cell and tissue research* 166(4):427-443.

8. Katoh K, Kano Y, Masuda M, Onishi H, & Fujiwara K (1998) Isolation and contraction of the stress fiber. *Molecular biology of the cell* 9(7):1919-1938.

9. Lazarides E & Burridge K (1975) Alpha-actinin: immunofluorescent localization of a muscle structural protein in nonmuscle cells. *Cell* 6(3):289-298.

10. Weber K & Groeschel-Stewart U (1974) Antibody to myosin: the specific visualization of myosin-containing filaments in nonmuscle cells. *Proceedings of the National Academy of Sciences of the United States of America* 71(11):4561-4564.

11. Colombelli J, *et al.* (2009) Mechanosensing in actin stress fibers revealed by a close correlation between force and protein localization. *Journal of cell science* 122(Pt 10):1665-1679.

12. Endlich N, Otey CA, Kriz W, & Endlich K (2007) Movement of stress fibers away from focal adhesions identifies focal adhesions as sites of stress fiber assembly in stationary cells. *Cell motility and the cytoskeleton* 64(12):966-976.

13. Peterson LJ, *et al.* (2004) Simultaneous stretching and contraction of stress fibers in vivo. *Molecular biology of the cell* 15(7):3497-3508.

14. Rossier OM, *et al.* (2010) Force generated by actomyosin contraction builds bridges between adhesive contacts. *The EMBO journal* 29(6):1055-1068.

15. Russell B, Curtis MW, Koshman YE, & Samarel AM (2010) Mechanical stress-induced sarcomere assembly for cardiac muscle growth in length and width. *Journal of molecular and cellular cardiology* 48(5):817-823.

16. Smith MA, *et al.* (2010) A zyxin-mediated mechanism for actin stress fiber maintenance and repair. *Developmental cell* 19(3):365-376.

17. Chapin LMB, E.; Smith, M.A.; Shiu Y.; Beckerle M.C. (2012) Lateral communication between stress fiber sarcomeres facilitates a local remodeling response. *Biophysical journal* 103(10).

18. Guolla L, Bertrand M, Haase K, & Pelling AE (2012) Force transduction and strain dynamics in actin stress fibres in response to nanonewton forces. *Journal of cell science* 125(Pt 3):603-613.

19. Reedy MB, G.; Fischman, D. (1973) How many myosins per cross-bridge? I. Flight muscle myofibrils from the blowfly, Sarcophaga bullata. *Cold Spring Harbor Symposia on Quantitative Biology* 37:397-421.

20. Cramer LP, Siebert M, & Mitchison TJ (1997) Identification of novel graded polarity actin filament bundles in locomoting heart fibroblasts: implications for the generation of motile force. *The Journal of cell biology* 136(6):1287-1305.

21. Satcher RL, Jr. & Dewey CF, Jr. (1996) Theoretical estimates of mechanical properties of the endothelial cell cytoskeleton. *Biophysical journal* 71(1):109-118.

22. Charras GT & Horton MA (2002) Determination of cellular strains by combined atomic force microscopy and finite element modeling. *Biophysical journal* 83(2):858-879.

23. Haga H, *et al.* (2000) Elasticity mapping of living fibroblasts by AFM and immunofluorescence observation of the cytoskeleton. *Ultramicroscopy* 82(1-4):253-258.

24. Russell RJ, Xia SL, Dickinson RB, & Lele TP (2009) Sarcomere mechanics in capillary endothelial cells. *Biophysical journal* 97(6):1578-1585.

25. Deguchi S, Ohashi T, & Sato M (2006) Tensile properties of single stress fibers isolated from cultured vascular smooth muscle cells. *Journal of biomechanics* 39(14):2603-2610.

26. Gordon AM, Huxley AF, & Julian FJ (1966) The variation in isometric tension with sarcomere length in vertebrate muscle fibres. *The Journal of physiology* 184(1):170-192.

27. Hoffman LM, *et al.* (2006) Genetic ablation of zyxin causes Mena/VASP mislocalization, increased motility, and deficits in actin remodeling. *The Journal of cell biology* 172(5):771-782.

28. Schoenberg RJPaM (2011) Force Generation and Shortening in Skeletal Muscle. *Comprehensive Physiology* Supplement 27: Handbook of Physiology, Skeletal Muscle:173-187.

29. Stachowiak MR & O'Shaughnessy B (2009) Recoil after severing reveals stress fiber contraction mechanisms. *Biophysical journal* 97(2):462-471.

30. Hill AV (1925) Length of muscle, and the heat and tension developed in an isometric contraction. *The Journal of physiology* 60(4):237-263.

31. Kaunas R, Hsu, H-J., and S. Deguchi (2011) Sarcomeric model of stretch-induced stress fiber reorganization. *Cell Health and Cytoskeleton* 3:13-22.

32. Amato PA & Taylor DL (1986) Probing the mechanism of incorporation of fluorescently labeled actin into stress fibers. *The Journal of cell biology* 102(3):1074-1084.

33. Kreis TE, Winterhalter KH, & Birchmeier W (1979) In vivo distribution and turnover of fluorescently labeled actin microinjected into human fibroblasts. *Proceedings of the National Academy of Sciences of the United States of America* 76(8):3814-3818.

34. Turnacioglu KK, Sanger JW, & Sanger JM (1998) Sites of monomeric actin incorporation in living PtK2 and REF-52 cells. *Cell motility and the cytoskeleton* 40(1):59-70.

35. Hotulainen P & Lappalainen P (2006) Stress fibers are generated by two distinct actin assembly mechanisms in motile cells. *The Journal of cell biology* 173(3):383-394.

36. Rassier DE (2012) The mechanisms of the residual force enhancement after stretch of skeletal muscle: non-uniformity in half-sarcomeres and stiffness of titin. *Proceedings. Biological sciences / The Royal Society*.

37. Cai Y, *et al.* (2010) Cytoskeletal coherence requires myosin-IIA contractility. *Journal of cell science* 123(Pt 3):413-423.

38. Schillers H, Walte M, Urbanova K, & Oberleithner H (2010) Real-time monitoring of cell elasticity reveals oscillating myosin activity. *Biophysical journal* 99(11):3639-3646.

39. Burridge K & Feramisco JR (1981) Non-muscle alpha actinins are calcium-sensitive actin-binding proteins. *Nature* 294(5841):565-567.

40. Esue O, Tseng Y, & Wirtz D (2009) Alpha-actinin and filamin cooperatively enhance the stiffness of actin filament networks. *PloS one* 4(2):e4411.

41. Cavnar PJ, Olenych SG, & Keller TC, 3rd (2007) Molecular identification and localization of cellular titin, a novel titin isoform in the fibroblast stress fiber. *Cell motility and the cytoskeleton* 64(6):418-433.

42. Frank D & Frey N (2011) Cardiac Z-disc signaling network. *The Journal of biological chemistry* 286(12):9897-9904.

43. Gautel M (2011) Cytoskeletal protein kinases: titin and its relations in mechanosensing. *Pflugers Archiv : European journal of physiology* 462(1):119-134.

CHAPTER 5

SUMMARY AND PERSPECTIVES

The field of cell mechanics is an exciting, growing field of cell biology. Cells in our bodies experience mechanical stimuli from their environment, and they are also capable of exerting forces outward on their surroundings. Advances in imaging have allowed us to mimic the contributions of the cellular environment on cell behavior, while advances in computational modeling have provided us with valuable information regarding the mechanisms of cell mechanics. By combining experimental data with data simulated from computational modeling we have provided better understanding of the complexities involved in mechanosensing and responding in living cells.

In this thesis I have summarized work that has contributed to the understanding of actin cytoskeletal remodeling and biomechanics. Specifically I have worked on projects that have revealed zyxin's role as a mechanosensitive protein involved in actin remodeling (1). I concluded this dissertation with the discovery of stress fiber (SF) sarcomere dynamics (2) and, in collaboration with Dr. Yan-Ting Shiu and Lowell Edgar, a Bioengineering PhD candidate, have further characterized the mechanics of sarcomeres; the individual subunits of SFs.

Moving forward there are even more opportunities to expand on this work and raise additional questions regarding the mechanics of actin remodeling. Specifically new advances in imaging will provide better resolution by which to study actin-binding proteins and the polymerization of actin monomers in vivo. For example, higher resolution imaging such as photoactivatable localization microscopy (PALM) allows for the tracking of structures as small as 30 nm (3, 4), which provides near EM-like resolution in the context of live cell microscopy (5-7).

Within the last few years PALM was used to capture filamentous-actin (F-actin) dynamics in dendritic spines (7) which revealed kinetics of actin polymerization and depolymerization in single actin filaments among multiple filaments bundled together. This kind of live cell microscopy would be a powerful tool for capturing details of actin polymerization along actin SFs.

In addition to the ability to collect highly resolved imaging data, advances in computational modeling will also improve the accuracy of our findings. Advances in computational modeling come in the form of fewer assumptions, and the greater use of experimentally determined variables. In an early model one assumption was that there is homogeneous sarcomere shortening and lengthening (8), though later it was shown not to be the case (9-12). Additionally, a few recent computational models have incorporated simultaneous solving of two processes (9), thereby providing a possibly more physiological context of testing. Being able to account for these variable, dynamic changes in the actin cytoskeleton will lead to more realistic predictions about live-cell biomechanics.

One additional way to strengthen assumptions would be to conduct more consistent, reproducible methods for testing single SF mechanics. For example, there is a wide variety of values for tensile breaking force for actin structures, as well as a wide range for the elastic modulus (Table 5.1). Methods of actin filament or SF isolation differ, as well as the instrumentation used for mechanical property testing. Consistency in this field as well as easily reproducible techniques would improve.

In this thesis I have outlined my involvement in advancing the field of actin remodeling biomechanics. Advancements in imaging to produce higher resolution of live cell dynamics, as well as improvements in mechanical testing of actin structures would lead to more reliable assumptions used in computational modeling.

Table 5.1: Mechanical properties of actin filaments and stress fibers

Assay and actin structure	**Unit**	**Reference**
Tensile strength of an actin filament	200 pN	(13)
Tensile strength of untwisted actin filament	400 pN	(13)
Max breaking force of single actin filament	600 pN	(13)
Breaking force of isolated actin SF	377 nN	(14)
Physiological tension on an actin filament	250 pN	(15)
Elastic modulus of isolated actin SF	1.45 MPa	(14)
Elastic modulus of synthesized F-actin	1.8 GPa	(16)
Elastic modulus of synthesized F-actin	2.6 GPa	(17)

5.1 References

1. Smith MA, *et al.* (2010) A zyxin-mediated mechanism for actin stress fiber maintenance and repair. *Developmental cell* 19(3):365-376.

2. Chapin LMB, E.; Smith, M.A.; Shiu Y.; Beckerle M.C. (2012) Lateral communication between stress fiber sarcomeres facilitates a local remodeling response. *Biophysical journal* 103(10).

3. Betzig E, *et al.* (2006) Imaging intracellular fluorescent proteins at nanometer resolution. *Science* 313(5793):1642-1645.

4. Hess ST, Girirajan TP, & Mason MD (2006) Ultra-high resolution imaging by fluorescence photoactivation localization microscopy. *Biophysical journal* 91(11):4258-4272.

5. Manley S, *et al.* (2008) High-density mapping of single-molecule trajectories with photoactivated localization microscopy. *Nature methods* 5(2):155-157.

6. Niu L & Yu J (2008) Investigating intracellular dynamics of FtsZ cytoskeleton with photoactivation single-molecule tracking. *Biophysical journal* 95(4):2009-2016.

7. Tatavarty V, Kim EJ, Rodionov V, & Yu J (2009) Investigating sub-spine actin dynamics in rat hippocampal neurons with super-resolution optical imaging. *PloS one* 4(11):e7724.

8. Iribe G, Helmes M, & Kohl P (2007) Force-length relations in isolated intact cardiomyocytes subjected to dynamic changes in mechanical load. *American journal of physiology. Heart and circulatory physiology* 292(3):H1487-1497.

9. Besser AS, U. S. (2007) Coupling biochemistry and mechanics in cell adhesion: a model for inhomogeneous stress fiber contraction. *Journal of New Physics* 9.

10. Guolla L, Bertrand M, Haase K, & Pelling AE (2012) Force transduction and strain dynamics in actin stress fibres in response to nanonewton forces. *Journal of cell science* 125(Pt 3):603-613.

11. Peterson LJ, *et al.* (2004) Simultaneous stretching and contraction of stress fibers in vivo. *Molecular biology of the cell* 15(7):3497-3508.

12. Russell B, Curtis MW, Koshman YE, & Samarel AM (2010) Mechanical stress-induced sarcomere assembly for cardiac muscle growth in length and width. *Journal of molecular and cellular cardiology* 48(5):817-823.

13. Tsuda Y, Yasutake H, Ishijima A, & Yanagida T (1996) Torsional rigidity of single actin filaments and actin-actin bond breaking force under torsion measured directly by in vitro micromanipulation. *Proceedings of the National Academy of Sciences of the United States of America* 93(23):12937-12942.

14. Deguchi S, Ohashi T, & Sato M (2006) Tensile properties of single stress fibers isolated from cultured vascular smooth muscle cells. *Journal of biomechanics* 39(14):2603-2610.

15. Liu X & Pollack GH (2002) Mechanics of F-actin characterized with microfabricated cantilevers. *Biophysical journal* 83(5):2705-2715.

16. Kojima H, Ishijima A, & Yanagida T (1994) Direct measurement of stiffness of single actin filaments with and without tropomyosin by in vitro nanomanipulation. *Proceedings of the National Academy of Sciences of the United States of America* 91(26):12962-12966.

17. Gittes F, Mickey B, Nettleton J, & Howard J (1993) Flexural rigidity of microtubules and actin filaments measured from thermal fluctuations in shape. *The Journal of cell biology* 120(4):923-934.

APPENDIX

INVESTIGATING THE RELATIONSHIP BETWEEN STRUCTURAL STRESS FIBER SARCOMERE DYNAMICS AND GENERATION OF TRACTION STRESS

A.1 Abstract

Actin stress fibers (SFs) have often been compared to muscle fibers. Each are made of individual contractile units, called sarcomeres. Traditionally SF contractility has been presumed to be directly linked to structural changes in sarcomere length, as is the case in muscle fibers. Here I investigated whether changes in sarcomere length in SFs could be directly linked to changes in contractility by coupling traction force microscopy with image analysis. In this study I tracked sarcomere dynamics in living cells using zyxin-GFP, and compared sarcomere length fluctuations with changes in traction stress at the SF's associated FA. Here I found no correlation between sarcomere shortening and increased contractility, and conversely there was no detectable, significant relationship between sarcomere lengthening and decreased contractility. Overall no trend emerged from the data. Herein I discuss experimental challenges and shortcomings of this set of experiments.

A.2 Introduction

Cells are able to generate contractile forces through their actin cytoskeleton, which can be especially important during cell migration and wound closure (1, 2). Actin stress fibers (SFs) and

nonmuscle myosin II are often implicated in these processes and SF contraction can be transferred to the underlying extra cellular matrix via focal adhesions (FAs) (3, 4).

SFs are organized into subunits much like sarcomeres in skeletal muscle fibers. SF sarcomeres are identified by α-actinin or zyxin borders, comparable to Z-line proteins in muscle fibers, with nonmuscle myosin II in the centers of individual sarcomeres (5, 6). The contractile dynamics and force generating abilities of skeletal muscle sarcomeres have long been characterized (7, 8), and SF sarcomeres are also thought to be contractile subunits of the actin cytoskeleton (9, 10). It has been hypothesized that shortening of SF sarcomeres may lead to increased contractile forces (11). However, unlike muscle fibers, the direct relationship between sarcomere dynamics and force transmission in actin SFs is largely unknown.

Living cells produce quantifiable traction stresses at their FAs. These stresses can be measured using live cell traction force microscopy. For this project, I tracked dynamics of SF sarcomeres with zyxin-GFP and compared it with the mechanical output of stress at the associated FA. Correlating measurements of a traditional measure of cell contraction with traction force microscopy, a quantitative method of measuring force, could allow for more accurate predictions of how contractile a cell is based on the shortening of SF sarcomeres alone.

A.3 Methods

A.3.1 Cell lines

As published elsewhere (12), fibroblasts were derived from a zyxin -/- mouse were rescued with a stably expressing zyxin-GFP (13). Cells were cultured in DMEM with 10% fetal bovine serum (Hyclone), sodium pyruvate, penicillin/streptomycin and L-glutamine.

A.3.2 Live cell traction force microscopy

Details of imaging conditions have been discussed previously (14). Briefly, cells were plated on 25 kPa polyacrylamide gels containing far red 0.02 μm beads (Invitrogen). Images were taken at 30 second time intervals for 20-30 minutes.

A.3.3 Image analysis

A detailed explanation of image analysis has been published (12). The combination of live cell traction force microscopy data and image analysis is illustrated in Fig. A1.

A.3.4 Traction stress analysis

Particle tracking velocimetry code was written in MATLAB (The MathWorks Natick, MA) (15, 16). Traction stress at specific pixel coordinates was determined by the peak stress within 16 pixels of the initial coordinate. This was measured using code written by Jonathan Stricker, for MATLAB.

A.4 Results

A.4.1 Fluctuations in SF sarcomere length are similar regardless of traction stress dynamics

The FA stress profile over time was broken up into a minimum of 1.5-minute stretches of continuous behavior: increasing, decreasing, or unchanging traction stress (Fig. A2 A). These particular fragments in the image sequence were paired with the changes in sarcomere length at the same time. Using the trends in traction stress, we grouped the range of sarcomere length fluctuations (Fig. A2 B). There is no significant difference between groups (Incres vs Decres $p = 0.53$, Incrs vs noChng $p = 0.77$, Decres vs noChng $p = 0.92$), indicating there is no relationship linking sarcomere length changes to trends in traction stress change.

A.4.2 There is no correlation between fluctuations of stress fiber sarcomere length and the changes in traction stress at the FA

Although there was no detectable difference between the means and ranges of sarcomere length changes according to groupings, we then paired the net change in sarcomere length with the change in traction stress. We first compared SF sarcomere length changes (um) with mechanical changes (Pa) in a scatter plot (Fig. A3 A). If the main hypothesis were true, we would expect greater amounts of shortening with greater amounts of traction stress generation. However, we found no correlation in either increasing or decreasing traction stress (Pearson's r = -0.0027, Pearson's r = -0.055, respectively) This was also done comparing percent change in both net change of sarcomere length and change in traction stress with no correlation (increasing Pearson's r = 0.23, decreasing Pearson's r = -0.18, Fig. A3 B). In this analysis we did not find a correlative relationship between change in sarcomere length and change in traction stress at the associated FA.

A.5 Discussion

Studies of muscle fiber sarcomere dynamics in conjunction with force generation have led to a similar hypothesis regarding SF sarcomere structure and function (11). Here we compared the length changes of the first four sarcomeres nearest the FA, with changes in traction stress detected at the FA. We separated the data into groups according to persistent increases, decreases, or no change in traction stress over a minimum of 1.5-minute stretches. We found there to be no detectable differences or correlations between these two sets of data.

Recently it was shown that SFs exposed to nN forces via AFM tip had no significant difference in sarcomere length fluctuations, though the standard deviations of mechanically perturbed SFs increased, indicating a greater range of fluctuations (11). No link was found between specific changes in sarcomere length and the force applied at the corresponding

attachment site of the AFM (11). One recent study did show a more subtle link between SF sarcomere length and force generation (17). In cells experiencing blebbistatin treatment and subsequent wash-out, forming actin bundles near the cell periphery shortened in length as traction force recovered to its prior magnitude (17). However, no direct link between changes in sarcomere lengths and changes in traction stress has been reported.

There were a number of experimental challenges in this project. Our zyxin -/- fibroblasts stably expressing zyxin-GFP did not adhere and spread as well on 25 kPa gels as they do on glass. It was difficult to find adequate looking cells, expressing zyxin-GFP, that remained adhered throughout the time of imaging. Frequently cells ripped themselves off the gel during image acquisition, presumably from phototoxicity from five images taken every 30 seconds for 30 minutes. Additionally, assuming cells remained adhered throughout the movie and cells were adequately expressing zyxin-GFP, it was not common to find a single SF attached to a single FA. Oftentimes multiple SFs attached to a single large FA, which would make it difficult to answer questions regarding single SF-FA relationship.

Aside from many experimental challenges, conceptually we were ignoring a number of different components of SF contractility; myosin II activity, strength of adherence of FA to the substrate, and signaling events.

What we have found speaks to a mechanical homeostasis, which complements our structural homeostatic conditions (12).

We have found there is no link between resting fluctuations in SF sarcomere length and resting, homeostatic changes in traction stress. When changes in either sarcomere length or traction stress occur outside the range of resting conditions, it is still unknown whether there is coordination between sarcomere length and force generation, as there is in muscle fibers.

A.6 Acknoweldgments

Margaret Gardel provided extensive training in both traction force microscopy and data analysis. Jonathan Stricker, a grad student in the Gardel lab, was also extremely helpful with image and data analysis. Additionally, both Margaret and Jonathan provided MATLAB code necessary for this project.

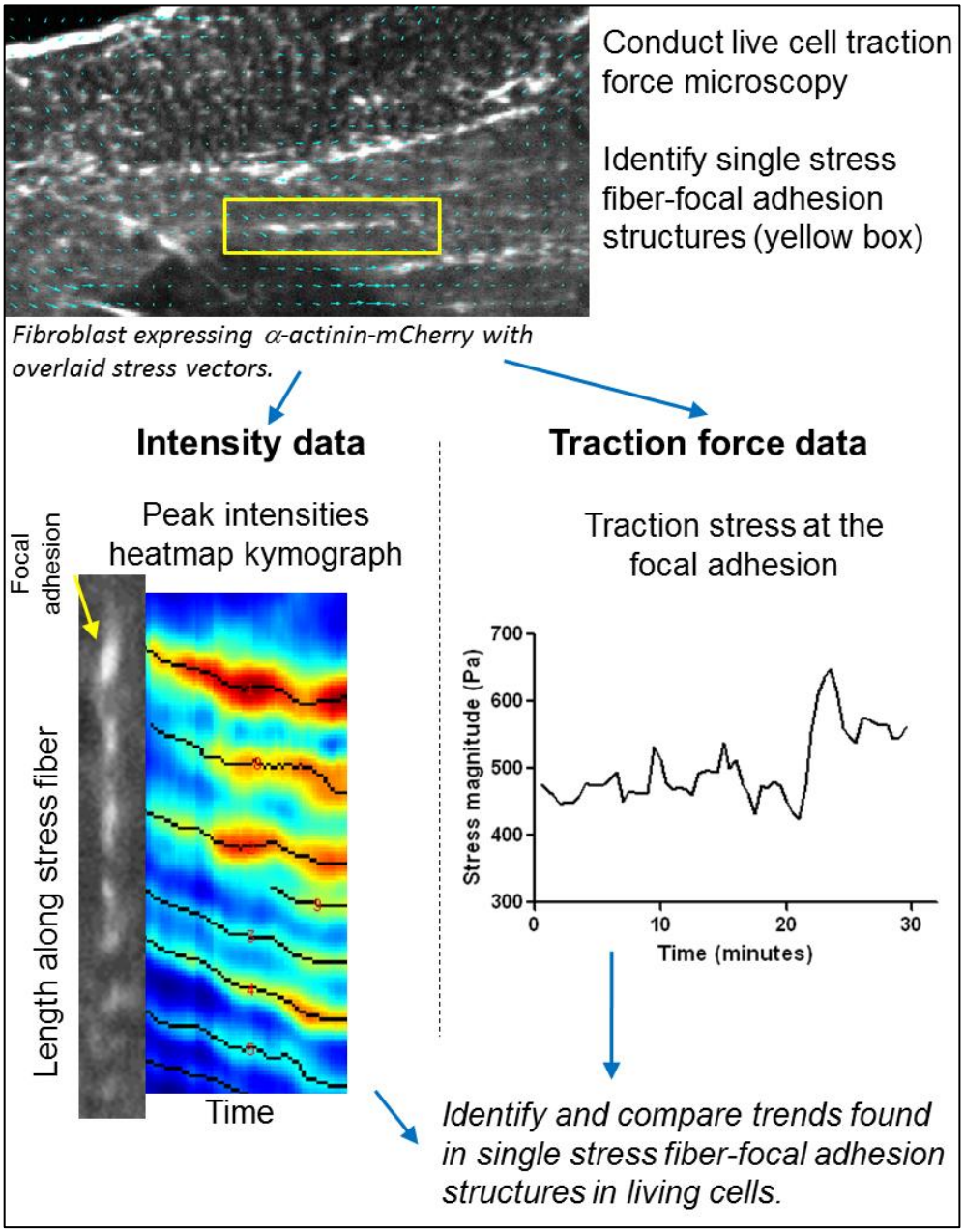

Figure A1: Sequence of events during data analysis. Simultaneously image α-actinin-mCherry-expressing cells that are plated on polyacrylamide gels embedded with fluorescent microbeads. Image analysis and collection of traction stress data occur in separate steps, though are later combined in order to test the relationship between SF structure and mechanical function.

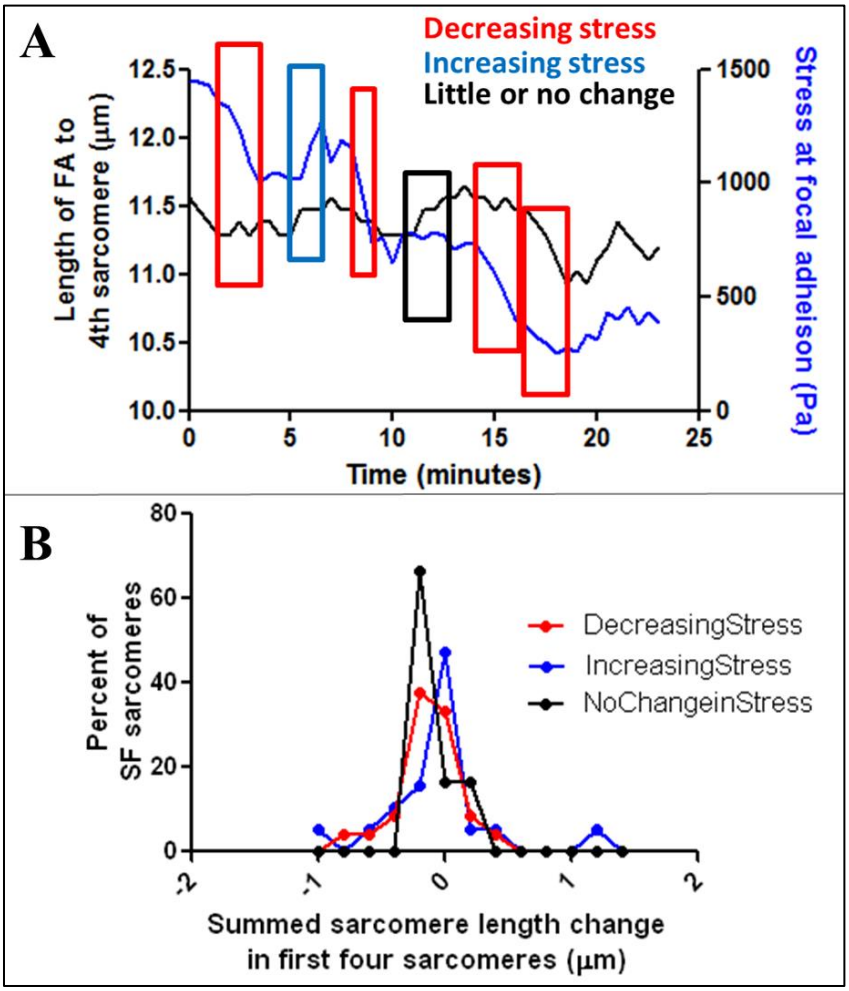

Figure A2: Similar changes in sarcomere length regardless of traction stress trend. (A) Stretches of time during continuous increasing, decreasing, or unchanging traction stress. (B) Summed lengthening and shortening of the first four closest sarcomeres to the FA during episodes of increasing, decreasing, and unchanging stress at the FA.

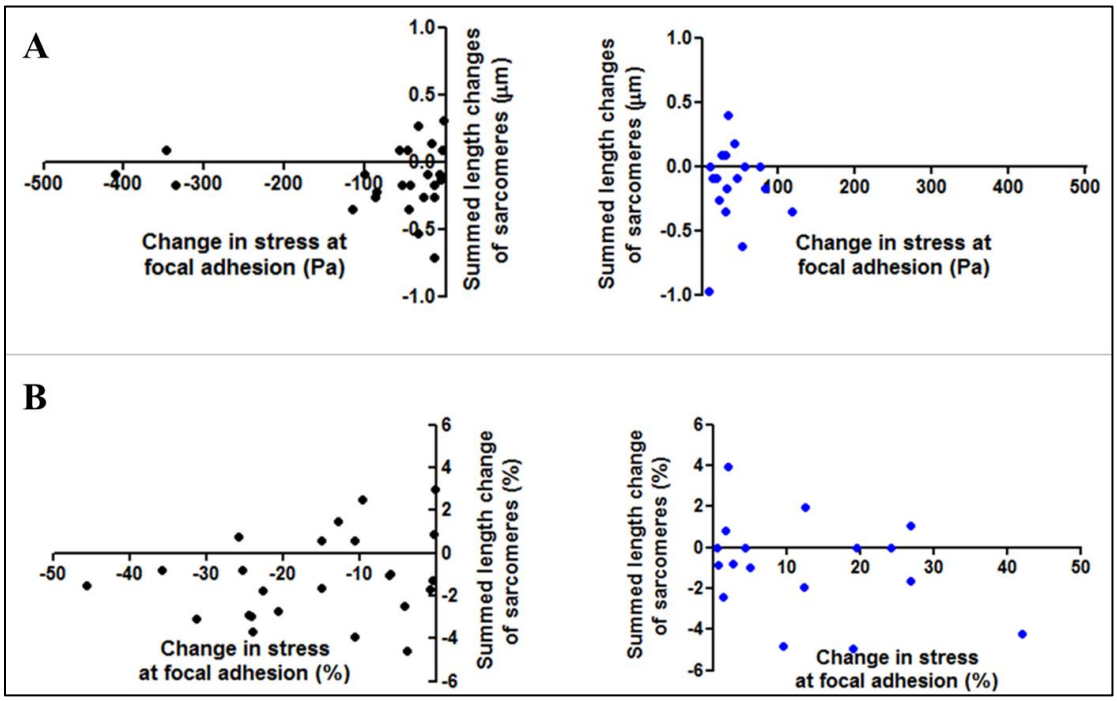

Figure A3: No correlation between changes in the four closest sarcomeres to the focal adhesion, and changes in traction stress. (A) Changes in sarcomere length given in distance (µm) compared to changes in traction stress (Pa). There is no significant correlation. (B) Changes in sarcomere length and traction stress given as percentages. Decreasing traction stress indicated by negative x-axis values shown as black scatter points in left-side plots, while increasing traction stress indicated by positive x-axis values is shown as blue scatter points on the right-side plots.

A.7 References

1. Disanza A, *et al.* (2005) Actin polymerization machinery: the finish line of signaling networks, the starting point of cellular movement. *Cellular and molecular life sciences : CMLS* 62(9):955-970.

2. Ridley AJ, *et al.* (2003) Cell migration: integrating signals from front to back. *Science* 302(5651):1704-1709.

3. Burridge K & Chrzanowska-Wodnicka M (1996) Focal adhesions, contractility, and signaling. *Annual review of cell and developmental biology* 12:463-518.

4. Parsons JT, Horwitz AR, & Schwartz MA (2010) Cell adhesion: integrating cytoskeletal dynamics and cellular tension. *Nature reviews. Molecular cell biology* 11(9):633-643.

5. Lazarides E & Burridge K (1975) Alpha-actinin: immunofluorescent localization of a muscle structural protein in nonmuscle cells. *Cell* 6(3):289-298.

6. Weber K & Groeschel-Stewart U (1974) Antibody to myosin: the specific visualization of myosin-containing filaments in nonmuscle cells. *Proceedings of the National Academy of Sciences of the United States of America* 71(11):4561-4564.

7. Edman KA (2010) Contractile performance of striated muscle. *Advances in experimental medicine and biology* 682:7-40.

8. Maruyama K (1995) Birth of the sliding filament concept in muscle contraction. *Journal of biochemistry* 117(1):1-6.

9. Isenberg G, Rathke PC, Hulsmann N, Franke WW, & Wohlfarth-Bottermann KE (1976) Cytoplasmic actomyosin fibrils in tissue culture cells: direct proof of contractility by visualization of ATP-induced contraction in fibrils isolated by laser micro-beam dissection. *Cell and tissue research* 166(4):427-443.

10. Katoh K, Kano Y, Masuda M, Onishi H, & Fujiwara K (1998) Isolation and contraction of the stress fiber. *Molecular biology of the cell* 9(7):1919-1938.

11. Guolla L, Bertrand M, Haase K, & Pelling AE (2012) Force transduction and strain dynamics in actin stress fibres in response to nanonewton forces. *Journal of cell science* 125(Pt 3):603-613.

12. Chapin LMB, E.; Smith, M.A.; Shiu Y.; Beckerle M.C. (2012) Lateral communication between stress fiber sarcomeres facilitates a local remodeling response. *Biophysical journal* 103(10).

13. Hoffman LM, *et al.* (2006) Genetic ablation of zyxin causes Mena/VASP mislocalization, increased motility, and deficits in actin remodeling. *The Journal of cell biology* 172(5):771-782.

14. Smith MA, *et al.* (2010) A zyxin-mediated mechanism for actin stress fiber maintenance and repair. *Developmental cell* 19(3):365-376.

15. Sabass B, Gardel ML, Waterman CM, & Schwarz US (2008) High resolution traction force microscopy based on experimental and computational advances. *Biophysical journal* 94(1):207-220.

16. Gardel ML, *et al.* (2008) Traction stress in focal adhesions correlates biphasically with actin retrograde flow speed. *The Journal of cell biology* 183(6):999-1005.

17. Aratyn-Schaus Y, Oakes PW, & Gardel ML (2011) Dynamic and structural signatures of lamellar actomyosin force generation. *Molecular biology of the cell* 22(8):1330-1339.